

Poly(ethylene oxide)-grafted Polycarbonates as Solvent-free Polymer Electrolytes for Lithium-Metal Batteries

Zur Erlangung des akademischen Grades eines
DOKTORS DER NATURWISSENSCHAFTEN
(Dr. rer. nat.)

von der KIT-Fakultät für Chemie und Biowissenschaften
des Karlsruher Instituts für Technologie (KIT)



genehmigte
DISSERTATION
von
Marvin Subarew

1. Referent: Prof. Dr. Patrick Théato
2. Referent: Prof. Dr. Michael Meier
Tag der mündlichen Prüfung: 13. Dezember 2022

MEINEN ELTERN GEWIDMET

We are neither gods nor geniuses.
We have to do everything step by
step, starting from the very bottom.
Looking for the rules behind the
things we don't understand and the
steady effort going into it, that's all
that science really is.

Ishigami Senkū (loosely translated)

Abstract

Solid-state electrolytes are considered to be a crucial step to increase the safety of battery cells, as well as allowing the employment of lithium metal anodes which achieve much higher energy densities. To this point, only materials based on poly(ethylene oxide) (PEO) have been commercially employed as such. In an effort to improve the understanding of PEO-based polymer electrolytes, the synthesis of an aliphatic polycarbonate bearing PEO sidechains *via* a thiol-ene post-polymerization modification approach is described. The complete suppression of crystallization in the system for all four PEO sidechain lengths was demonstrated. The influence of the sidechain lengths and different LiTFSI concentrations on the thermal behavior and the ionic conductivity of the polymer electrolyte was illustrated in a systematic approach. The PEO sidechain with around 12 repeating units displayed some positive interactions with the polycarbonate backbone, resulting especially in quite high lithium ion transference numbers for a PEO-based electrolyte with up to 0.19. Ultimately, the highest ionic conductivity achieved for this system was $9.9 \times 10^{-3} \text{ mS cm}^{-1}$ at ambient temperature and $2.3 \times 10^{-1} \text{ mS cm}^{-1}$ at 70 °C with the PEO sidechain containing 23 repeating units. Unfortunately, these polymer electrolytes were very lacking in mechanical stability, resembling a honey-like, highly viscous mass. Two different solidification approaches were examined to improve the mechanical properties. Controlled thiol-ene crosslinking yielded highly flexible solid films that could still achieve an ionic conductivity one order of magnitude worse than the grafted system. The second approach planned on the integration of a polystyrene block, but control over the polymerizations was insufficient and the resulting polymer electrolyte films were very brittle and demonstrated a noticeable loss of ionic conductivity. Nonetheless, a deeper insight into the structure-property relationship of PEO-grafted polymer electrolytes was provided, strengthening the understanding of PEO sidechain architectures. The demonstrated system of PC-*gr*-PEO showcased some interesting properties that warrant further investigation.

Zusammenfassung

Festkörperbatterien werden als wesentlicher Schritt angesehen, um die Sicherheit von Batteriezellen zu erhöhen, sowie auch den Einsatz von Lithiummetall-Anoden zu ermöglichen, die deutlich höhere Energiedichten erzielen. Bis zum jetzigen Zeitpunkt wurden nur Materialien auf Basis von Polyethylenoxid (PEO) kommerziell hierfür eingesetzt. Um das Verständnis für PEO-basierte Polymerelektrolyte zu verbessern, wird die Synthese eines aliphatischen Polycarbonats mit PEO-Seitenketten über einen Thiol-En-Postfunktionalisierungsansatz beschrieben. Die vollständige Unterdrückung der Kristallisation im System wurde für alle vier PEO-Seitenkettenlängen bewiesen. Der Einfluss der Seitenkettenlängen und unterschiedlicher LiTFSI-Konzentrationen auf das thermische Verhalten und die Ionenleitfähigkeit des Polymerelektrolyten wurden in einem systematischen Ansatz dargestellt. Die PEO-Seitenkette mit etwa 12 Wiederholungseinheiten zeigte einige positive Wechselwirkungen mit dem Polycarbonat-Rückgrat, was insbesondere zu relativ hohen Lithiumüberföhrungszahlen für einen PEO-basierten Elektrolyt mit bis zu 0.19 führte. Letztlich war die höchste erreichte Ionenleitfähigkeit für diese System $9.9 \times 10^{-3} \text{ mS cm}^{-1}$ bei Umgebungstemperature und $2.3 \times 10^{-1} \text{ mS cm}^{-1}$ bei 70°C mit der PEO-Seitenkette mit 23 Wiederholungseinheiten. Diesen Polymerelektrolyten fehlte es allerdings sehr an mechanischer Stabilität, eher einer honigartigen, hochviskosen Masse ähnelnd. Zwei unterschiedliche Ansätze zur Verfestigung wurden untersucht, um die mechanischen Eigenschaften zu verbessern. Die kontrollierte Thiol-En-Vernetzung ergab äußerst flexible, feste Filme, die immer noch eine Ionenleitfähigkeit eine Größenordnung schlechter als das gepropfte System erreichen konnten. Der zweite Ansatz sah die Integration eines Styrolblock vor, aber die Kontrolle über die Polymerisationen war unzureichend und die entstandenen Polymerelektrolytfilme waren sehr spröde und zeigten einen nennenswerten Verlust an Ionenleitfähigkeit. Nichtsdestotrotz wurde ein tieferer Einblick in die Struktur-Eigenschafts-Beziehung für PEO-gepropfte Polymerelektrolyte zur Verfügung gestellt, was das Verständnis von PEO-Seitenkettenarchitekturen stärken sollte.

Das demonstrierte System aus PC-*gr*-PEO zeigte einige interessante Eigenschaften, die weitere Untersuchungen rechtfertigen.

Danksagung

Zunächst möchte ich meinen ausdrücklichen Dank an PROF. DR. PATRICK THÉATO aussprechen. Ohne ihn wäre diese Arbeit nicht zustande gekommen. Danke für das Bereitstellen des Themas, der Labore, der Chemikalien und allem Weiteren, das man so für den Laboralltag gebrauchen kann und für das man bei ihm nie betteln musste. In diesem Sinne möchte ich mich auch bei dem BUNDESMINISTERIUM FÜR BILDUNG UND FORSCHUNG (BMBF) im Rahmen des FESTBATT Clusters und beim KARLSRUHE HOUSE OF YOUNG SCIENTISTS (KHYS) für die finanziellen Mittel bedanken, die diese Forschung überhaupt erst ermöglicht haben.

Mein Dank gilt außerdem PROF. DR. MICHAEL MEIER für die problemlose Übernahme der Zweitkorrektur dieser Dissertation, sowie PROF. DR. HELMUT EHRENBERG, PROF. DR. JOACHIM PODLECH und PROF. DR. FRANK BREHER in deren Funktion als Promotionsprüfungsausschuss.

Ich möchte auch DR. DOMINIK VOLL ganz herzlich dafür danken, dass er mir einen riesigen Batzen administrativer Aufgaben in Form der *de facto*-Leitung des Campus (Wild Wild) West von den Schultern genommen hat. Ich habe mit dem Aufbau und der Strukturierung des Westens viel gelernt und bin als Mensch daran gewachsen. Ich möchte diese Erfahrung nicht missen, bin aber gleichzeitig froh, dass ich den Stress abgeben konnte und mich dann auch mehr meiner Forschung widmen konnte.

In demselben Atemzug sei auch DR. HATICE MUTLU gedankt. Was Dominik administrativ geleistet hast, war sie für viele AKT-Mitglieder auf wissenschaftlicher Ebene. Ich durfte sie über die Jahre als überaus fleißige und hart arbeitende Wissenschaftlerin kennenlernen, die niemals gezögert hat ihr Wissen zu teilen und ihre Hilfe anzubieten. Ich bin fest davon überzeugt, dass sie eine herausragende und inspirierende Professorin wird und wünsche ihr nur das Beste auf ihrem weiteren Weg.

Mein nimmer endender Dank gilt außerdem KATHARINA KUPPINGER. Sie hält mit einer Leichtigkeit und Selbstverständlichkeit den kompletten Arbeitskreis am Laufen und ihre Hilfsbereitschaft kennt gefühlt keine Grenzen. Ohne ihr Zutun wäre schon unzählige

Male alles gegen die Wand gefahren, oder abgesoffen, oder wie ein Kartenhaus zusammengestürzt. Ich hoffe sehr, dass sie auch in Zukunft Anerkennung dafür finden wird.

Auch BIRGIT HUBER sei in gleichem Maße gedankt, die sich um alle Gerätschaften am Soft Matter Lab kümmert und immer gerne bereit war ihre Zeit zur Verfügung zu stellen. Ich möchte mich auch dafür bedanken, dass sie ihr Wissen in diesen Dingen, aber besonders im Rahmen der GPC, so bereitwillig geteilt hat und mir bei jeder Frage schnellstmöglich helfen konnte. Ich konnte viel über dieses Gerät lernen, das doch mit dem Herzblut eines jeden Polymerchemikers läuft.

BÄRBEL SEUFERT-DAUSMANN war immer freundlich und immer hilfsbereit und damit ein absoluter Kontrast zu ihrer Vorgängerin. Besten Dank, dass sie sich immer schnell um alle administrativen und organisatorischen Angelegenheiten gekümmert, vieles davon auch einfach hinter den Kulissen übernommen hat und dass es ihr wichtig war, mit der Transportkarte an die Schranke zu laufen, damit ich nicht selbst laufen musste. Größter Dank geht auf jeden Fall an ISABELLA WEISS, meiner Partnerin in Uncrime. Wir haben über die vergangenen Jahre einiges erlebt und uns dabei gegenseitig den Rücken frei gehalten. Gerade in der Anfangszeit konnte niemand wissen, was am nächsten Tag am Campus West auf einen warten würde. Deswegen war es beruhigend zu wissen, dass es zumindest eine Person gab, bei der man wusste, dass die Dinge gut werden und man sich nicht selbst um alles kümmern muss. Das Büro mit ihr und mit niemandem sonst zu teilen, war eine fantastische Entscheidung. Gemeinsam stellten wir uns auch diesem Ungetüm, das sich FestBatt nannte und drohte unsere Freude an der Chemie zu zermalmen.

Letztlich möchte ich auch DR. ANDREAS BUTZELAAR, dem Dritten im Bunde FestBatt-Batterie-Menschen, danken. Er hatte immer den besten Draht zu unseren Kollegen in Münster und war es schließlich auch, der viel Knowhow transferiert hat. Ich danke auch explizit für die wissenschaftlichen Diskussionen, wenn es in meinen Ergebnissen Unstimmigkeiten oder Fragen gab, mit denen ich mich an niemanden sonst hätte wenden können.

Ich möchte mich ebenso bei den Studenten bedanken, die mich über die Jahre

unterstützt haben. Das waren ANASTASIA CEPOI und ihr unglaublicher Wissensdurst, FRANZISKA SAUER, die leider nie ihre Arbeit abgegeben hatte, aber wenigstens die erhobenen Daten hinterließ, und DAVID GEISS, der viele Misserfolge hinnehmen musste, damit ich später die eine funktionierende Lösung hatte.

Unbedingt muss ich auch meinen Dank an DR. PATRICK-KURT DANNECKER richten. Er war nur relativ kurz ein Teil des Arbeitskreises, aber es war zu einer wichtigen Zeit, in der ich eine ganze Menge von ihm lernen konnte und die mir meine eigene Anfangszeit in den Doktorandenalltag erheblich erleichterte.

Ich bedanke mich auch bei der Gesamtheit des Arbeitskreises Théo für die letzten Jahre. Es war wahrlich nicht immer leicht, aber ich nehme dennoch auch eine Menge positive Erinnerungen mit. Explizit möchte ich dabei den folgenden Personen für ihre Unterstützung, ob privat oder wissenschaftlich, für die Gemeinsamkeit und für ihre Freundlichkeit danken: VICTORIA LE außerdem dafür einfach super zu sein, DAVID SUNDERMANN nicht nur für das gemeinsame Leiden sondern auch für das gemeinsame Siegen, YUNJI XIE for being three helping hands at once, JOHANNES SCHEIGER für seine Art mit allen klar zu kommen, ALEXANDER GRIMM und DANIEL DÖPPING für das Halten der Stellung, MERYEM AKDEMIR for just pushing through with us, DR. YOSUKE AKAE for always being open and interested, NICO ZUBER dafür alles immer auf 110% zu drehen, SERGEJ BARABAN für seine überraschend ehrliche Offenheit und letztlich auch KLARA URBSCHAT als das junge Blut.

Aus tiefster Seele möchte ich an dieser Stelle meiner besten Freundin DR. KATJA KRELL meine Dankbarkeit zum Ausdruck bringen. Wir sind beide von Natur aus Pessimisten, rechnen immer mit dem Schlimmsten und haben deswegen auch schon einen Plan F parat. Und trotz dessen oder vielleicht auch gerade deshalb schaffen wir es irgendwie ein Leuchtfeuer der Positivität für den jeweils anderen zu sein. Wir bauen uns gegenseitig auf, wie wir es für uns selbst nicht können. Ohne ihr Vertrauen und ihre aufbauenden Worte weiß ich nicht, ob ich nicht schon am Weg gescheitert wäre. Ein großes Dankeschön gilt ihr außerdem für das Gegenlesen dieser Dissertation und ihren Input dahingehend.

Ebenso zu Dank verpflichtet bin ich meinen beiden anderen besten Freunden KARSTEN

DIEKHOFF und ARMIN HERZOG. Sie stellten immer genau das zur Verfügung, das ich gerade brauchte: Ablenkung um den Kopf zu resetten, ein offenes Ohr als Gesprächspartner oder guten Zuspruch, wenn die Luft raus war. Über die Studienjahre und jetzt auch nochmal während der Promotion habe ich nur immer mehr zu schätzen gelernt, wie wichtig es ist, jemanden wie die beiden zu haben.

Auch meinem Chaos Squad MARK RUTSCHMANN und DR. MARCO SCHÖNIG sei an dieser Stelle gedankt. Ob sie nun wollen oder nicht, sie werden ihrem Namen nicht gerecht; ganz im Gegenteil. In den letzten Jahren, in denen sich ein Tag wie der andere angefühlt hat, vor allem wenn die Arbeit einen einmal mehr übermannt hat, haben unsere wöchentlichen/halbwochentlichen Eskapaden eine gewisse Struktur gebracht, einen freudigen Termin, auf den man sich jedes Mal aufs Neue freuen konnte.

Auch danken möchte ich LAURA SELLRICH. Kaum zu glauben, wie lange wir nun schon befreundet sind. Sie ist mit großem Abstand meine langjährigste Freundin. Und selbst wenn man mal über Wochen und Monate nichts voneinander hört, weil einen der Stress ertränkt, ist doch wieder sofort alles beim Alten, wenn man sich meldet. Hoffentlich gibt es dazu jetzt wieder mehr Gelegenheiten.

An letzter und damit an besonders hervorgehobener Stelle möchte den beiden Menschen danken, denen auch diese Arbeit gewidmet ist: EV-LIANE und MICHAEL SUBAREW. Sie sind mein Anker und mein Ruhepunkt, haben mir schon immer erlaubt und mich ermutigt meine eigenen Entscheidungen zu treffen, waren aber immer bereit mich aufzufangen oder mir aufzuhelfen, wenn ich auf die Nase gefallen bin. Meine Mami, du hast dein Schicksal nicht verdient, aber ich hoffe, dass du eine Möglichkeit findest, mit der Sache deinen Frieden zu schließen, damit wieder ein bisschen mehr Lebensfreude bei dir einkehren kann. Mein Papi, dir wünsche ich wieder mehr Gelassenheit. Manche Dinge kann man im Leben leider einfach nicht ändern und dann muss man sich entweder damit abfinden oder gehen.

Contents

Abstract/Zusammenfassung	i
Danksagung	iv
1 Introduction	1
2 Theoretical Background	2
2.1 Polymerization Techniques	2
2.1.1 Step-Growth Polymerization	2
2.1.2 Chain-Growth Polymerization	4
2.1.3 Ring-Opening Polymerization	8
2.2 Post-Polymerization Modification	11
2.2.1 Thiol-ene Addition Chemistry	12
2.3 Lithium-Ion Batteries	14
2.4 Polymer Electrolytes	17
2.4.1 PEO as Polymer Electrolyte	18
2.4.2 Polycarbonates as Polymer Electrolytes	21
3 Motivation and Aim	24
4 Results and Discussion	26
4.1 Polymer Synthesis	26
4.1.1 Initial Considerations and Test Reactions	26
4.1.2 Updated Synthesis Pathway	30
4.1.3 Thiolation of PEO	35
4.1.4 Post-Polymerization Functionalization	37
4.2 Thermal Characterization	42
4.3 Ionic Conductivity	48
4.4 Multifunctionalization	56
4.5 Solidification Approaches	59
4.5.1 Crosslinking	59

4.5.2	Microphase Separation	61
4.5.3	Characterization of Solidified Samples	67
5	Conclusion and Outlook	70
6	Experimental Protocols	73
6.1	Materials	73
6.2	Instrumentation and Procedures	74
6.3	Synthesis of Cyclic Carbonates	78
6.3.1	Trimethylene Carbonate (TMC)	78
6.3.2	2-Allyloxymethyl-2-Ethyltrimethylene Carbonate (AOMECE)	80
6.3.3	2-Butyl-2-Ethyltrimethylene Carbonate (BEC)	82
6.4	Anionic Ring-Opening Polymerization	84
6.4.1	Synthesis of Thiourea Cocatalyst (TUC)	84
6.4.2	Polymerization of TMC	86
6.4.3	Polymerization of AOMECE	87
6.4.4	Polymerization of BEC	88
6.5	Thiolation of PEO	90
6.5.1	Tosylation	90
6.5.2	Xanthation	91
6.5.3	Aminolysis	92
6.6	Thiol-ene Addition	94
6.6.1	General Procedure for Post-Polymerization Modification	94
6.6.2	Crosslinking	95
6.7	PS Block Copolymerization Approach	96
6.7.1	RAFT Polymerization of Styrene	96
6.7.2	CTA Endgroup Removal <i>via</i> Radical Displacement	97
6.7.3	CTA Endgroup Removal <i>via</i> Aminolysis	98
6.7.4	AROP Chain Extension	99
6.7.5	Thiol-ene Addition and Electrolyte Film Preparation	101
6.8	Multifunctionalization	103

6.8.1 Bromination of PAOMEC	103
List of Abbreviations	A
List of Figures	E
List of Tables	G
Bibliography	H
Author Information	T

1 Introduction

Fossil fuels are a finite resource. This simple realization triggered a massive worldwide push towards more renewable energy sources. However, this change will also result in an unprecedented demand for fast and efficient storage of electrical energy.^[1–3] While state-of-the-art lithium-ion batteries still feature some very advantageous properties,^[4] battery cells will require higher energy densities in the future, especially for electric vehicles.^[5] Additionally, current lithium-ion batteries employ mixtures of small liquid organic molecules as electrolyte.^[4,6] These are, however, volatile, flammable, and toxic compounds, resulting in an enormous safety concern.^[7–9]

Solid-state electrolytes are a promising alternative to the conventional electrolytes. By removing all liquid and volatile components from a battery cell, dangers of fire, explosion, and leakage of toxic material are massively decreased.^[10,11] Furthermore, it is known that a solid-state electrolyte can allow the usage of lithium metal as anode material in a cell. This would substantially increase the energy and power densities of batteries.^[12–15] Despite this prospect, solid-state electrolytes are still limited in their practical application due to their very low ionic conductivity.^[16–18]

However, a sole polymer-based solid electrolyte actually could achieve the commercial level in combination with a lithium metal anode. This electrolyte is based on poly(ethylene oxide) (PEO) and displays a variety of advantageous properties.^[19,20] Unfortunately, PEO typically suffers from high crystallinity at the same time. This massively reduces the ionic conductivity below its melting point, thus requiring quite high operational temperatures.^[21–23] The research focus on PEO has shown that there are avenues and ways to elevate this issue, but no ideal solution was found yet to overcome all challenges.

This thesis aims to give further insights on some of the properties of PEO-based polymer electrolytes.

2 Theoretical Background

2.1 Polymerization Techniques

The International Union of Pure and Applied Chemistry (IUPAC) defines a polymer as a “substance composed of macromolecules”, which are “molecule[s] of high relative molecular mass, the structure of which essentially comprises the multiple repetition of units derived [...] from molecules of low relative molecular mass”, which we call monomers. The “process of converting a monomer or a mixture of monomers into a polymer” is called a polymerization.^[24] However, there are two big classes of polymerization reactions that can be differentiated fundamentally: Step-growth polymerization comprises techniques where all monomers are reactive at once. On the other side, the term chain-growth polymerization covers methods where only a few chain ends are reactive at once. Both classes and relevant techniques will be discussed in the following sections.

2.1.1 Step-Growth Polymerization

In step-growth polymerizations, the monomers need to be bi- or multifunctional and share two different reactive functional groups between them. The growth of the polymer proceeds by the individual reaction between any two functional groups, slowly building up bigger and bigger units. The kinetics of step-growth polymerizations are nicely defined by the Carothers' equation:^[25]

$$P_n = \frac{1+r}{1+r-2rX}$$

The degree of polymerization P_n , meaning the number of repeating units in the polymer, is limited by both, the ratio between the two functional groups r and the conversion X of the polymerization. Ultimately, this means that for step-growth polymerizations the

equimolarity of the reactive groups is extremely important and the reactions have to be necessarily driven to very high conversions to reach reasonable molecular weights. Already 1 % of excess from one functional group and only reaching 99 % conversion limits the maximum degree of polymerization to around 66. This also restricts the range of chemistries employable for step-growth polymerizations to reactions that can reach high conversions.

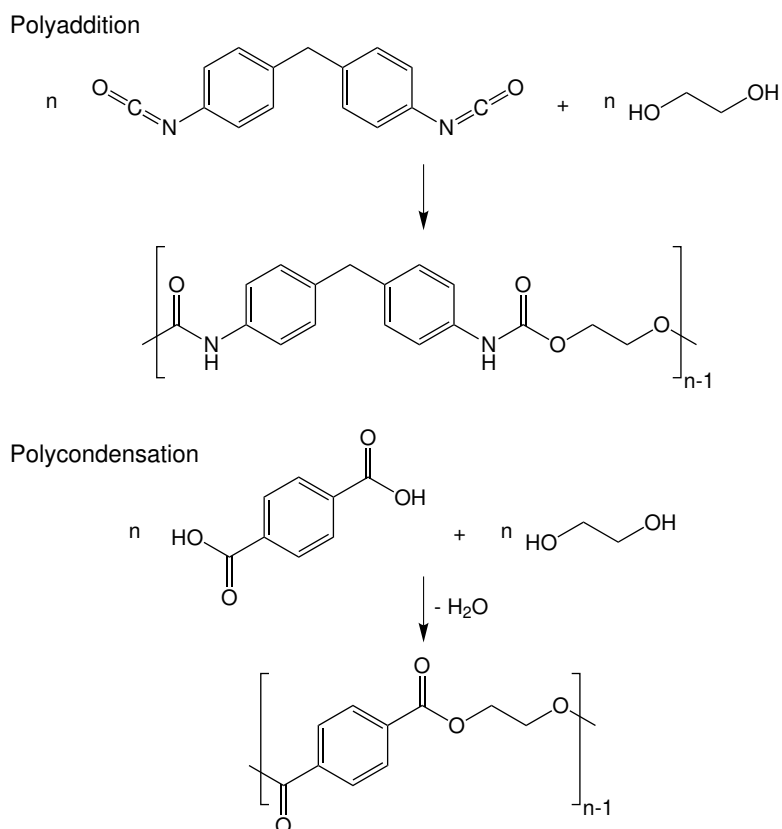


Figure 1: Two exemplary step-growth polymerizations are given. The top reaction shows the polyaddition between methylene diphenyl diisocyanate and ethylene glycol to form a polyurethane. The lower reaction shows the polycondensation between terephthalic acid and ethylene glycol to poly(ethylene terephthalate) (PET), a polyester.

Step-growth polymerizations can be further divided into two subclasses: polyadditions and polycondensations, with the latter also producing a small molecule with each reaction step that usually needs to be constantly removed during the reaction.^[25] One example for each subclass is given in figure 1. Due to the mechanism of step-growth

polymerizations, the reaction product from the two functional groups remains within the mainchain of the polymer. This gives rise to functional polymers like polyesters, polyamides, and polyurethanes.^[26–28]

2.1.2 Chain-Growth Polymerization

The second big class of polymerization reactions are the chain-growth polymerizations. These are distinguished by constantly adding monomer units to an active chain end of the polymer. Radical polymerizations, ionic polymerizations, and coordination polymerizations are all part of this class. A selection will be described below.

FREE RADICAL POLYMERIZATION (FRP)

FRP is one of the most straightforward and widespread polymerization methods. Nearly all vinyl monomers can be polymerized by FRP with undemanding reaction conditions.^[29,30] To start the polymerization, an initiator is added that produces a radical species. The mechanism is detailed in figure 2.^[29] According to the kinetic of a FRP, high degrees of polymerization are reached already at low conversions, reducing the need for long reaction times.^[29] The resulting polymers typically feature quite high dispersities ($\bar{D} = 1.5\text{--}3.0$).^[31] Nonetheless, just short of half of all industrially synthesized polymers are polymerized with FRP.^[32]

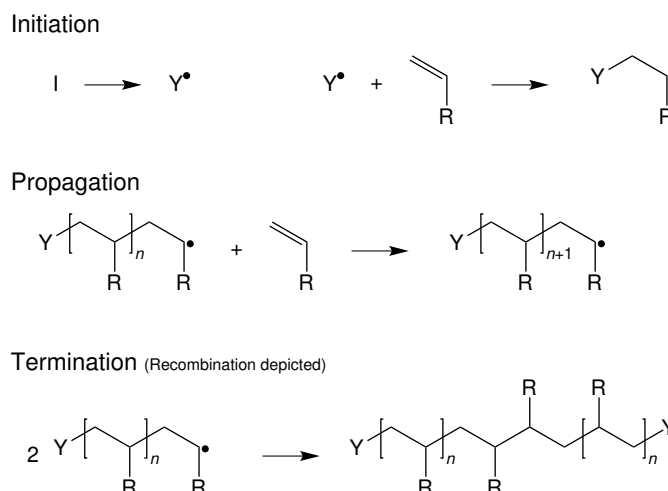


Figure 2: The mechanism of a FRP is illustrated: First, a radical initiator decomposes and produces an active radical, which attacks the double bond of a vinyl monomer. In the same fashion, the radical chain end of the growing chain can attack further monomer units. Eventually, two radicals terminate each other either by recombination or by a chain transfer reaction.

ANIONIC (LIVING) POLYMERIZATION

The anionic polymerization follows the same general reaction mechanism as the FRP, but with an anion as the reactive chain end opposed to a radical. This difference results in a fundamental change of polymerization kinetics as formally no termination reaction can occur: Two radicals will eventually react with each other, but two ions with the same charge simply repel each other.^[29] Because of the lack of termination, this type of polymerization is also named ‘living polymerization’, as first reported by Szwarc *et al.* in 1956.^[33] Anionic polymerization allows outstanding control over the molecular mass, determined by the monomer-to-initiator ratio, and growing linearly with the monomer conversion. Additionally, anionically synthesized polymers show the lowest dispersity of all polymerization methods (\bar{M} below 1.1). Another feature of the living nature of the anionic polymerization is the complete control over the end groups, enabling the synthesis of block copolymers and various other architectures.^[34] However, the anionic polymerization demonstrates an extremely high sensitivity towards residual impurities, has low tolerance for functionalized monomers, and limits the use of reagents and solvents.^[29]

REVERSIBLE-DEACTIVATION RADICAL POLYMERIZATION (RDRP)

In an effort to combine the excellent control and living nature of anionic polymerization with the simple reaction setup, undemanding reaction conditions, and high tolerance of FRP, multiple RDRP techniques have been developed.^[30] The general aim of these polymerization methods is to decrease the likeliness of termination reactions. As the termination of radical species can never be completely avoided, RDRPs are not truly living.^[35] Nonetheless, low dispersities (\bar{D} below 1.5) are achieved, the degree of polymerization grows linearly with the conversion, and the control over endgroups allows the synthesis of block copolymers and other complex topologies.^[36]

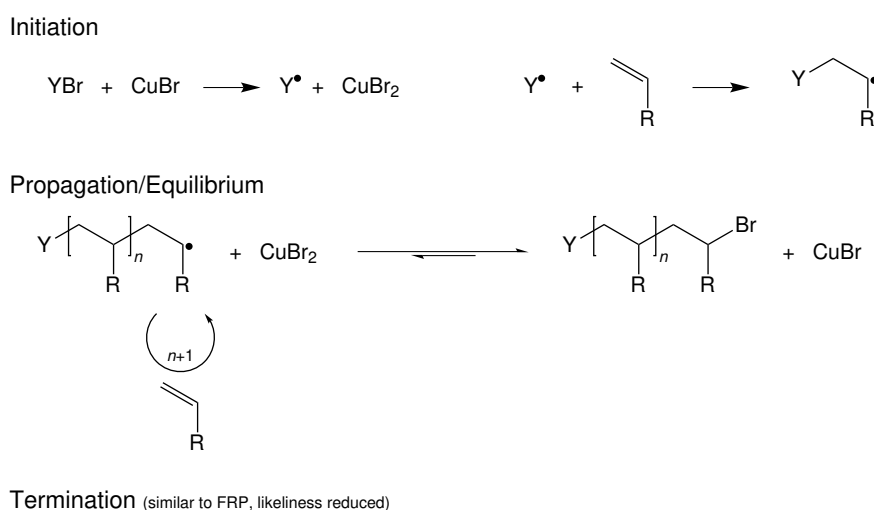


Figure 3: The mechanism of an ATRP is illustrated: Initially, the redox reaction between copper(I) bromide and an alkyl halide produces a radical, which can initiate radical chain growth. The active chain is in equilibrium with a dormant macromolecular halide by the reverse reaction. It is crucial for the rate of deactivation to be orders of magnitude bigger than the rate of activation to ensure that most chains are in the dormant state and the radical concentration is kept low. This reduces the likeliness of radical termination reactions. The mechanism is exemplary demonstrated with copper bromide, but different halides and transition metal catalysts have been reported as well.^[37]

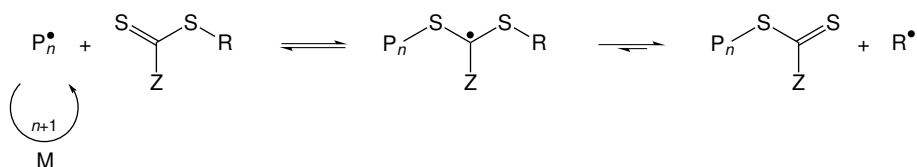
There are two different approaches to reduce termination: In the first, an equilibrium between a dormant and an active species lowers the concentration of free radicals

drastically, which lowers the probability of termination, but also decreases the polymerization speed.^[38] Atom transfer radical polymerization (ATRP) as described almost independently by Matyjaszewsky and Sawamoto in 1995 is demonstrated in figure 3 as example for this type of RDRP.^[39,40] The second type of RDRP forces a continuous radical chain transfer between all chains, which is favored over the termination reaction.^[41] The most prominent representative of this type, reversible addition-fragmentation chain transfer (RAFT) polymerization, was discovered by Rizzardo and Moad in 1998 and is described in figure 4.^[42,43]

Initiation



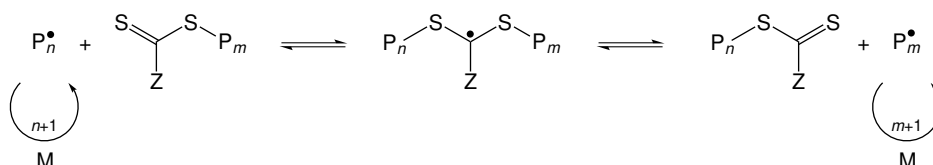
Chain Transfer



Reinitiation



Chain Equilibrium



Termination (similar to FRP, likelihood reduced)

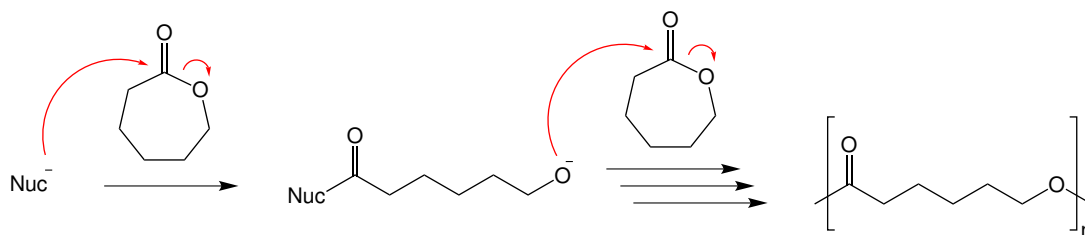
Figure 4: The mechanism of a RAFT polymerization is illustrated: RAFT polymerizations are initiated by conventional radical initiators similar to FRP. However, a chain transfer agent (CTA) transfers the active radical to its leaving group R, which can reinitiate further chain growth. Eventually, all growing chains will be in an equilibrium with all other growing chains *via* the CTA. This allows uniform growth for all chains and reduces termination reactions. It is vital for the stabilizing group Z of the CTA to be suitable for the respective monomer.^[43]

2.1.3 Ring-Opening Polymerization

Besides the two big classes of polymerizations, ring-opening polymerizations (ROP) are sometimes counted as their own third class. From a mechanistical point of view, most ROPs classify as chain-growth polymerizations. However, there are more complicated mechanisms, exceptions, and polymerizations involving activated monomers, all of which renders a generalization difficult.^[44] This problematic nature can be easily demonstrated by comparing the mechanisms for the anionic ROP (AROP) of ϵ -caprolactone and of ϵ -caprolactam, with both being shown in figure 5. Despite this discussion, the resulting polymers after ROP often resemble polymers synthesized by step-growth polymerizations with functional moieties directly in the polymer backbone.^[44]

All polymerizations described prior to ROP feature a chemical change between the monomer and the polymer, like the conversion from double bonds to single bonds, or the conversion from carboxylic acids and alcohols to esters. That is not the case for ROPs. Instead, the driving force is solely the ring strain of the cyclic monomer. This in turn also means that strain-free rings generally do not polymerize.^[44] Additional rotational degrees of freedom when going from cyclic rings to linear polymers might give another driving force in some cases.^[45] Another important consideration for ROPs is that in a lot of cases the ring-opening is in an equilibrium with a ring-closing depolymerization. The result is a considerable influence of monomer concentration and temperature on the achieved conversion of the polymerization.^[46]

Chain-Growth Mechanism



Activated Monomer Mechanism

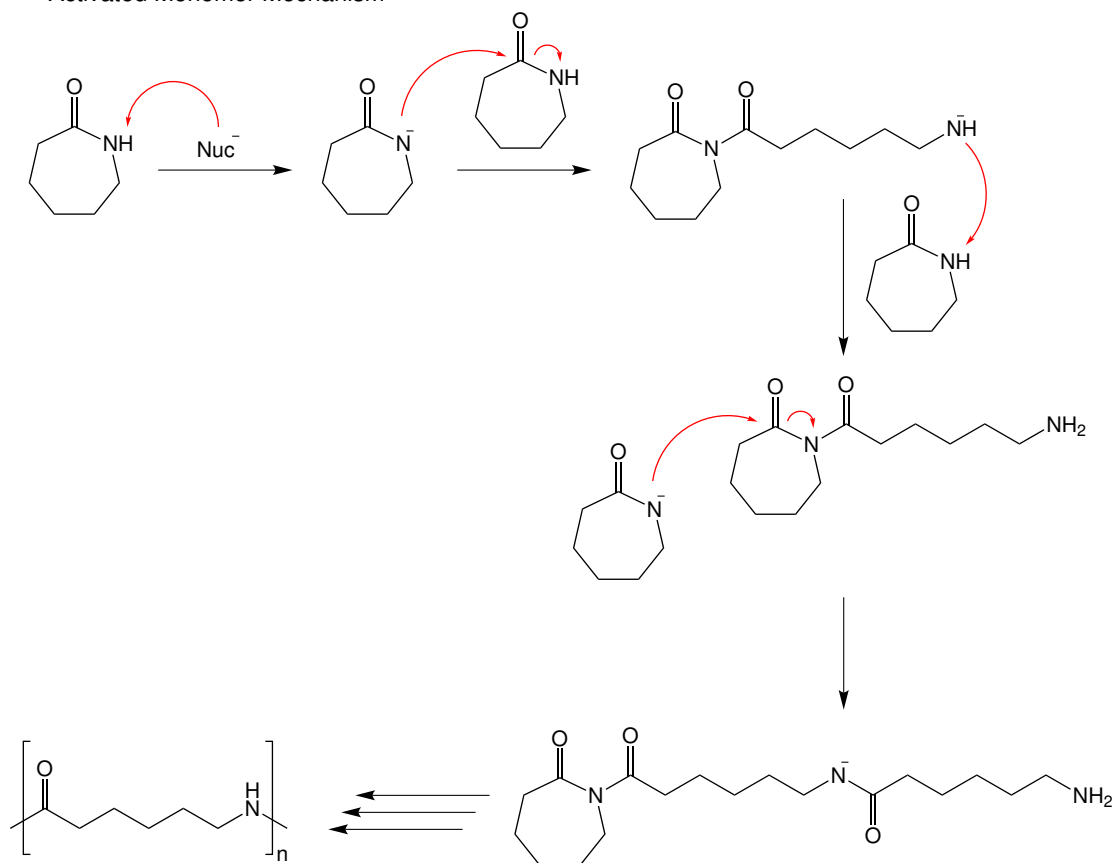
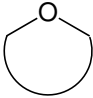
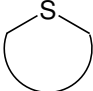
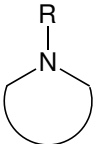
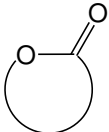
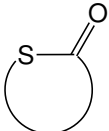
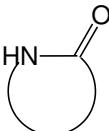
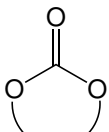
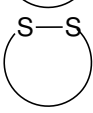
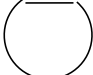


Figure 5: The AROP of ϵ -caprolactone follows a chain-growth mechanism: An anion attacks the monomer nucleophilic and opens the ring. The new chain end is an anion once again that can attack the next monomer. This mechanism is a nucleophilic attack of the propagating chain end to a monomer. On the other side, the AROP of ϵ -caprolactam follows an activated monomer mechanism: The initiating anion deprotonates the monomer, which can then attack another monomer nucleophilic. The chain end of the opened monomer deprotonates a new monomer that can then attack a polymer chain. This mechanism is a nucleophilic attack of an activated monomer to the polymer chain end.^[46]

2 Theoretical Background

Beyond the aforementioned AROP, there exist radical ROP (RROP) and cationic ROP (CROP) as well, which differ mostly in the type of active species and the reactive monomers. A fourth quite common type of ROP relies on metathesis chemistry, the ring-opening metathesis polymerization (ROMP).^[44] Table 1 demonstrates a selection of monomers for ROP.

Table 1: Overview over a selection of typical cyclic monomers and their usual ring-opening polymerization mechanism (adapted from literature^[45]).

name	structure	ring size	mechanism
ether		3–5, 7	CROP, AROP
thioether		3, 4	CROP, AROP
amine		3, 4, 7	CROP
lactone		4, 6–8	AROP, CROP
thiolactone		4–8	AROP, CROP
lactam		≥4	AROP, CROP
carbonate		6–8, ≥20	AROP
disulfide		≥8	RROP
olefin		4, 5, 8	ROMP

2.2 Post-Polymerization Modification

The functionalization of polymers after their polymerization is another potent tool for polymer chemistry.^[47] This process allows the synthesis of a wide variety of materials, some of which would not even be accessible by the direct polymerization of a respective monomer.^[48,49] The usage of post-polymerization modification reactions even traces back to a time before polymers themselves were an established concept. One such example would be the hardening of natural rubber by crosslinking with sulfur in the vulcanization process described by Goodyear and Hancock in 1839.^[50]

In a more modern sense, it is vital for post-polymerization modification reactions to exploit highly efficient chemistries, ideally with quantitative conversions. This is considered necessary, since the separation of fully functionalized macromolecules from only partially functionalized ones is in most cases simply impossible. This renders click chemistry the ideal choice for post-polymerization modification approaches,^[51,52] but also other highly efficient reactions like transesterifications and amidations of active ester moieties (*N*-hydroxysuccinimide, pentafluorophenyl) have been successfully employed.^[47,53]

The term click chemistry was coined by Sharpless in 2001 and asks for a number of criteria a reaction has to satisfy: Click chemistry has to provide nearly quantitative yields, by-products have to be the exception and then have to be easily removable without chromatographic methods, the reaction conditions have to be mild and especially include an insensitivity towards oxygen and water, the reaction has to be specific and orthogonal to other organic reactions, and importantly the reaction has to be modular and wide of scope.^[54] Only a few reactions can be truly considered click chemistry, for instance the Huisgen 1,3-dipolar cycloaddition between azides and alkynes, the [4+2] Diels-Alder cycloaddition, the nucleophilic ring-opening reaction of small strained rings, or the addition of thiols to double bonds.^[51,55] Just this year, the very concept of click chemistry, but in particular modifications of the Huisgen cycloaddition in the copper(I)-catalyzed azide-alkyne cycloaddition (CuAAC) and the ring strain-promoted azide-alkyne cycloaddition (SPAAC) were honored with the Nobel Prize in Chemistry

to Carolyn R. Bertozzi, Morten P. Meldal, and K. Barry Sharpless.^[56] Ultimately, all of the aforementioned reactions have also found applications in the post-polymerization functionalization of polymers.^[51,52,57] Below, the thiol-ene addition is examined closer because of its relevance to this thesis.

2.2.1 Thiol-ene Addition Chemistry

The term thiol-ene addition actually encompasses two different reactions, which often are not sufficiently differentiated. Both are hydrothiolations of a carbon double bond (ene component) and yield the anti-Markownikow product.^[51] The radical thiol-ene addition is triggered by conventional radical initiators as depicted in figure 6. The resulting thiyl radical adds to the ene in a propagation step. The formed carbon radical then abstracts a hydrogen in a transfer step from another thiol, reforming a thiyl radical in the process.^[55] Typically, any terminal ene is capable of radical thiol-ene addition, whereas internal double bonds react too slow. Electron-rich or ring-strained double bonds react much more readily than electron-poor or conjugated ones (norbornene > vinyl ether > alkene > allyl ether > acrylate > maleimide > methacrylate > styrene > conjugated diene).^[51,55]

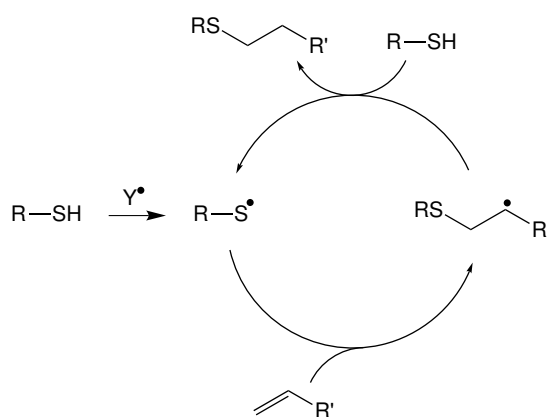


Figure 6: The mechanism of a radical thiol-ene addition is illustrated: A radical initiator abstracts a hydrogen from the thiol to form a thiyl radical, which then attacks the ene component in an anti-Markownikow addition. Following that, another radical transfer takes place to form the thiol-ene addition product and another thiyl radical that triggers the cycle again.

Opposed to this, the second variant is often called thiol-Michael addition, which is a catalytic process. The initiation is triggered either in an alkaline mechanism by tertiary amines or in a nucleophilic mechanism by phosphines or primary amines.^[58] In that regard, the mechanism between the two variants is similar, with the thiol-Michael addition focusing on an anion instead of the radical.^[59] Importantly, an electron-deficient ene (e.g. maleimide, methacrylate, acrylate) is required to stabilize the anion in the process.^[51,59,60]

Although thiol-ene and thiol-Michael additions are usually both mentioned under the term of click reactions, some issues have to be acknowledged. In a broad sense both meet the required criteria like high yields, mild reaction conditions, the formation of a single regioselective anti-Markownikow, insensitivity towards oxygen and water and a broad versatility of thiols and enes.^[59,60] However in a radical process, side reaction can never be excluded completely: homopolymerization of the ene-component and disulfide formation by radical-radical termination may occur. The anions in the thiol-Michael addition have no terminating capabilities by coupling, resulting in this reaction being much closer to the ideal click criteria (especially for maleimides as ene component).^[60]

Nonetheless, both reactions are used as powerful synthetic tools in polymer chemistry. They find application in the direct formation or crosslinking of essentially perfect networks. One of their most widespread utilization is the rapid sidechain or endgroup post-polymerization modification^[51,55,60] or the surface modification.^[61] Beyond that, click thiol-Michael chemistry allows for the synthesis of copolymers from telechelic polymers or for a simple high-yield bioconjugation (e.g. with the thiol in cysteine).^[62] Another related process is the radical thiol-yne addition. This is a radical addition of a thiol to an alkyne and leads to a vinylthioether. This product is typically still reactive to perform a subsequent thiol-ene addition. The addition of two thiols to a single functionality is useful for the synthetic route of multifunctional compounds,^[63] hyperbranching polymers and dendrimers.^[64]

2.3 Lithium-Ion Batteries

The commercialization of the first rechargeable lithium-ion battery (LIB) in 1991 initiated a revolutionization of our world. In particular, the market for portable electronic devices, like mobile phones and laptops, experienced a never before seen upsurge.^[65] Since then, the demand for batteries only continued to grow and is expected to further explode in the future.^[1,66] LIBs offer many advantageous properties like high voltage and high energy density, while being fairly light weight and providing a longer lifespan compared to other battery systems.^[4] In 2019, the outstanding importance and impact of LIBs were honored by awarding the Nobel Prize in Chemistry to John B. Goodenough, M. Stanley Whittingham, and Akira Yoshino for their contributions in the development of this technology.^[67] However, the limited nature of fossil fuels constantly drives and necessitates a push towards renewable energy sources. In turn, this increases the demand for the fast and efficient storage of electrical energy and requires continued innovation and improvements.^[2,3]

At its core, a battery is a device that converts chemically stored energy into electrical energy. A battery cell consists of a negative electrode called anode, a positive electrode called cathode, and an electrolyte between them (figure 7). The difference in chemical potential between the electrodes triggers a redox reaction. As the electrolyte is an electrical insulator, the electron flow from the anode to the cathode is forced through an external circuit providing power. At the same time, the electrolyte allows ion transport within the cell, ensuring that electroneutrality is maintained. In a rechargeable battery (also called secondary battery), this process is reversible by applying a voltage in the opposite direction.^[4,68] Current commercially available LIBs employ lithium transition metal compounds as cathode materials, like LiCoO_2 (LCO), LiMn_2O_4 (LMO), LiFePO_4 (LFP), or $\text{LiNi}_x\text{Mn}_y\text{Co}_z\text{O}_2$ (NMC), while the anode consists of lithiated graphite.^[4,6] State-of-the-art electrolytes are based on lithium salts dissolved in liquid polar organic solvents, typically mixtures of small carbonates like ethylene carbonate, propylene carbonate, or dimethyl carbonate.^[4,6]

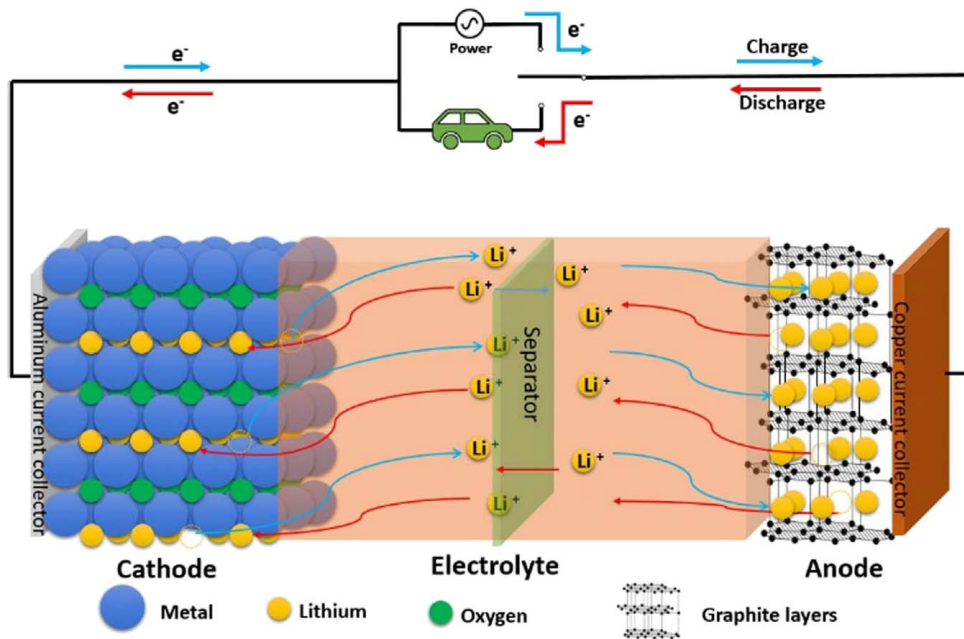


Figure 7: The working principle of a LIB is depicted as a schematic (image taken from literature^[69], with permission from Elsevier).

Despite the massive success story of LIBs, multiple important considerations remain, especially in light of their approaching large-scale commercialization in the automotive industry.^[65,68] Electric vehicles will require battery cells with higher energy densities in the future.^[5] One potential approach is to replace the lithiated graphite anode with a lithium metal anode, which provides a substantially higher gravimetric specific capacity (around one order of magnitude).^[16,70] However, conventional liquid electrolytes are incompatible with lithium metal anodes due to the formation of an unstable solid electrolyte interphase (SEI). Furthermore, lithium ions deposit in a non-uniform way on a lithium metal anode. This leads to the formation of what is referred to as lithium dendrites, which will continue to grow until they reach through the complete cell, eventually resulting in short circuit as illustrated in figure 8.^[71] Another relevant aspect are the safety hazards originating from liquid electrolytes. They are volatile and flammable compounds, leading to the risk of fire or explosions in case of mechanical, thermal, or electrical failure of the battery cell.^[7-9] Furthermore, the reaction of liquid electrolytes with other materials in the battery may release toxic gases under such runaway

conditions.^[72]

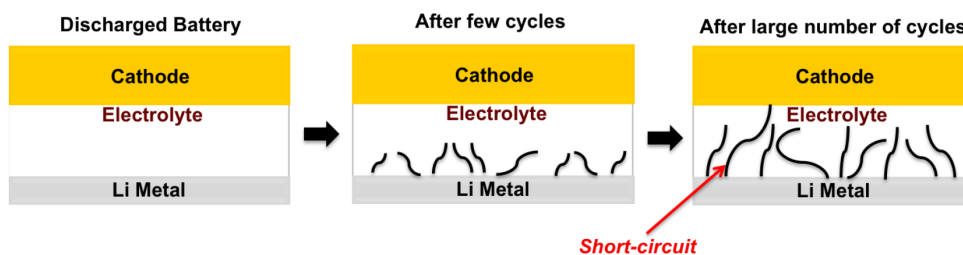


Figure 8: The cycling of battery cells with lithium metal anodes leads to the growth of lithium dendrites. Eventually, the dendrites will pierce through the electrolyte and reach the cathode. Consequently, the battery short-circuits due to the electrical conductivity of lithium metal (image taken from literature^[73]).

Most of the safety issues related to organic liquid electrolytes can be mitigated by substituting them with solid-state electrolytes. The exclusion of volatile compounds from the battery massively reduces the flammability and toxicity of the cells.^[10,11] Besides being safer alternatives, solid-state electrolytes are, as the name suggests, solids. Their mechanical strength can enable the usage of lithium metal anodes by suppressing the growth of dendrites, allowing for much higher energy and power densities.^[12–15] It also prevents the leakage of electrolyte from a punctured battery, and gives rise to more fabrication possibilities regarding the size and geometry of cells.^[74,75]

Solid-state electrolytes are still limited in their practical application, however, despite their immense potential. Namely, the performance of a battery cell is very dependent on a high ionic conductivity of the electrolyte. However, the slow kinetics in solids typically result in much lower ionic conductivities compared to conventional liquid electrolytes.^[16–18] Thus, they remain subject of exploration and research to overcome this disadvantage.

Solid-state electrolytes can be differentiated into inorganic solid electrolytes and polymer electrolytes,^[10,74] the latter of which will be described further in the following chapter.

2.4 Polymer Electrolytes

In general, polymer electrolytes can be further divided into solid polymer electrolytes (SPE) and gel polymer electrolytes (GPE). SPEs are, as the name suggests, a combination of a solid polymer and a lithium salt that is dissolved into the polymer matrix. The polymer chains coordinate the dissociated lithium ions and transport them through segmental motion and short intra- or interchain jumps between coordination sites.^[76] Thus, the flexibility of the polymer chains is a decisive property for the ion mobility in SPEs. As a direct consequence, the polymers should have large dimensions of their amorphous domains and a high degree of free volume. This also necessitates the operation of a SPE battery at a temperature well above the glass transition temperature T_g of the polymer to allow sufficient ionic conductance.^[77,78] Since there is no liquid involved, SPEs can be considered as dry systems. A distinctive advantage of polymer electrolytes opposed to other solid-state electrolytes ensues from the flexible and viscoelastic nature of most polymers. As a result of elastic deformation, they are able to compensate the volume changes of the electrodes during charging and discharging, improving contact of the electrolyte with the electrodes.^[7,79] Yet, SPEs are still faced with a low ionic conductivity, even at elevated temperatures, when compared to conventional organic liquid electrolytes.^[74]

GPEs combine the principles of SPEs and liquid electrolytes by trapping solvents or other small liquid molecules as plasticizers in the polymer. Depending on the composition, this improves the ionic conductivity either by improving the polymer mobility *via* a reduction of intramolecular interactions, or by shifting the ion transport to the liquid phase based on the movement of the swelling agent whereas the polymer only functions as stabilizing matrix.^[20,80,81] In that sense, GPEs provide better ionic conductivity compared to SPEs while maintaining a much higher mechanical stability compared to liquid electrolytes. However, the integration of liquids into the polymer lowers the mechanical properties and raises the safety concerns established for liquid electrolytes.^[69] For this reason, ionogels using ionic liquids with low volatility as plasticizer for GPEs are regarded as a promising development.^[82]

The subsequent two sections will present and discuss polymers in their use as SPEs: poly(ethylene oxide) (PEO) and polycarbonates (PC).

2.4.1 PEO as Polymer Electrolyte

The research interest in polymer electrolytes arose from the work of Wright *et al.* in the mid-70s. They discovered the ion conductance of alkali metal ions in poly(ethylene oxide) (PEO).^[83,84] The application of PEO in a lithium metal battery was successfully demonstrated by Armand *et al.* only a few years later.^[85–87] Since its inception as polymer electrolyte, PEO continues to be the most examined polymer matrix for lithium ion conduction^[19,88,89] with an ever increasing amount of in-depth studies and reviews.^[81,87,90–95] Beyond that, PEO-based electrolytes are the sole commercially employed electrolyte for any solid-state batteries so far. The Bolloré group introduced their lithium-metal polymer (LMP) battery to the automotive market in 2011, which features a lithium metal anode, a LiFePO_4 (LFP) cathode, and PEO as SPE at an operating temperature between 60 °C and 80 °C.^[21–23]

The research focus on and the commercial application of PEO is a consequence of its multitude of beneficial features: It has good chain flexibility following from its low T_g , great solubilizing properties for conductive lithium salts *via* a multidentate chelating coordination (see figure 9), high chemical stability, especially a remarkable electrochemical stability against lithium metal, low costs compared to other SPEs, and a facile processability.^[19,20] As stated above in general for SPEs, the coordinated lithium ions can perform jumps between coordination sites within one PEO chain (intrachain hopping) or to a different chain (interchain hopping). These effects have a very short range, however. The main portion of the ionic conductivity of PEO is dependent on the mobility of the PEO chains, allowing the ions to move longer distances with the chain and facilitating the aforementioned hopping mechanisms.^[19,20,96]

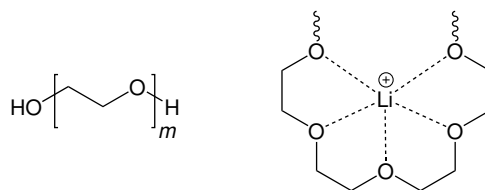


Figure 9: The chemical structure of poly(ethylene oxide) (PEO) is shown. Additionally, the chelating polyether coordination between the lithium cation and the PEO backbone is depicted. According to calculations and simulations, four to six oxygen atoms participate in the coordination of a single lithium ion.^[94,97]

Unfortunately, PEO also is a semicrystalline polymer with comparatively high crystallinity (75–80 % at room temperature).^[98] The formation of crystalline domains inhibits the chain segmental motion to a large degree, leading to a massively reduced ion conductivity of PEO below its melting point (65 °C).^[19,99,100] For instance, a SPE made from PEO and lithium bis(trifluoromethanesulfonyl)imide (LiTFSI) only achieves an ionic conductivity of around 10^{-3} – 10^{-4} mS cm⁻¹ at ambient temperatures.^[101] This is four orders of magnitude below the ionic conductivity of liquid electrolytes and three orders of magnitude below the general aim of 0.1 mS cm⁻¹ for SPEs.^[93,100]

Various optimization strategies have been proposed to reduce or remove the crystallinity of PEO and thereby improve the ionic conductivity at lower temperatures. One approach is adding conductive or non-conductive materials to the PEO electrolyte to restrict the neat chain alignment, such as plasticizers,^[102–104] nanofillers,^[105–107] or blending with another polymer.^[108,109] The second, chemically more sophisticated approach is based on the chemical modification of the polymer structure to interrupt chain alignment and crystallization, for instance via crosslinking.^[110–113] Of particular interest in this regard are polymers with grafted PEO sidechains. The crystallinity in those is efficiently reduced by anchoring one chain end to the backbone. A selection of PEO-grafted structures is depicted in figure 10. These polymer electrolytes typically reach ionic conductivities of 10^{-1} mS cm⁻¹ at ambient temperatures.^[114]

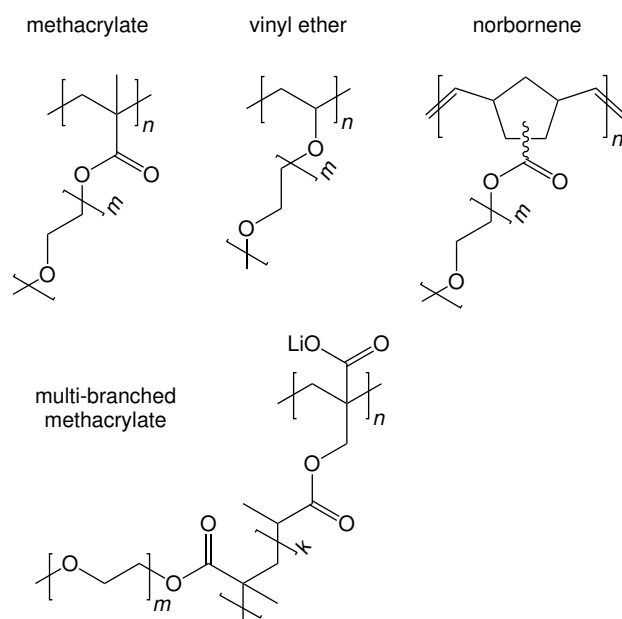


Figure 10: Some examples of PEO-grafted structures from literature are depicted: methacrylates,^[115,116] vinyl ethers,^[117,118] norbornenes,^[116] and a multi-branched methacrylate.^[119]

Unfortunately, the reduced crystallinity results in a tradeoff in mechanical properties for the polymer electrolyte. Fully amorphized PEO-based materials, like the aforementioned, are typically only highly viscous fluids due to the low T_g of PEO at around $-65\text{ }^\circ\text{C}$.^[19,120] On the other side, a system with a higher T_g and therefore higher mechanical stability results in reduced ionic conductivity. It is necessary to tune both properties independently from each other to yield a SPE with both suitable mechanical stability to eliminate dendrite growth and suitable ionic conductivity at mild temperatures.

The introduction of a non-polar block with high T_g connected to the polar PEO block was showcased to be able to achieve such properties.^[121,122] In these microphase-separated block copolymers, the polar PEO domain contributes the ion conductance whereas the non-polar domain provides mechanical stability.^[123,124] Although their mechanical stability is massively improved, they still suffer the loss of some ionic conductivity to about $10^{-1}\text{ mS cm}^{-1}$ at $60\text{--}70\text{ }^\circ\text{C}$.^[125–129]

2.4.2 Polycarbonates as Polymer Electrolytes

Besides PEO, multiple other polymer host materials for lithium ion transport have been proposed and investigated.^[20,130,131] Akin to the structure of small organic carbonates employed as conventional liquid electrolytes, polycarbonates have attracted the most research interest within these non-PEO SPEs.^[20] They are able to coordinate the lithium cation mostly *via* their carbonyl oxygen and the resulting ion mobility is directly linked to the chain flexibility of the polymer matrix, similar to many other SPEs.^[78,132] The well-known engineering polycarbonates typically bear aromatic groups in the mainchain (such as materials based on bisphenol-A). Thus, their high T_g and slow polymer dynamics lead to very limited ionic conductivities.^[133]

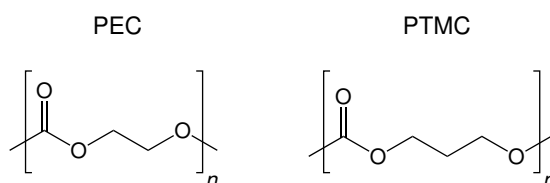


Figure 11: The chemical structures of the aliphatic polycarbonates PEC and PTMC are shown.

Instead, most research focuses on one of two aliphatic polycarbonates: Tominaga *et al.* pioneered poly(ethylene carbonate) (PEC),^[134,135] while Mindemark *et al.* demonstrated poly(trimethylene carbonate) (PTMC).^[136,137] Both structures are contained within figure 11. PEC is typically not polymerized from ethylene carbonate, as five-membered cyclic carbonates require harsh conditions during ROP,^[138] but is usually formed from the copolymerization of CO₂ and an epoxide.^[134] Opposed to that, trimethylene carbonate (TMC) is a six-membered cyclic carbonate and can be easily polymerized in a ROP with high control. Additionally, this synthesis allows the incorporation of sidechains into PTMC.^[139]

Both polycarbonate systems are highly amorphous with low T_g (9 °C for PEC, -15 °C for PTMC)^[136,140] and their feasibility in solid-state batteries, even at room temperature, could already be successfully shown.^[141,142] Despite this, polycarbonates typically

exhibit an ionic conductivity below fully amorphized PEO at around 10^{-2} mS cm⁻¹ at ambient temperature.^[20] At the same time however, polycarbonate-based electrolytes reach lithium transference numbers t_+ close to 0.5 to 0.6 (opposed to 0.1 to 0.2 for PEO-based electrolytes), meaning a significantly higher portion of the overall ionic conductivity can be attributed to the movement of lithium ions and thus contributes to the performance of the battery.^[143–145] The high transference numbers are the major selling point for polycarbonates as SPEs and are a direct consequence from the much weaker carbonyl coordination compared to the polyether coordination in PEO.^[20] Additionally, polycarbonates display a high oxidative stability.^[136,146]

PEC (and to a lesser extent also PTMC) demonstrates a very unique property at high concentrations of lithium salt, where the T_g decreases with higher salt ratios and the ionic conductivity is increased in accordance.^[134,147] The transference number is also further increased and reaches 0.8 at 80 °C.^[135,143] This composition is known as polymer-in-salt electrolyte and it is proposed that at high salt contents ion conductance becomes possible by percolation type movement, decouples from chain segmental movement.^[135,148]

In an effort to improve the ionic conductivity of PTMC, a common strategy has become to introduce flexible sidechains. These increase the free volume in the polymer and thus reduce T_g .^[149–152] However, the improvements to the ionic conductivity are often much smaller than the lowered T_g would suggest, probably due to some form of sterical hindrance for the ion transport along the backbone.^[153] Nonetheless, functionalization of the polycarbonates can still open up possibilities for materials with tailored properties.^[150,154,155]

For instance, there have been some attempts in combining the useful properties of polycarbonates, specifically the high transference numbers, with the generally high ionic conductivity of PEO-based electrolytes. The most common strategy relies on the integration of short oligo(ethylene oxide) units into the mainchain between carbonate moieties,^[156,157] but also longer PEO units in the mainchain have been explored in-depth.^[158–160] Although polycarbonates grafted with PEO sidechains are known in the literature for application other than polymer electrolytes,^[161–164] the only studies of

PEO-grafted aliphatic polycarbonates in the context of ion conducting materials focus on just short oligo(ethylene oxide) sidechains (1–3 repeating units).^[165]

3 Motivation and Aim

Since the discovery of its ionic conductivity nearly 50 years ago, PEO continues to be the poster child of polymer electrolytes. Its multitude of advantageous properties like the low T_g , the resulting high chain flexibility, the great stability against lithium metal, and the great solubilization of lithium conductive salts have lead it to be the most studied and explored ion conducting polymer matrix. Beyond that, PEO is the sole commercially employed solid-state electrolyte for batteries with lithium metal anodes to this day. This serves to show that PEO is still relevant, even in the face of the enormous advances attained for other SPEs. Despite this, the ionic conductivity for pure PEO itself is usually quite low due to its high tendency for crystallinity, especially at ambient temperatures. Various methods are known to reduce the crystallinity for PEO, but grafting PEO sidechains to a backbone seems to be the most efficient route to suppress the crystallinity. Nonetheless, PEO-based electrolytes still suffer from a very low lithium transference number of around 0.1.

A second polymer matrix that provides outstanding properties are the class of polycarbonates, akin to the liquid organic carbonate electrolytes. Above all, they possess a lithium transference number up to 0.6. This not only means that a higher portion of the ionic conductivity actually provides a benefit during cycling, but also that a significantly lower cell polarization is build up. There have been quite some attempts in combining the useful properties of PEO and polycarbonates, but there has not been an in-depth study for PEO-grafted polycarbonates yet. As described above, the anchoring of PEO sidechains is known to suppress its crystallization efficiently, enhancing segmental mobility and thus the ionic conductivity. Furthermore, the high inherent amorphicity and chain flexibility of polycarbonates were envisioned to further facilitate ionic conductivity. The interaction between the PEO sidechains and polycarbonate backbone were important to track as well, especially in terms of potential improvements for the lithium transference number.

Ultimately, the aim of the thesis was to synthesize polycarbonates with PEO sidechains

in a systematical fashion to then correlate polymer parameters with the electrochemical performance. This structure-property correlation was intended to gain a deeper understanding and expand the portfolio of detailed studies for PEO-grafted electrolyte systems. Additionally, it allows for predictability, assessability, and optimization of this system. It was expected that the resulting solid polymer electrolyte would be lacking in terms of mechanical properties. Thus, explorations for the improvement in this regard were targeted as well.

4 Results and Discussion

4.1 Polymer Synthesis

4.1.1 Initial Considerations and Test Reactions

To allow the greatest possible synthetic control over the polycarbonate mainchain, especially in terms of molecular weight, an approach by ring-opening polymerization (ROP) was chosen as opposed to any step-growth mechanism. As briefly touched upon in chapter 2.4.2, ethylene carbonates do not readily undergo ROP or need harsh conditions due to the high stability of the five-membered cyclic carbonate structure.^[138,139] Therefore, trimethylene carbonate (TMC) derivatives as six-membered cyclic carbonates are the monomer of choice. Furthermore, it was decided to employ anionic ROP (AROP) using purely organic catalysts. This approach has the clear advantage of guaranteeing that no metal ions from reactants or catalysts remains in the polymer that might impact the ionic conductivity later down the line, if not sufficiently removed.

Unfunctional TMC was synthesized from 1,3-propanediol by ring-closing with ethyl chloroformate and purified by multiple recrystallization steps. Subsequently, this TMC was used in an AROP to gauge polymerization conditions, using 1,8-diazabicyclo(5.4.0)undec-7-ene (DBU) as the catalytic base. However, the molecular mass distribution of the resulting poly(trimethylene carbonate) (PTMC) revealed a bimodal distribution for all tested conditions. Figure 12 depicts this observation for one example. The secondary distribution was found to be always around twice the molecular mass of the main distribution. This suggested the presence of some bifunctional initiator, like water or unreacted 1,3-propanediol. According to calculations from various kinetic studies, only 0.23–0.41 % of the monomer mass consisted of this bi-initiator, which could not be detected by nuclear magnetic resonance (NMR) spectroscopy due to the low concentration. Despite these circumstances, the linear relationship between the conversion and the molecular mass clearly indicated the living nature of this polymerization.

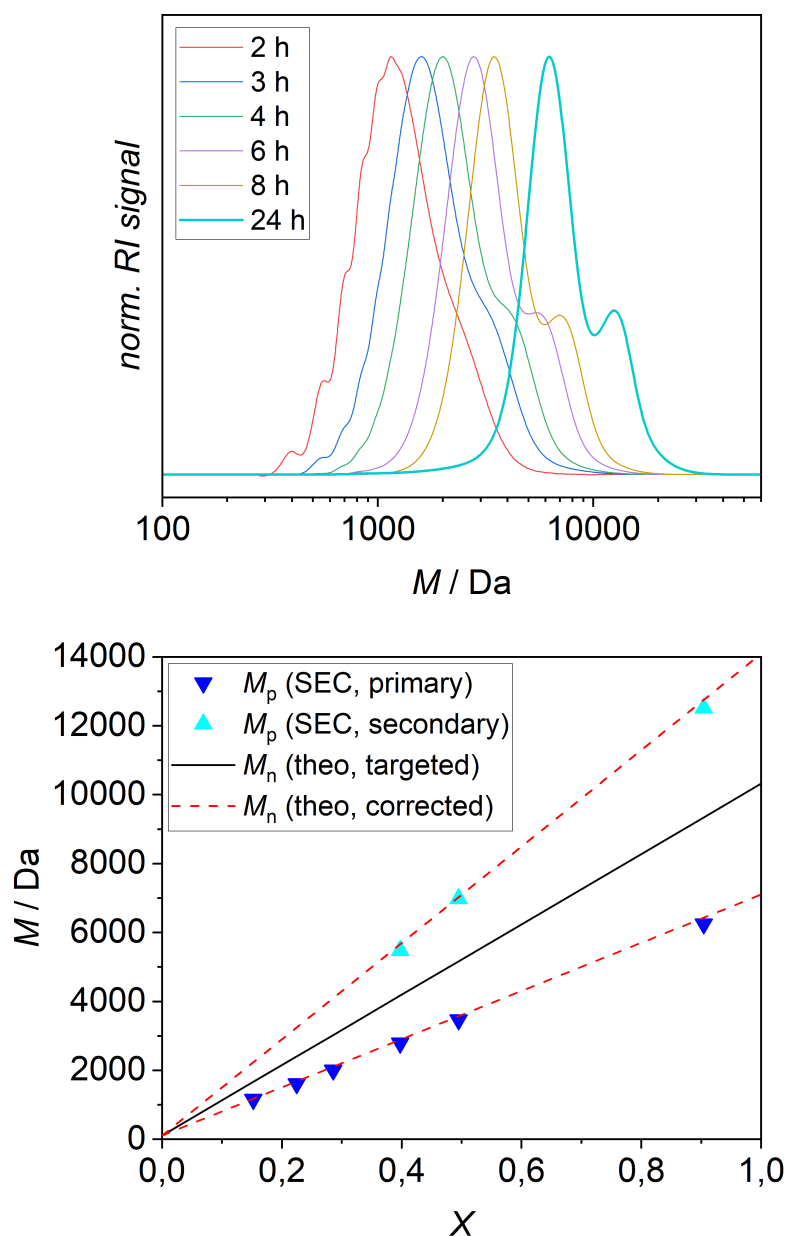


Figure 12: A kinetic study for the AROP of TMC is visualized. The top plot shows the evolution of the molecular mass distribution according to size exclusion chromatography (SEC) over time. A secondary distribution at approximately double the molecular mass is clearly visible. The bottom plot connects the peak molecular weight M_p of both distributions from SEC to the conversion X calculated from NMR. The black line describes the expected trend for the initial monomer to initiator ratio of 100:1. The red dashed line corrects this theoretical behavior with an additional monomer to bi-initiator ratio of 100:0.23 to fit the observed measurements.

Water was ruled out as bi-initiator, as the polymerization solution was always dried prior to initiation by stirring over molecular sieves or CaH_2 overnight, and the nitrogen used as inert gas was passed through a drying column with silica gel. Further recrystallization steps, as well as recrystallizations from different solvent mixtures massively reduced the yield of the monomer synthesis, while still always producing the secondary distribution. Purification of the TMC by column chromatography was not easily realized as the carbonate decomposed quickly in contact with the silica gel.

Additionally, other carbonate cyclization agents like 1,1'-carbonyldiimidazole (CDI) were evaluated, however to significantly worse results in terms of both purity and yield. Ethyl chloroformate is very efficient for the ring-closing to cyclic carbonates due to the wildly different reactivity of its two sides. The acid chloride analogue reacts quickly in an initial step at lowered temperatures, whereas the carbonic ester then completes the cyclization entropically favored from the release of ethanol at ambient temperatures. Other cyclization agents, like the aforementioned CDI, produced substantial amounts of linear side products due to incomplete cyclizations or potentially forming short linear oligomers.

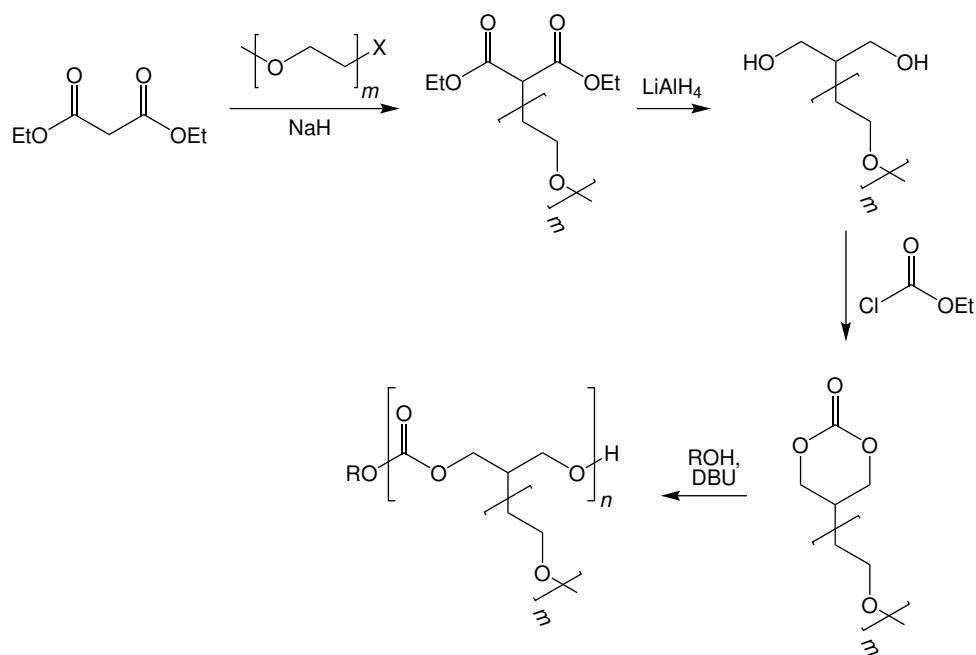


Figure 13: The abandoned initial synthesis pathway is depicted. It relied on the direct functionalization of a malonic ester using its α -acidity. Afterwards, the reduction of the malonate with LiAlH_4 would result in a PEO-functionalized 1,3-diol that could be ring-closed to a cyclic carbonate and eventually polymerized by ring-opening polymerization to yield a PEO-grafted polycarbonate.

As the polymerization of TMC was only meant as a test reaction, the reaction conditions and purification steps were not further optimized. However, these issues helped reveal inherent flaws of the initial synthesis strategy, illustrated in figure 13. The plan was to exploit the α -acidity of the 1,3-dicarbonyl from malonic esters for the functionalization, followed by the reduction to a 1,3-diol, the carbonate cyclization and the AROP. One clear advantage of this pathway is the direct attachment of the sidechain to the carbonate backbone without the need for a linker. This would have increased the comparability of this system with other PEO-grafted polymers.

However, the purity of the cyclic carbonate is of utmost importance for an AROP as just established. Typically, the cyclization reaction does not reach quantitative conversion and even very little amounts of unreacted starting material leads to side reactions. Unfortunately, attaching the PEO directly to the monomer before polymerization results in a major challenge during purification. Essentially, the purification would require the

exhausting, if not impossible separation of PEOs with only differing endgroups. Another more practical reason to abandon this route is the need to complete the whole synthesis for every single sidechain. Ultimately, a post-polymerization modification approach was envisioned to achieve the desired PEO-grafted polycarbonate architectures which is detailed in the following chapters.

4.1.2 Updated Synthesis Pathway

The direct functionalization of the polycarbonate after polymerization avoided the obstacles described above, but in turn demanded a very efficient reaction to allow complete conversion. Further requirements had to be met for the chemistry of choice to be suitable: The functional moiety on the side of the polycarbonate should not interfere with the carbonate cyclization or the AROP. Additionally, it was important for the reaction to be neither acidic or basic, nor nucleophilic to ensure no degradation of the polycarbonate backbone would occur during the functionalization. Similar to the reason for choosing AROP, the post-polymerization functionalization also should avoid metal-containing catalysts. Another vital consideration was for the moiety that was left after the grafting to be as unfunctional and small as possible to keep its influence on the battery performance to a minimum. Lastly, it was necessary for the reactive group at the PEO chain end to be available from a facile synthesis with full conversion for the same reasons as described above, or alternatively be commercially available and affordable.

Radical thiol-ene addition meets all the aforementioned conditions and was chosen for the post-polymerization functionalization. An outline for the synthesis route is depicted in figure 14. As a thiol would negatively impact the ring-opening polymerization as another potential initiation site, a polycarbonate bearing a reactive double bond was targeted. Radical thiol-ene addition works best with electron-rich double bonds.^[51,55] Hence, an allyl ether double bond was a suitable choice. Alongside its high reactivity in radical thiol-ene additions, allyl ethers also feature the clear advantage to be fairly unreactive in a competing radical homopolymerization.

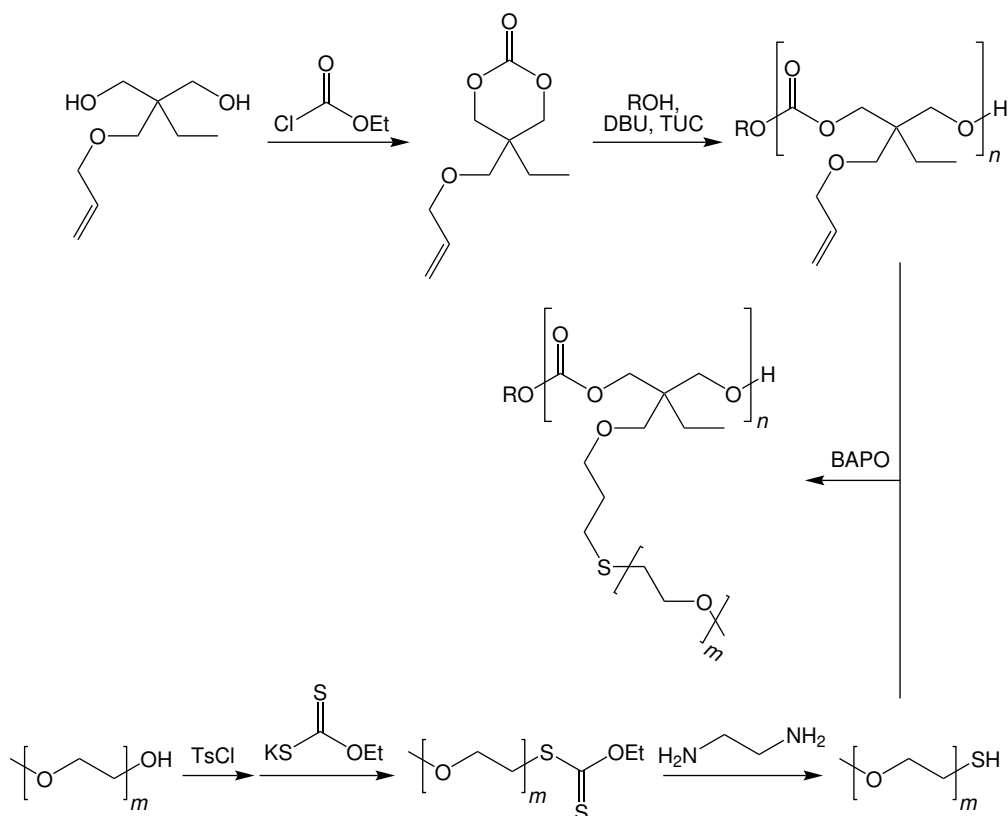


Figure 14: The synthesis route towards the intended PC-*gr*-PEO is shown. The top path outlines the synthesis of the double bond bearing, aliphatic polycarbonate PAOMEC by firstly ring closing trimethylolpropane allyl ether to a cyclic carbonate with subsequent ring opening polymerization. The lower half focuses on the endgroup modification of PEO to a thiol *via* a xanthate. Post-polymerization functionalization by radical thiol-ene addition is then used to converge both paths to the PC-*gr*-PEO.

Trimethylolpropane monoallyl ether, a 1,3-diol bearing an allyl ether moiety, is commercially available and very affordable and was ultimately chosen as the starting point. The cyclic carbonate monomer 2-allyloxymethyl-2-ethyltrimethylene carbonate (AOMEC) was synthesized following the same cyclization procedure as before. Opposed to the crystalline needles of TMC, AOMEC is a oily liquid due to the impeding nature of its two sidegroups on the crystallization. This fact allowed the purification to be realized by fine vacuum distillation. Although this demanded quite harsh conditions (boiling point of AOMEC: 135 °C at 0.5 mbar, typically heating of the feed flask above 200 °C was required), yields were much better compared to the multiple recrystallization steps

necessary for TMC.

As experienced by the PTMC test polymerizations, the purity of a cyclic carbonate monomer could not be judged by NMR spectroscopy alone, as difficult to detect trace amounts of remaining 1,3-diol, even below 0.2 %, would compete with the AROP initiation. Instead, a test polymerization of AOMECE was conducted. The SEC traces revealed two notable differences between poly(2-allyloxymethyl-2-ethyltrimethylene carbonate) (PAOMECE) and the previous PTMC. Firstly, the resulting PAOMECE displayed a monomodal molecular mass distribution, indicating that the the purity of the monomer after distillation was sufficient. Secondly, whereas the PTMC reached above 90 % conversion according to NMR despite the bi-initiation, the polymerization of PAOMECE was limited to about 50 % conversion, even at higher polymerization times (depicted in figure 15).

The conditions of an AROP also allow for the backbiting of the active chain end. Instead of attacking a carbonate monomer, the anionic chain end can attack one carbonate unit in the backbone of a polycarbonate, which results in chain degradation and the elimination of cyclic carbonates. Due to the high stability of a six-membered cyclic carbonate, backbiting usually occurs with the carbonate moiety closest to the chain end, leading to the reformation of a monomer unit. Thus, an equilibrium is formed between the ring-opening polymerization and a ring-closing depolymerization.^[46] This equilibrium is the deciding factor for the maximum conversion possible in an AROP. The sidegroups of AOMECE seem to negatively impact this equilibrium compared to TMC, potentially due to sterical hindrance.

To shift the equilibrium for the AROP of AOMECE to higher conversions, *N*-(3,5-bis(trifluoromethyl)phenyl)-*N'*-cyclohexylthiourea (thiourea cocatalyst, TUC) was synthesized in a simple one-step reaction. This cocatalyst is known to improve conversions in AROP reactions due to an additional activation of the monomer carbonyl group.^[166,167] The polymerization of AOMECE employing TUC in the same concentration as DBU improved the conversions to about 73 % as demonstrated in figure 15. The polymerization speed was also increased substantially.

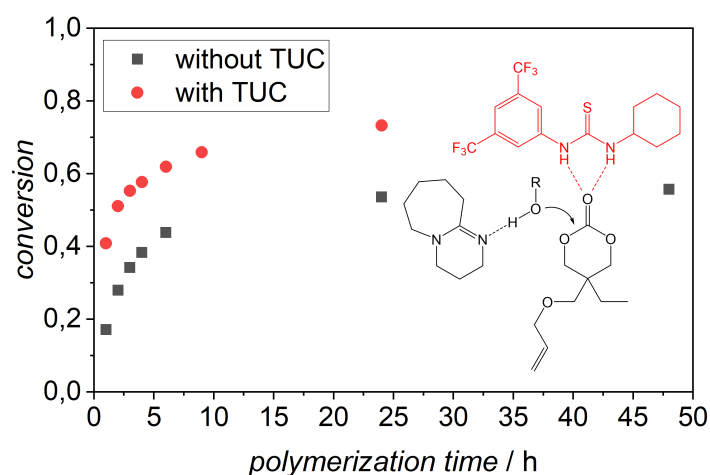


Figure 15: The influence of catalysis with TUC is shown. The polymerization of AOMEC stagnates at around 55% conversion after 24 h without TUC. The addition of TUC increases the equilibrium conversion to above 73%. The monomer activation is depicted as insert as well.

A few further kinetic studies were conducted to test the influence of various parameters. Namely, the monomer concentration was expected to be vital to the equilibrium conversion. In most ring-opening or ring-closing reactions, the ring-chain equilibrium tends to shift to the side of the ring for low concentrations and the side of chains for high concentrations. The results in figure 16 clearly reflect this expectation. A 5 M monomer solution even achieved above 90% conversion. However, the higher concentrations came at a price in practicability. The 3 M solution was already viscous to a point, at which regular readjustments of the stirring was necessary to keep it stirring. On the other side, the 5 M solution was unable to be stirred with a magnetic stirring plate and would have required a mechanical stirrer. In both cases, the low scale of the polymerizations probably helped to alleviate this issue, but upscaling would have been challenging. Hence, polymerizations were fixed to 2 M monomer concentrations, as the 73% conversion was also deemed sufficient.

Figure 16 also demonstrates the influence of the initial monomer-to-initiator ratio ($[M]/[I]$). Ideally, the equilibrium conversion should be independent from $[M]/[I]$ due to the living nature of an AROP. This is observed for a ratio of 50 (with which prior AOMEC poly-

merizations were conducted) and 25. An initial $[M]/[I]$ ratio of 100 results in a much lower conversion with only 50%. This result is only marginally improved even at much higher concentrations (although the lack of stirring due to the concentration could be responsible for this last batch as well). Judging from these results, there seems to be some form of upper limit for the maximum chain length achievable under these conditions. Nonetheless, no further optimization was investigated.

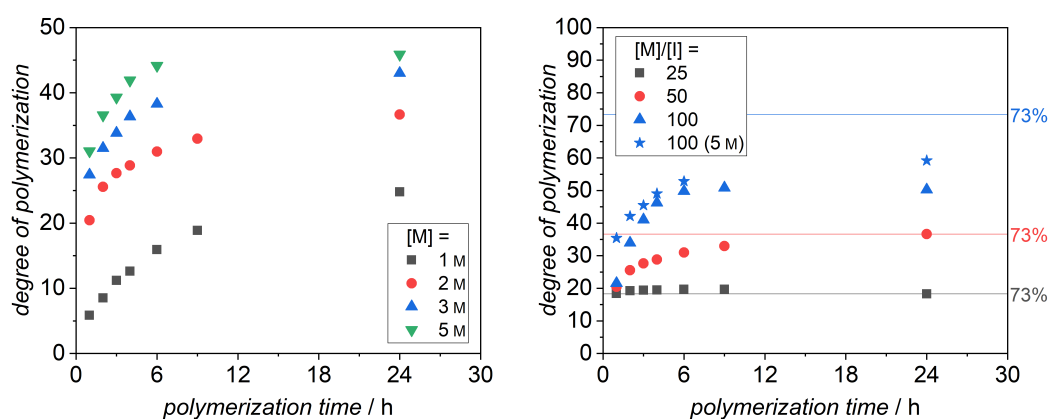


Figure 16: Further kinetic studies for the AROP of AOMEc are shown. The left plot depicts the influence of the monomer concentration. The equilibrium conversion increases with increased monomer concentration. The plot on the right side demonstrates different polymerizations with varying initial $[M]/[I]$ ratios at a 2 M monomer concentration. The two lower ratios of 25 and 50 reached the expected equilibrium conversion of 73%. For a polymerization with $[M]/[I]$ at 100, noticeably lower conversions were obtained, even at higher monomer concentrations.

As the polymerization of TMC was not satisfactorily completed, a second unfunctionalized polycarbonate was targeted to perform as a reference. For this purpose, 2-butyl-2-ethyltrimethylene carbonate (BEC) was synthesized in an identical fashion to AOMEc. BEC had a similar boiling point and was purified under identical conditions as well. Ultimately, poly(2-butyl-2-ethyltrimethylene carbonate) (PBEC) was polymerized following the established protocol to an comparable conversion of 64%.

4.1.3 Thiolation of PEO

The length of the PEO sidechain was considered one of the most important factors for the structure-property correlation, which this work aimed to establish. Prior studies and considerations that will be discussed in chapter 4.3 suggested a sweet spot between too short and too long sidechains. This length was suspected to be between a few and a few dozen repeating units (RU). The functionalization at the allyl ether of PAOMEC required a PEO with a thiol endgroup (EG). As thiol-functionalized PEOs are rather expensive and the available range for their lengths is very limited, the thiols had to be synthesized.

Four methoxy-PEO-OH (mPEO-OH) with different lengths were chosen as starting materials. When differentiation between those lengths is necessary, they will be denoted with the average molecular weight as specified by the supplier (M_n : 400 Da/550 Da/1000 Da/2000 Da). The methoxy endgroup limited all transformations to the other endgroup and avoided any bifunctionalization, which would have been difficult to separate and produced crosslinked samples as opposed to the targeted grafted structures. Additionally, the methoxy group produces an easily identifiable and sharp signal in NMR spectroscopy that can be used to quantify the success of the reactions. An overview of various pathways for the transformation of mPEO-OH to mPEO-SH is given in figure 17. As discussed earlier, it is of utmost importance for the reaction steps during the thiolation to be quantitative as the separation of PEOs with only different endgroups is nearly impossible to realize. An easy, single-step thiolation of alcohols is often reported in literature by the Steglich esterification with 3-mercaptopropionic acid. Although this might have been the fastest way towards a thiol-PEO, this method introduces an additional ester bond and increased linker distance. Both of these modifications should be avoided, especially the introduction of a carbonyl, which would compete with the carbonate moieties and the PEO for the coordination with Li^+ cations.

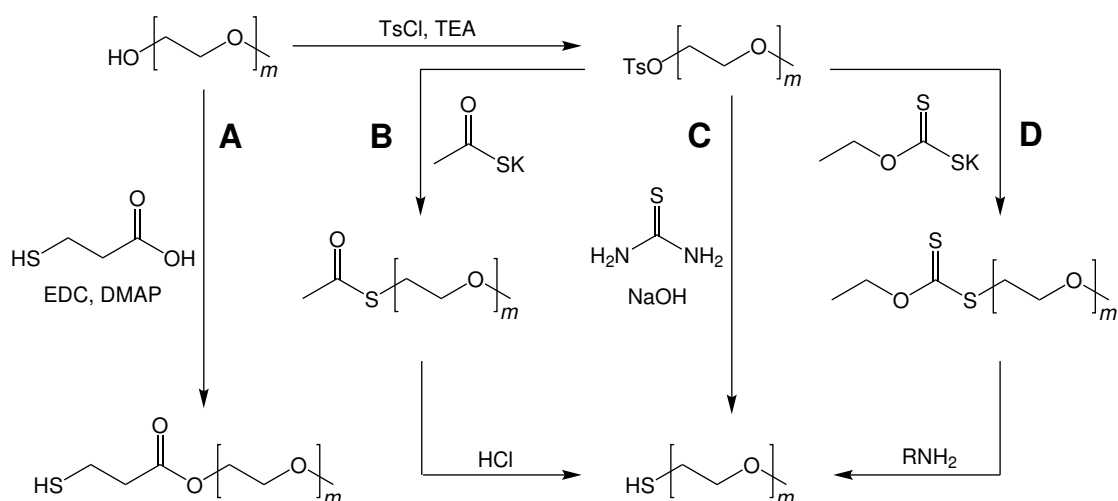


Figure 17: Various routes for the transformation of an alcohol into a thiol are given. Path A shows the one-step functionalization *via* the Steglich esterification with mercaptopropionic acid. The remaining three variants require a better leaving group, exemplary shown with a tosylate. From those, path B depicts the the functionalization with thioacetate and path C with thiourea as the two most employed techniques. The path D describes the synthesis which was ultimately decided upon: firstly the functionalization with an ethylxanthate, followed by the cleavage to a thiol by aminolysis with a primary amine.

The remaining thiolation variants require an increase in reactivity of the alcohol by exchanging it for a better leaving group. Halides are an option in that regard, but usually tosylate (*p*-toluenesulfonate, TsO^-) and mesylate (methanesulfonate, MsO^-) are the leaving groups of choice due to being more readily attached. Afterwards, a nucleophilic attack of a sulfur compound introduces a protected thiol group, which can then be liberated in a following step.

One common pathway uses thiourea as nucleophile to form an isothiuronium intermediate that is typically not isolated and directly cleaved under alkaline conditions.^[168,169] The other common pathway employs a thioacetate, which is then cleaved by either alkaline or acidic conditions.^[170–172] A clear advantage of the latter variant is the stability of the thioacetate compound. It can be prepared in a bigger batch, stored, and then cleaved to the thiol in smaller batches when needed. This avoids the oxidation of thiols to disulfides in air. In both cases, the modification requires elevated temperatures

and harsh conditions for cleavage. Furthermore, quick test reactions for both pathways revealed incomplete conversions or difficult purifications in either of the steps.

Hence, another pathway was pursued and optimized. Potassium *O*-ethylxanthate (KXEt) was employed as an alternative nucleophile (figure 17 route D). There have been reports of it being used to produce thiols or analogous compounds,^[173,174] but it is mostly used to produce CTAs.^[175,176] Nonetheless, yields for this transformation are usually very high and the reaction proceeds under mild conditions. Similarly, it was found that the recovery of the thiol from the xanthate *via* aminolysis proceeds very efficiently under ambient temperature, thus reducing side reactions and facilitating purification.

All three reaction steps, the tosylation, the xanthation, and the aminolysis, could be performed to relatively high yields (50–70 % over all steps, lowest yields for longer PEO chains). Notably, only stirring overnight or at most cooling in an ice bath during addition of reagents was required, and purification was achieved with only washing and extraction steps. The complete functionalization for the tosylation and xanthation was proven with NMR spectroscopy by comparing the signal integrals of the methoxy endgroup and the methyl groups of the respective moieties. Additionally, the absence of any signals from the previous steps demonstrated the successful purification. As is typical for any thiol, the oxidation of mPEO-SH in air to a disulfide was unavoidable. Depending on the time between synthesis and analysis, up to 30 % were oxidized, but around 10 % were more common. Similarly to the thioacetate, the functionalized mPEO-XEt could also be stored easily over long times without degradation. The mPEO-SH could then be quickly produced on demand. Alternatively, thiol samples that were stored for longer were reduced with TCEP·HCl (tris(2-carboxyethyl)phosphine hydrochloride) to a similar state as freshly prepared mPEO-SH.

4.1.4 Post-Polymerization Functionalization

A PAOMEC with 35 repeating units ($M_n = 7.1$ kDa) was synthesized in a substantially bigger batch to be used as the starting material for all further functionalizations. This

was done to increase comparability between the results. Initial test reactions of the radical thiol-ene post-polymerization functionalization were done thermally initiated using AIBN (azobis(isobutyronitrile)) as radical source. However, only partial conversion was achieved. To rule out any influence of the synthesized mPEO-SH, the thiol-ene was repeated under identical conditions with commercially available dodecylthiol, which resulted in similarly lower conversion. At the same time, a photoinitiated test reaction revealed full double bond conversion. Instead of trying to optimize the conditions for the thermal initiation, BAPO (bis(2,4,6-trimethylbenzoyl)phenylphosphine oxide, also known as Irgacure 819) was used as a photoinitiator for all thiol-ene additions. Besides reaching higher conversions, the photoinitiation was about twice as fast to reach completion, which was also easily observed by the decolorization of BAPO.

For the radical thiol-ene addition, the mPEO-SH had to always be employed in excess. Firstly, this ensured a sufficient amount of thiol despite its inevitable partial oxidation. Secondly, this served to drive the functionalization to quantitative conversion. In this specific case, a twofold excess of mPEO-SH proportional to the allyl ether double bond from PAOMEC was sufficient for most PEO lengths. The longest examined sidechain length with mPEO2000 required four equivalents of the thiol to reach complete functionalization.

Ultimately, this excess had to be removed after the successful reaction as to not falsify the ionic conductivity results. As PEO chains have a high tendency to adhere to each other, this proved to be rather difficult, and no extraction, washing, or precipitation steps were successful. In the end, purification could only be realized by dialysis with regenerated cellulose membranes. Despite the high PEO content of PC-*gr*-PEO, the solubility of this polymer in water was limited and always resulted in turbid solutions. Thus, dialysis was performed in THF. Unfortunately, the molecular weight cutoff (MWCO) for the dialysis membranes is only defined in aqueous solutions. Trial and error was necessary to determine suitable purification conditions. The lowest MWCO for which complete removal of free PEO was observed, formed a near linear relationship with the molecular mass of the PEO (MWCO: 8 kDa for mPEO400; 15 kDa for mPEO550; 25 kDa for mPEO1000; 50 kDa for mPEO2000). Typically, a dialysis time of seven

days was sufficient to remove unreacted mPEO-SH, as well as formed disulfide, but a dialysis time of thirty days was necessary for the purification of PC-*gr*-PEO2000. The success of the functionalization was proven by NMR spectroscopy. As allyl ethers do not undergo homopolymerization, the conversion of the double bond should be sufficient to judge the reaction. Still, the comparison of the methoxy endgroup from the PEO sidechain to the methyl group from the polycarbonate backbone was always monitored as well (see figure 18). The latter analysis also served to demonstrate the success of the purification by dialysis. Additionally, a uniform shift of the SEC traces towards higher molecular weights was observed, indicating that no side reactions occurred (e.g. coupling or crosslinking). Similarly, the distributions for the thiol and the disulfide disappeared after completed dialysis (see figure 19).

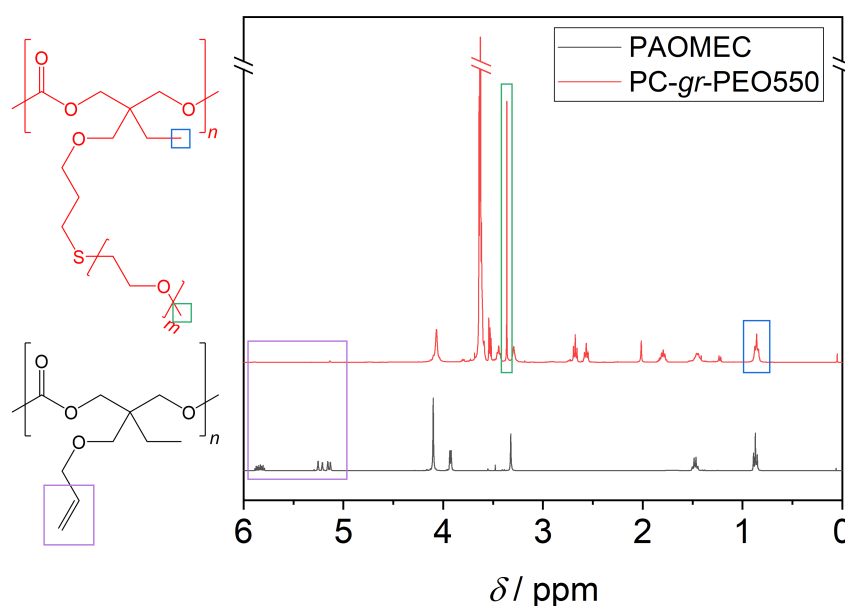


Figure 18: The quantitative functionalization of the polycarbonate was proven by ^1H -NMR spectroscopy. The radical thiol-ene addition consumed the double bond from the polycarbonate entirely (purple box). Additionally, the integrals of the methyl group from the polycarbonate backbone (blue box) and of the methoxy endgroup from the PEO (green box) are identical. The other integrals fit the expectations as well.

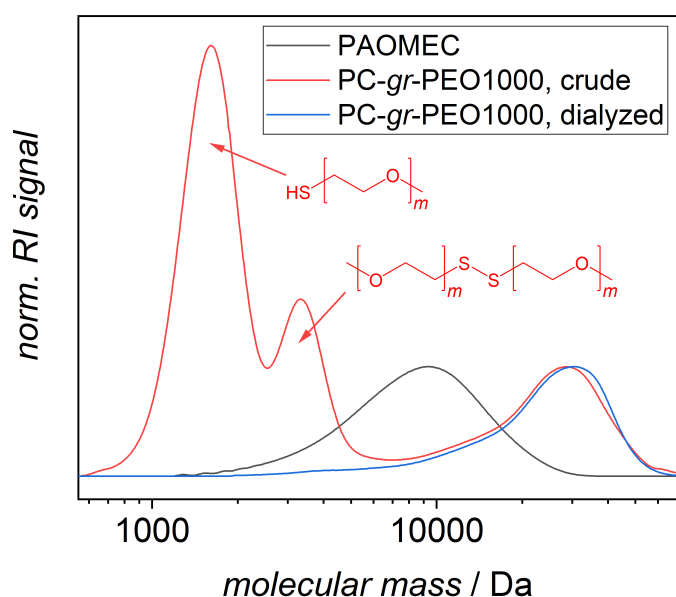


Figure 19: The SEC traces show a uniform shift after thiol-ene addition, exemplary demonstrated for PC-*gr*-PEO1000. The crude reaction mixture prior to dialysis still clearly contains unreacted mPEO1000-SH as well as formed disulfide. The dialysis successfully removed this free PEO.

Yet, the resulting values for the molecular weight of the PC-*gr*-PEO polymers according to the column calibration in SEC were much lower than expected. This was especially the case for longer sidechain lengths, as is listed in table 2. Generally, the accuracy of SEC results largely depend on the selection of a standard that is similar or ideally identical to the analyzed polymer. The considerable architectural difference between the grafted polycarbonate and the linear standards used in calibration rendered the molecular mass results unusable. Albeit the determined value was different from the truth, the results were reproducible and consistent for PC-*gr*-PEO within the same sidechain length, meaning they could be used to give an estimate for the conversion of the thiol-ene addition as well.

Due to this observation, multiangle light scattering (MALS) coupled with SEC had to be employed to validate the molecular weight of the polymers. Both of the unfunctionalized polycarbonates, PAOMEC and PBEC, were too small to produce reliable results with this technique. The results from the conventional column calibration were regarded

as more accurate due to their linear nature. In the case of the various PC-*gr*-PEO, a close agreement between the theoretical molecular weight calculated from individual degrees of polymerization and the molecular weight determined by MALS analysis was observed. These results confirm by another method that indeed full conversion is achieved during the thiol-ene addition. The large difference between the conventional column calibration and the MALS results are depicted in figure 20.

Table 2: ¹H-NMR and SEC results of the examined polymers.

polymer	$P_n(\text{PC})$	$P_n(\text{PEO})^a$	$M_{n,\text{theo}}^b / \text{kDa}$	$M_{n,\text{SEC}}^c / \text{kDa}$	$M_{n,\text{MALS}} / \text{kDa}$
PAOMEC	35	-	7.1	7.0	(8.0)
PBEC	32	-	6.1	6.2	(7.9)
PC- <i>gr</i> -PEO400	35	8.5	21.9	19.7	21.2
PC- <i>gr</i> -PEO550	35	12.5	28.1	25.9	27.3
PC- <i>gr</i> -PEO1000	35	23	44.3	26.7	44.5
PC- <i>gr</i> -PEO2000	35	48	82.8	32.5	81.4

^a calculated by ¹H-NMR integrals, ^b calculated from individual P_n , ^c calibrated using PMMA standards

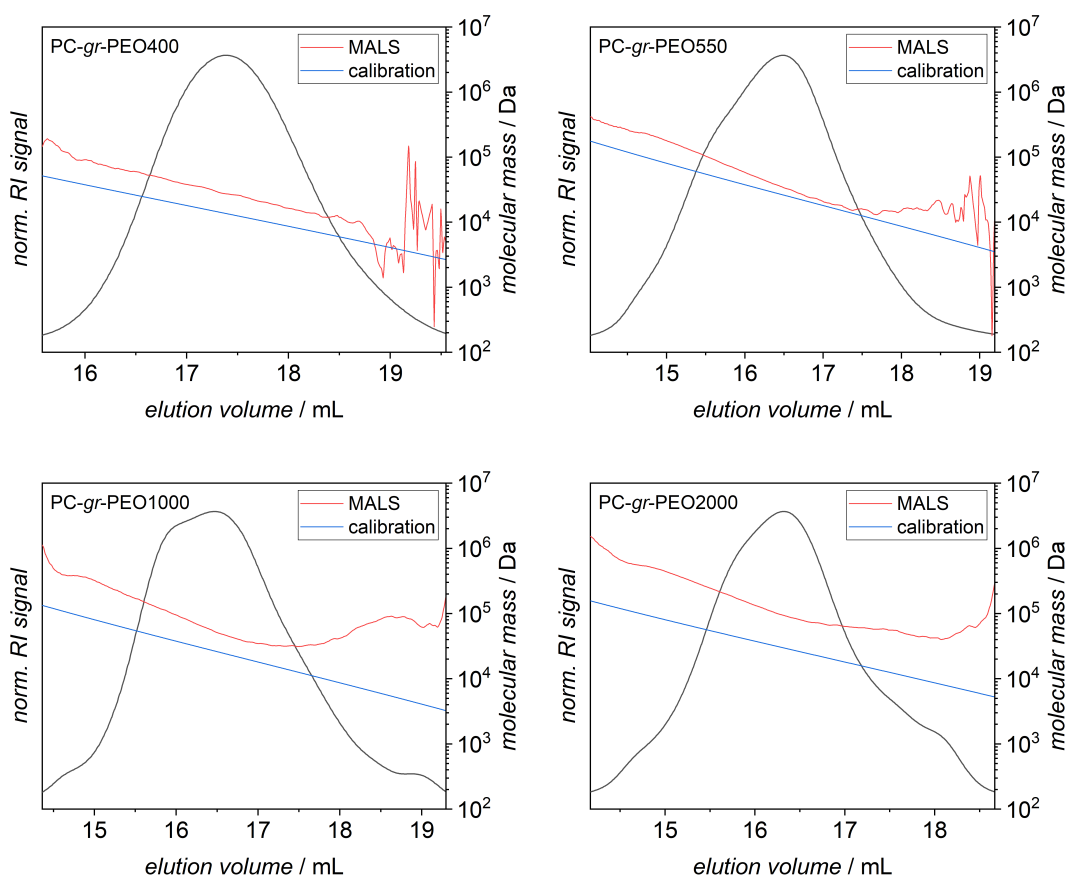


Figure 20: The results from MALS are compared to the conventional column calibration with PMMA standards. In all cases, the MALS determined a molecular mass noticeably above the SEC, which was much closer to the expected value calculated from NMR spectroscopy.

4.2 Thermal Characterization

The mechanism of ion transport in PEO relies on the mobility of the polymer chains. Following from this fact, ion conductance is only possible to a sufficient degree in the amorphous region of the polymer, whereas crystalline regions majorly reduce the ionic conductivity.^[20,96] As both glass transition temperature T_g and melting temperature T_m correlate with the mobility of polymer chains, the analysis of the thermal behavior by differential scanning calorimetry (DSC) is a vital aspect for the comprehensive evaluation of a polymer electrolyte. The results of the DSC measurements are summarized in

table 3 and the traces for one exemplary series of polymers is plotted in figure 21 (on page 45).

Table 3: Thermal properties of the examined polymers as determined by DSC measurements, as well as a comparison with pure PEO.

polymer	$T_g / ^\circ\text{C}$	$T_m / ^\circ\text{C}$	$\Delta H_m / \text{Jg}^{-1}$	mPEO of respective length			red. cryst. ^b
				$T_g^a / ^\circ\text{C}$	$T_m / ^\circ\text{C}$	$\Delta H_m / \text{Jg}^{-1}$	
PAOMEC	-42	-	-				
PBEC	-33	-	-				
PC- <i>gr</i> -PEO400	-61	-3	0.2	-50	0	82.2	99.8 %
PC- <i>gr</i> -PEO550	-36	15	73.1	-43	15	128.1	43.0 %
PC- <i>gr</i> -PEO1000	-10	33	89.4	-34	34	131.8	32.2 %
PC- <i>gr</i> -PEO2000	-6	45	103.7	-25	52	163.0	36.4 %

^a taken from literature^[177], ^b reduction of crystallinity calculated by ratio of ΔH_m before and after functionalization

The unfunctionalized PAOMEC already features a relatively low T_g of -42°C and showed no melting transition. This was expected and indicative of the high chain flexibility and amorphicity for which aliphatic polycarbonates are known.^[150] Similarly, PBEC also only featured a T_g at -33°C .

The post-polymerization functionalization of PAOMEC with mPEO-SH of different lengths resulted in both a shift in T_g and the emergence of a melting point T_m . The T_g of PC-*gr*-PEO is strongly dependent on the length of the PEO sidechain. This behavior is similar to the trend in T_g for pure PEO of similar length.^[177] Besides PC-*gr*-PEO400, the samples showed a T_g above the T_g of pure PEO of the same chain length. This effect can probably be attributed to the additional restraint of the grafting points which slightly lowers the mobility of the sidechains compared to free PEO. On the other side, the T_g of PC-*gr*-PEO400 was found to be below the T_g of mPEO400. Typically, the crystallinity of a polymer restricts the free movement of the chains and consequently also increases the T_g . As PC-*gr*-PEO400 demonstrates nearly a complete suppression of crystallization, this effect is absent for this shortest examined sidechain, resulting in an overall reduction of T_g .

Whereas T_g correlates with the chain mobility, T_m is the manifestation of the crystallinity

of a polymer. As PEO is a highly crystalline polymer,^[98] it is not surprising to see that the PEO-grafted polycarbonates still featured melting points. These were positioned at nearly the same values as the T_m of pure mPEO, with a slightly bigger deviation for PC-*gr*-PEO2000. However, it has to be noted that the area of the melting peak for the grafted polymers is considerably lower than for pure PEO. The integral of this peak is equal to the melting enthalpy ΔH_m (required energy to melt the crystalline phases) which in turn is an efficient quantification for the crystallinity. Thus, comparing ΔH_m of PC-*gr*-PEO with pure PEO of respective chain lengths allowed to calculate the reduction of crystallinity of the PEO sidechains. This shows the efficacy of the grafting approach and in turn also proves the accomplished goal to reduce the crystallization tendencies in PEO. For PC-*gr*-PEO400, this even led to a reduction of crystallinity above 99%. The effect of this approach naturally lessens with increased length of the sidechain, as those are influenced less by the constraint of their grafted chain end and have opportunity to crystallize at their free chain ends again. Nonetheless, even for the longer PEO sidechains an impressive reduction of crystallinity between 32% and 43% is achieved.

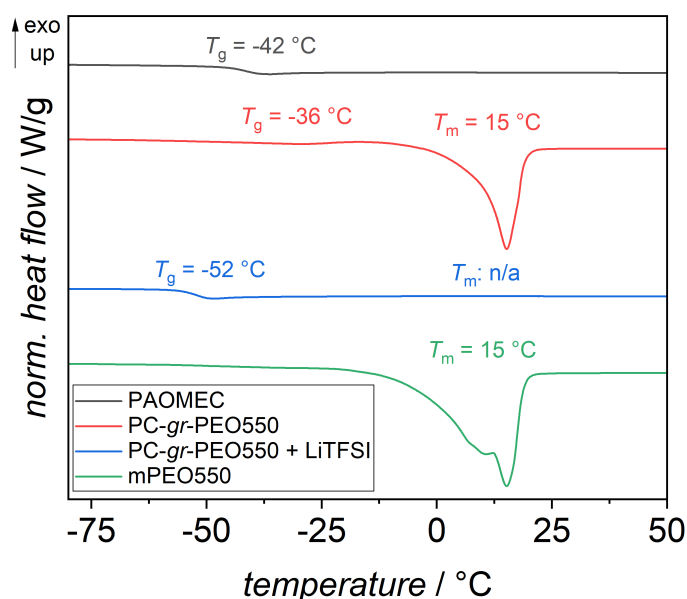


Figure 21: DSC plots for the polymer series resulting from PEO550 are given. The lower integral of the PEO melting peak after the grafting process is a direct indication for the reduction of crystallinity. Additionally, the melting peak vanishes after the addition of LiTFSI as conducting salt, showing the complete suppression of the crystallization of PEO in the polymer electrolyte. The glass transition temperature is reduced with the addition of LiTFSI suggesting an increase in chain mobility.

However, it is arguably more fruitful to discuss the thermal behavior of the polymer electrolytes as they will be employed in battery cells. Thus, PC-*gr*-PEO was mixed with LiTFSI, the state-of-the-art lithium salt for this purpose.^[19] This results in two interplaying effects: plasticizing and quasi-ionic crosslinking.^[97,117,118] The latter describes the fact that the coordination of lithium ions by the PEO sidechains inevitably also leads to mixed coordination of one lithium ion by two or more PEO sidechains, generating physical crosslinks. These additional restraints decrease the chain mobility and thus increase T_g . At the same time, this chain coordination also disrupts the neat alignment of the chains, thus further reducing crystallization. On the other hand, the TFSI⁻ anion with its bulky structure functions as a plasticizer, increasing the free volume in the polymer and resulting in a reduction of crystallinity as well. As most

of the PC-*gr*-PEO polymers prior to mixing with LiTFSI still showed crystallinity, the complete amorphization of these material should result in increased chain mobility and a decreased T_g .

Three different polymer electrolytes with $[\text{Li}^+]/[\text{O}]$ ratios of 1:10, 1:15, and 1:20 were prepared for each of the four PEO sidechain lengths and evaluated by DSC analyses, the results of which can be found in table 4. Importantly, no melting peaks was detected for any of the polymer electrolytes, even at the lowest $[\text{Li}^+]/[\text{O}]$ ratio. This proved the success in the complete suppression of crystallization for the PEO sidechains. Notably, pure PEO requires a substantially higher amount of LiTFSI between 1:6 and 1:12 to reach full amorphicity,^[178] demonstrating the efficacy of the grafting approach. For the longer sidechains, this change in material properties could even be macroscopically observed as is illustrated in figure 22.

Table 4: Thermal properties of the polymer electrolytes after the addition of LiTFSI

polymer	$T_g / ^\circ\text{C}$				$T_m / ^\circ\text{C}$
		[Li ⁺]/[O] ratio			[Li ⁺]/[O] ratio
	0	1:20	1:15	1:10	$\geq 1:20$
PAOMEC	-42	-36	-34	-34	-
PBEC	-33	-23	-36	-33	-
PC- <i>gr</i> -PEO400	-61	-43	-39	-34	-
PC- <i>gr</i> -PEO550	-36	-52	-50	-46	-
PC- <i>gr</i> -PEO1000	-10	-48	-44	-40	-
PC- <i>gr</i> -PEO2000	-6	-43	-43	-41	-

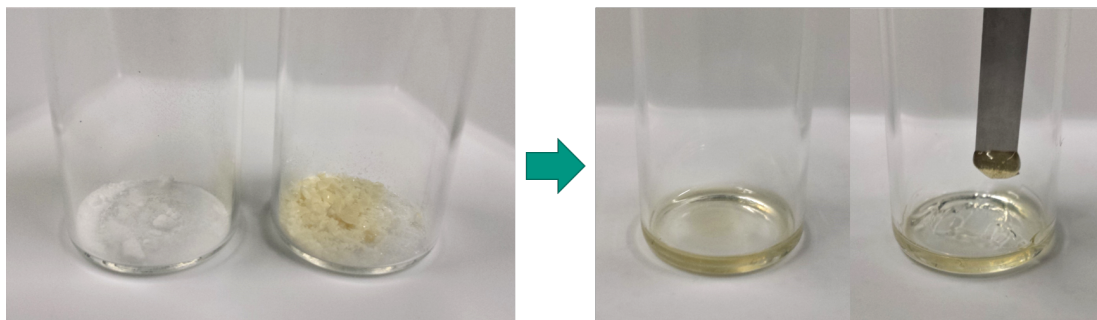


Figure 22: The picture on the left shows two vials: the left one containing LiTFSI and the right one PC-*gr*-PEO2000. Both of the compounds are powdery solids. After dissolving in acetone, mixing, and removing the solvent again, the viscous mass from the vial in the right picture is obtained. In a sense, this phenomenon macroscopically demonstrates the amorphization by LiTFSI.

The glass transition temperatures of the examined polymer electrolytes seemed to strike a balance between the effects from the LiTFSI on one side and the influence of the PEO sidechain length on the other side, somewhat canceling each other. This resulted in a T_g for all examined electrolytes in a similar range of about -50 to -40 °C, irrespective of the sidechain length. This meant an increase in T_g for PC-*gr*-PEO400 which was nearly fully amorphous before the addition of LiTFSI. Thus, the additional restraints from the quasi-ionic crosslinking have the biggest impact on the chain mobility. On the other side, the T_g was lowered for the longer sidechains for which the addition of LiTFSI completed the suppression of crystallinity. This resulted in a significantly increased mobility of sidechains which is only partially counteracted by the quasi-ionic crosslinking.

Typically, a higher concentration of LiTFSI results in a higher T_g due to the higher number of quasi-ionic crosslinks from the increased number of Li^+ cations.^[117] This trend is reflected in the T_g of all examined electrolytes. However, going from shorter to longer PEO sidechains, a decrease of the range of glass transition temperatures between the highest and the lowest LiTFSI concentrations can be observed. One possible explanation for this behavior could be the naturally lower grafting density of the herein reported PC-*gr*-PEO as opposed to most literature known PEO-grafted polymers, which typically feature a grafting point every other atom on the mainchain or

only a statistically reduced grafting density.^[19] This higher average distance of PEO chains might reduce the number of quasi-ionic crosslinks compared to intra-chain coordinations. At the same time however, shorter PEO chains have a lower tendency to form intra-chain coordinations due to the smaller number of coordination sites per chain and the relatively higher restriction in mobility from the grafting point. As a result, short PEO sidechains are expected to form more inter-chain crosslinks, leading to a bigger loss of chain mobility from a higher number of Li⁺ cations and thus a greater increase in T_g .

Interestingly, the PC-*gr*-PEO550 shows a slightly lower T_g after the addition of LiTFSI compared to the other sidechain lengths. Thus, it seems to be the ideal sidechain length that is long enough to support the reduced occurrence of quasi-ionic crosslinking due to the grafting distance, while still being short enough to profit from reduced interaction between sidechains due to the fixation from the grafting. Nonetheless, the T_g is still well below ambient temperature for all examined polymer electrolytes which is an important metric for their temperature dependent ionic conductivity.

4.3 Ionic Conductivity

As described above, polymer electrolytes were prepared by blending the synthesized polymers with LiTFSI in three [Li⁺]/[O] ratios (1:10, 1:15, and 1:20). These electrolytes were sandwiched between two stainless steel electrodes to conduct electrochemical impedance spectroscopy (EIS) at various temperatures. However, the PC-*gr*-PEO and LiTFSI mixtures were viscous, honey-like masses regardless of the length of the PEO sidechain due to the lack of a melting point and the low T_g . This fluidity, especially at elevated temperatures, necessitated a Mylar foil ring spacer in between the electrodes. Filling the cavity with the electrolyte prevented leakage and gave dimensional consistency. Mylar (a biaxially-oriented poly(ethylene terephthalate)) is often employed for this and similar purposes due to its high mechanical strength,

chemical and thermal resistance, and insulating properties, both in terms of electrical and ionic conductivity. The Nyquist plots from the EIS measurements allowed the determination of the bulk resistance of the polymer electrolytes, from which the ionic conductivities were derived. The conductivity plots are compiled in figure 23, which contains the measurements from two pure polycarbonates as references as well.

PAOMEC shows nearly no changes in conductivity from different $[Li^+]/[O]$ ratios, which is in line with its T_g . Additionally, PBEC was included to make sure that the measurements of PAOMEC were not affected by any adverse effects of the double bond. Both polycarbonates possessed ionic conductivities in a similar range, with PBEC being slightly better. Nonetheless, the resulting values are about one order of magnitude smaller at 70 °C and about two orders of magnitude smaller at 0 °C compared to the PEO-grafted polycarbonates.

As was described prior, the ion conduction of PEO-based materials strongly depends on the chain mobility of PEO. As such, effects discussed for the chain mobility in regards to the thermal behavior of the polymers are continued. However, there is no clear mapping between trends in the thermal properties and trends in the ionic conductivity. This fact clearly indicates that further influences figure into the ionic conductivity which are not captured in DSC analyses and optimization according to a single perceived parameter may not lead to an improved polymer electrolyte overall.

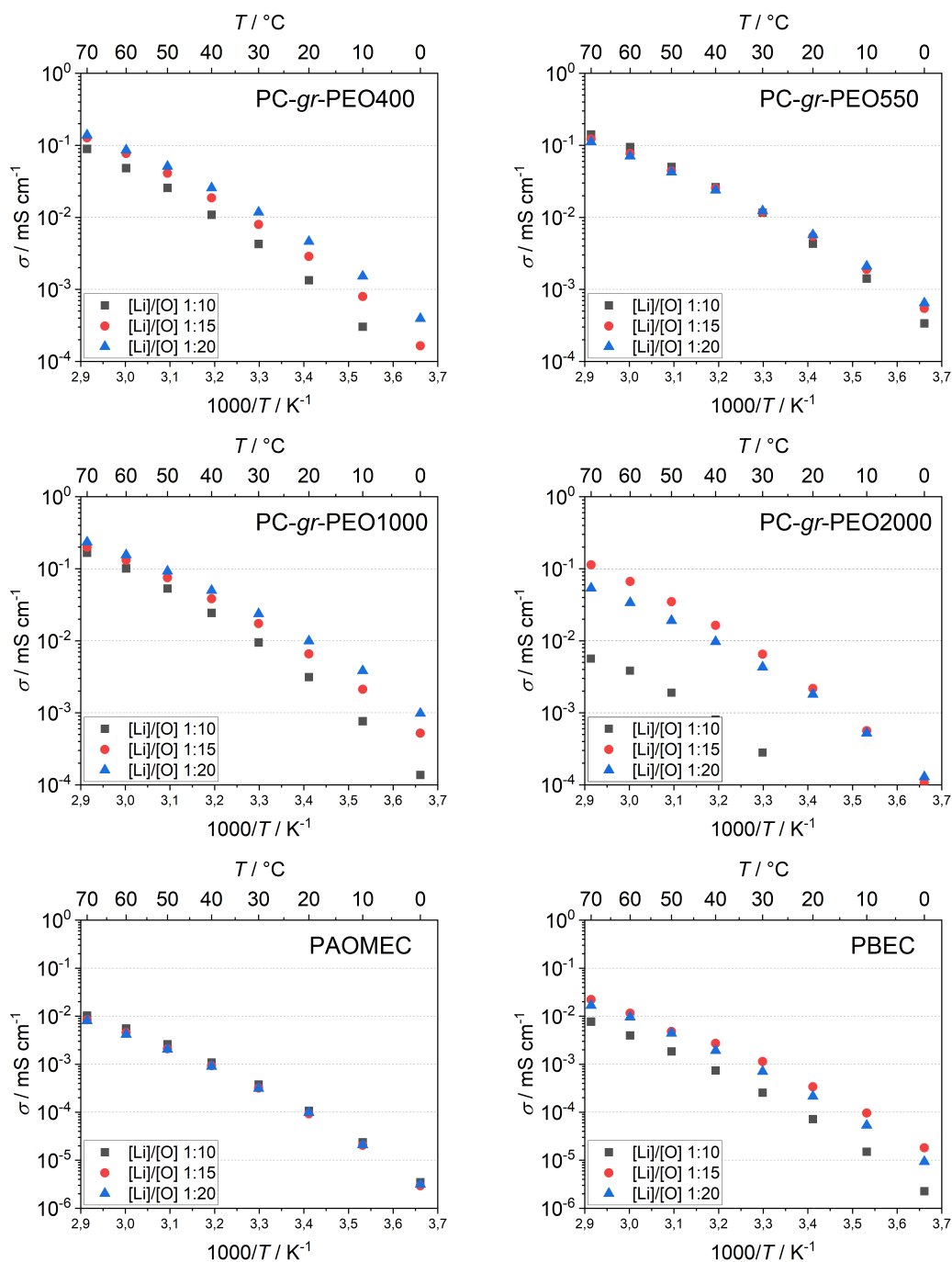


Figure 23: Overview of the temperature-dependent ionic conductivity for all examined polymers derived from electrochemical impedance spectroscopy measurements. The top four plots show the PC-gr-PEO with the four different PEO sidechain lengths. The bottom two plots show the conductivities of the unfunctionalized polycarbonates PAOMEC and PBEC as references.

For example, the lowest T_g for all electrolytes was always observed for the lowest amount of LiTFSI. At the same time, only half of the electrolytes also show their highest ionic conductivity with the lowest amount of LiTFSI. PC-*gr*-PEO550 and PC-*gr*-PEO2000 even exhibited an inversion point between 30 °C and 40 °C or between 0 °C and 10 °C, respectively. Below these inversion temperatures, they followed the general trend and had their highest ionic conductivity with a $[Li^+]/[O]$ ratio of 1:20, whereas above, the highest ionic conductivity resulted from a $[Li^+]/[O]$ ratio of 1:10 in the case of PC-*gr*-PEO550 and 1:15 for PC-*gr*-PEO2000. The main function of the Li^+ cations in the electrolytes is that of the charge carriers. A higher number of charge carriers should result in a higher ionic conductivity. However, an increasing number of Li^+ cations increases the number of quasi-ionic crosslinks at the same time. This results in a lowered chain mobility which in turn should theoretically reduce the ionic conductivity. At higher temperatures, quasi-ionic crosslinking constitutes a naturally lesser role due to the generally increased mobility of both the polymer chains and the ions. This results in a shift in the balance between these opposing effects, favoring the higher number of charge carriers at high temperatures, which is observed in the inversions.

Due to its lower T_g , PC-*gr*-PEO550 was hypothesized to be close to the ideal sidechain length at which quasi-ionic crosslinking plays a minor role, while still profiting maximally from the grafting approach. The existence of the inversion for this polymer may further strengthen this assumption, as a lower influence of the quasi-ionic crosslinking may be easier overcome. Additionally, the ionic conductivity for this polymer is overall only marginally influenced by the $[Li^+]/[O]$ ratio, which is reminiscent to the behavior of unfunctionalized PAOMEC. Hence, there might also be some beneficial interplay between the polycarbonate backbone and the PEO sidechain for this specific sidechain length. The other polymer demonstrating this inversion behavior was PC-*gr*-PEO2000. Following the above argumentation would mean that most Li^+ cations are coordinated by single chains and only form quasi-ionic crosslinks to a lesser degree. However, the ionic conductivity for this polymer drops by more than one order of magnitude for the highest $[Li^+]/[O]$ ratio of 1:10. It seems like there exist a critical concentration, above which quasi-ionic crosslinking is necessary to accommodate for all Li^+ cations.

Overall, the ionic conductivity results follow the expected trend regarding the chain length of the PEO sidechain: The mobility of short PEO sidechains is restrained significantly by the fixation of their chain end by the grafting. On the other side, very long chains are virtually unfazed by the grafting approach, but start crystallizing at their free chain ends again.^[114] Consequently, a sweet spot of highest chain mobility and thus also highest conductivity should exist between these extremes. The ionic conductivities measured at various temperatures in relation to the length of the sidechain is depicted in figure 24. Despite the better performance of PBEC, PAOMEK is included as comparison. It was reasoned that the unpolar butyl moiety was a bad stand-in as reference for the polar PEO sidechains, as well as PAOMEK being structurally closer in relationship to the examined system.^[149]

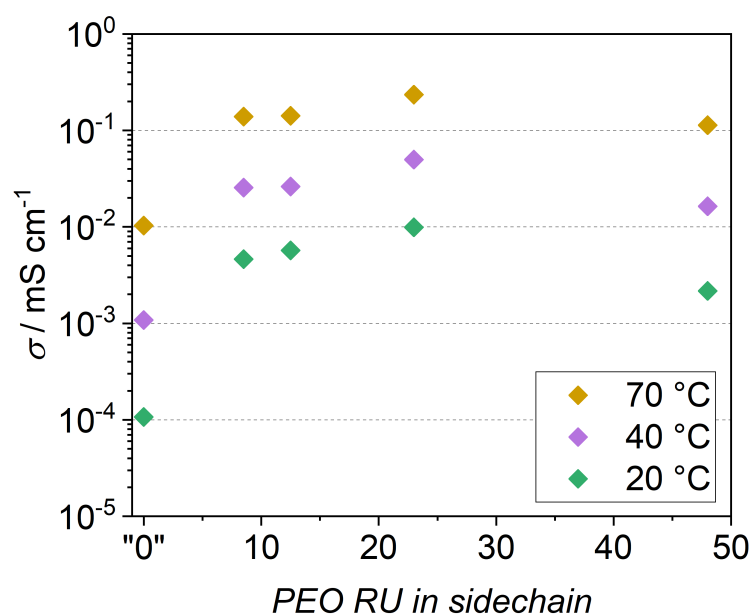


Figure 24: The ionic conductivity of PC-*gr*-PEO with all four PEO sidechains is shown in dependence of the length of the sidechain (given as number of repeating units (RU)). Only the best performing $[\text{Li}^+]/[\text{O}]$ ratio at the respective temperatures are depicted (1:20 for PEO400 and PEO1000, 1:10 for PEO550, and 1:15 for PEO2000). Additionally, PAOMEK is included as a reference and denoted with a sidechain of "0" RU of PEO.

PC-*gr*-PEO1000 achieved the highest ionic conductivity at all temperatures. The two shorter sidechains performed relatively similar to each other, but slightly below the maximum. The ionic conductivity from PC-*gr*-PEO2000 as the electrolyte with the longest examined sidechain was found to be only slightly lower at high temperatures, but performed considerably worse at low temperatures. The cause for this observation is most probably the reduced chain mobility due to increased chain interactions and quasi-ionic crosslinking. As already mentioned above, all PEO-grafted polycarbonates had substantially higher ionic conductivities compared to the unfunctionalized polycarbonate. This clearly demonstrates the validity and the positive influence of grafted PEO sidechains on the ionic conductivity.

Interestingly, there is a clear mismatch between the sidechain with the lowest T_g (PEO550), and thus postulated with the highest sidechain mobility, and the sidechain with the highest ionic conductivity (PEO1000). Although the sidechain mobility is one of the most important metrics for PEO-based electrolytes, multiple other properties and effects influence the ionic conductance as well, which are not captured by the thermal behavior of the polymeric material. For instance, both PEO400 and PEO550 sidechains are able to coordinate only a single Li^+ cation per chain, whereas PEO1000 is already able to accommodate for multiple Li^+ at one chain, facilitating ionic conductivity further.^[94,97] Another notable difference between the four PC-*gr*-PEO polymer electrolytes is the relative ratio of polycarbonate and PEO. As every polycarbonate repeating unit is grafted with a PEO sidechain, longer sidechains consequently lead to polymers with less PC overall. Typically, polycarbonates yield lower ionic conductivities compared to PEO-based electrolytes. Thus, the higher ionic conductance measured for PC-*gr*-PEO1000 might be ascribed to this property as well.

The ionic conductivity calculated from EIS corresponds to the combination of the mobility of anions and cations. However, only the transport of Li^+ cations contributes to the actual performance of a battery cell. Thus, the lithium ion transference number t_+ was determined by the Bruce-Vincent method^[179,180] to identify the portion of the overall conductivity constituting the Li^+ conductivity.

If a potential is applied to a battery cell, both anions and cations start to migrate according to the electrical field. In the Bruce-Vincent test both electrodes are lithium. Thus, Li^+ can be reduced at the negative electrode and become uncharged lithium metal, whereas at the positive electrode lithium metal is oxidized to Li^+ cations. The result is a constant current of Li^+ through the electrolyte. On the other hand, the electrodes are not reversible for the anions. Hence, they accumulate at the positive electrode and build a concentration gradient. This gradient leads to diffusion opposed to the migration in the electrical field until a steady state is reached and no more net movement of anions occurs. This means that only Li^+ cations provide ionic conductivity in the steady state. This effect is illustrated in the polarization plot in figure 25. The lithium ion transference number t_+ as the ratio of currents at steady state and the beginning of polarization is then additionally corrected by changes of the electrode interfacial resistances (determined by EIS directly before and after polarization).

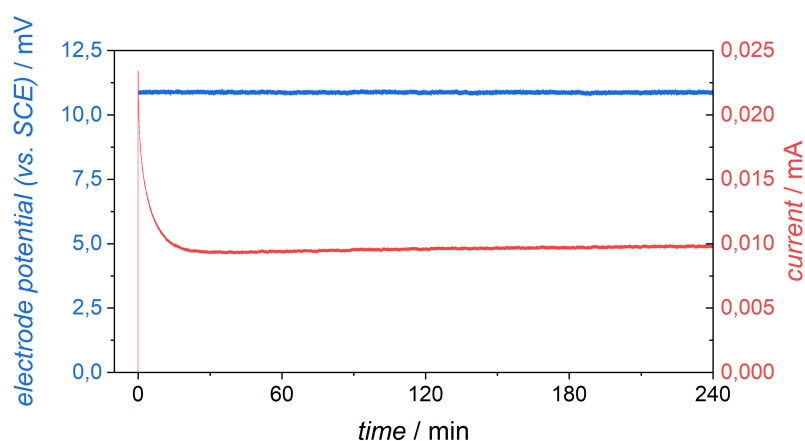


Figure 25: An exemplary polarization plot for PC-*gr*-PEO550 with a $[\text{Li}^+]/[\text{O}]$ ratio of 1:20 is depicted. After a constant potential is applied to the symmetric Li||Li cell, the resulting current is at its maximum and rapidly declines. After about 30 min, steady state with a constant current is reached, indicating only cation migration takes place as the anions are blocked by the electrodes and form a concentration gradient working against the electrical field.

The determined t_+ values are listed in table 5 and the corrected Li^+ conductivity of the polymers is visualized in figure 26. PC-*gr*-PEO2000 was omitted since it featured the

lowest ionic conductivity, while having the lowest polycarbonate content as well. Similarly to the other trends for different $[\text{Li}^+]/[\text{O}]$ ratios, t_+ was always highest with the lowest amount of LiTFSI for all PEO-grafted electrolytes. Moreover, a massive drop of t_+ was observed for PC-*gr*-PEO400 and PC-*gr*-PEO1000 with a $[\text{Li}^+]/[\text{O}]$ ratio of 1:10. On the other side and also mirroring the ionic conductivity results, PAOMEC displayed only negligible changes in t_+ with different $[\text{Li}^+]/[\text{O}]$ ratios. Again indicating some positive interplay between the polycarbonate with PEO sidechains, PC-*gr*-PEO550 still had a similar reduction of t_+ with increasing $[\text{Li}^+]/[\text{O}]$ ratios, however without the larger drop-off at 1:10. This polymer electrolyte also achieved transference numbers notably higher than the other sidechain lengths.

Table 5: Lithium ion transference numbers t_+ of selected polymers at 60 °C.

polymer	$[\text{Li}^+]/[\text{O}]$ ratio		
	1:10	1:15	1:20
PAOMEC		0.407	0.405
PC- <i>gr</i> -PEO400	0.076	0.145	0.156
PC- <i>gr</i> -PEO550	0.173	0.187	0.194
PC- <i>gr</i> -PEO1000	0.076	0.128	0.136

Nonetheless, all three PC-*gr*-PEO electrolytes reach a t_+ above 0.1 at sufficiently low amounts of LiTFSI, which is the typical transference number for pure PEO. PC-*gr*-PEO550 even features a t_+ near 0.2. This seems to be the upper limit for modified PEO-based electrolyte systems.^[116,181] The t_+ determined for PAOMEC is substantially higher at 0.4, which is expected for aliphatic polycarbonates.^[143–145]

These results confirm that the ionic conductivity of PC-*gr*-PEO is mostly based on the PEO sidechains. This is probably due to the much stronger chelating polyether coordination from PEO, whereas the polycarbonate coordination plays only a minor role.^[20] Although the highly flexible polycarbonate backbone together with the PEO-grafting approach resulted in substantially increased transference numbers compared to pure PEO, no further increase of t_+ beyond sophisticated PEO-based electrolytes could be detected.

The highest overall pure Li^+ cation conductivity is still achieved by PC-*gr*-PEO1000 despite the significantly higher t_+ of PC-*gr*-PEO550. Likewise, the Li^+ conductivity of PAOMEC is still lower than for the worst performing PC-*gr*-PEO, even after correction by the massively bigger t_+ of the polycarbonate.

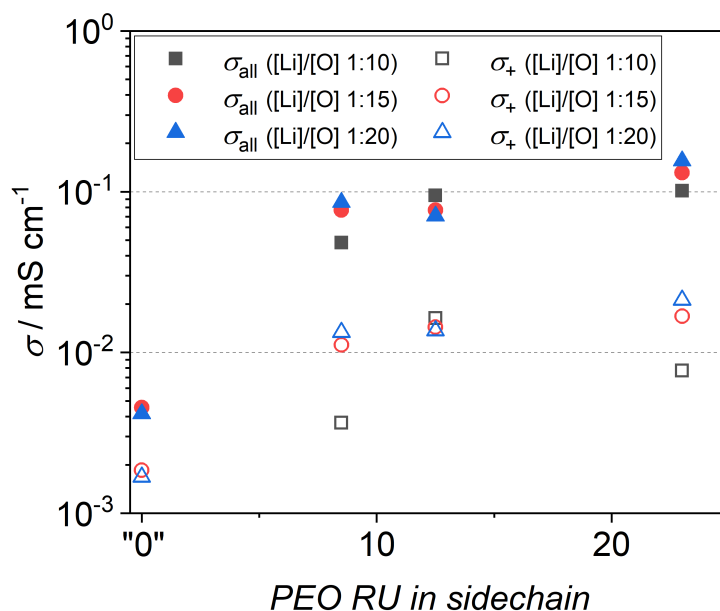


Figure 26: The overall ionic conductivity at 60 °C of PC-*gr*-PEO with the three best performing sidechains is shown (filled symbols). The pure Li^+ cation conductivity corrected by the transference number t_+ is plotted for comparison as well (hollow symbols). PAOMEC is included once again and denoted with a sidechain of "0" RU.

4.4 Multifunctionalization

As multiple of the interesting properties of PC-*gr*-PEO are proposed to be the results of the constant, bigger grafting distance, another synthesis approach was planned to increase the grafting density. The aim was to graft two PEO sidechains to every polycarbonate repeating unit. These two sidechains would then be in a similar spatial proximity compared to usual PEO-grafted polymer architectures, while still maintaining a bigger distance between pairs. This strategy was envisioned to boost the ionic

conductivity of the shortest sidechain length in particular, as the PC-*gr*-PEO400 seemed to be limited by its lacking ability to coordinate the Li^+ cations mostly in an intra-chain fashion. Another potentially interesting comparison could have been between a single PEO sidechain of double the length with the doubly grafted PEO sidechains, practically representing the longer sidechain being attached in the middle of the chain opposed to a chain end.

In an effort to reuse as much of the previous syntheses as possible, the double bond of the established PAOMEC was planned to be brominated. The bromine atoms were then to be substituted by the PEO chains as depicted in figure 27. The bromination of PAOMEC was easily realized by the addition of Br_2 with complete conversion and nearly quantitative yield. However, the substitution turned out to be much more challenging than anticipated.

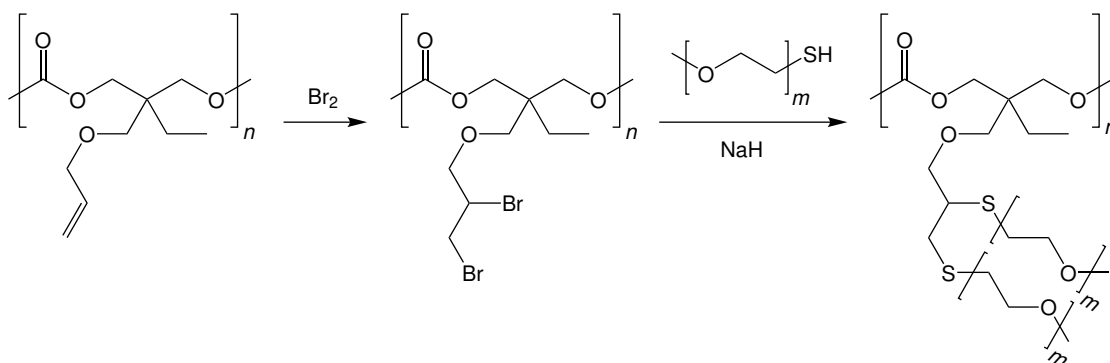


Figure 27: The planned difunctionalization approach is illustrated. Initially, the allyl ether double bond of PAOMEC was brominated. Subsequently, nucleophilic substitution with a deprotonated mPEO-S^- was intended to introduce two PEO sidechains per polycarbonate repeating unit.

Initially, the mPEO-SH was intended to be deprotonated irreversibly by NaH to a thiolate, which is a potent nucleophile. Nonetheless, only partial substitution was observed after addition of the brominated PAOMEC at reduced temperatures. Additionally, the reemergence of the double bond according to crude NMR spectra (figure 28) suggested that a competing elimination reaction took place. The multiplicity of the signals indicated the re-formation of an unfunctionalized double bond, meaning no hydrogen was eliminated. This left the disulfide, bromine, or a sulfenyl bromide as

potential elimination products. The same elimination was observed with a moderate base like Cs_2CO_3 as well.

To avoid any base-catalyzed elimination, the substitution was attempted directly with mPEO-SH, although the thiol is a much weaker nucleophile compared to the thiolate. Thus unsurprisingly, no reaction occurred under these conditions. Another attempt was to employ an alkoxide by deprotonating mPEO-OH. Although an alkoxide is a stronger base than a thiolate, it was reasoned that at least the elimination of a peroxide could be avoided due to the instability of such a compound. However, the strong basicity of the alkoxides resulted in the complete decomposition of the polycarbonate backbone as evident in figure 28.

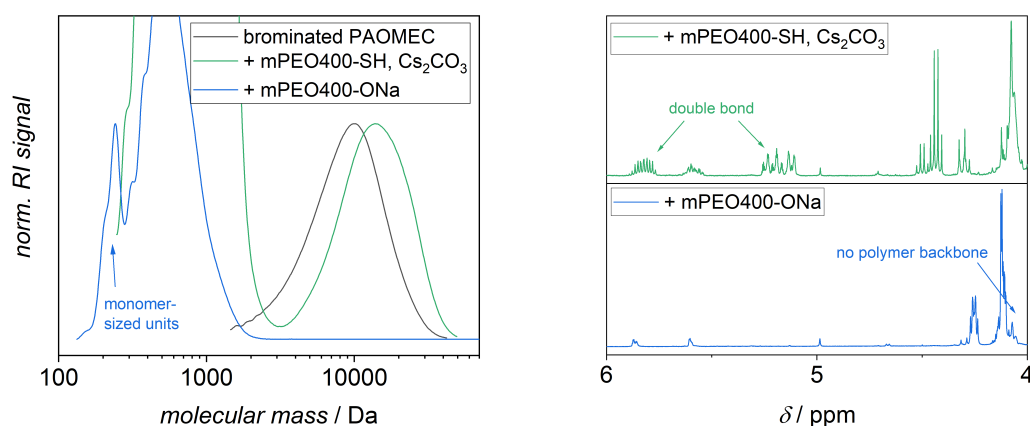


Figure 28: SEC and NMR results from the unsuccessful substitution attempts are depicted. A thiolate (green) was formed by deprotonation of mPEO400-SH with Cs_2CO_3 . This substitution resulted in a shift towards higher molecular masses, albeit still substantially lower than PC-*gr*-PEO. At the same time, double bonds are reformed during this step according to NMR spectroscopy. The substitution attempt with an alkoxide (blue), which was formed by prior deprotonation with NaH, led to a complete decomposition of the polycarbonate backbone into monomer-sized units.

Ultimately, this difunctionalization approach was shelved. It would require fine kinetic control for the substitution with thiolates to reduce or remove the occurrence of elimination reactions. Potentially, the dropwise addition of thiolate to keep the concentration of free base low might be helpful, too. An alternative pathway towards the same product

could be to employ a polycarbonate bearing a triple bond and then performing radical thiol-yne addition. This, however, would require the establishing of a completely new monomer synthesis, probably with the need for an adjusted purification procedure, as well as the optimization of the functionalization conditions. Nonetheless, thiol-yne addition might be an interesting pathway for the future, either way.

4.5 Solidification Approaches

Ultimately, a key advantage of polymer electrolytes is the potential they show as solid-state electrolytes for the reasons discussed at the end of chapter 2.3. As it stands, all polymers described until this point were honey-like, viscous masses. Their fluidity was typically relatively low, meaning they did not flow in an angled or upended vial. However, the samples could be easily parted with a spatula and then flowed back together into a single mass relatively quickly. The PC-*gr*-PEO, as is, would not demonstrate a sufficient resistance against lithium dendrite growth. The increase in mechanical stability to a point of solidification was thus very necessary.

4.5.1 Crosslinking

The immediate consideration was the crosslinking of the polymer. Random radical crosslinking is a well-known technique employed for the solidification of PEO as polymer electrolyte. The random nature of a radical as crosslinking source hinders reproducibility, however. On the other side, the double bond of PAOMEC gave the opportunity for defined crosslinking using a α,ω -dithiol in the radical thiol-ene addition. The idea was to use some of the double bonds for crosslinking, while grafting PEO to the remaining double bonds as before. Essentially, one would trade some of the conductivity for the solidification of the material. Bis(mercaptoethoxy)ethane (BMEE) was used as a commercially available crosslinker (basically a very short PEO with three repeating units). However, it was found that up until 60 % of the double bonds are functionalized

with a crosslinker, no discernible change in material properties occurred. Furthermore, at least 80% double bond conversion was needed to produce an insoluble, swellable solid (figure 29). With only a fifth of the double bonds remaining for grafting with PEO, the ionic conductivity was expected to drop substantially.

Instead, another path was considered in combining the function of the PEO as ion-conducting sidechain and as crosslinker. For this approach, a PEO1000 with a thiol at both chain ends was synthesized from bishydroxy-PEO1000 following the identical protocol as before. The resulting flexible, free-standing network was extensively dried (figure 29). As the chain mobility of a crosslinker that is fixated to the backbone at both its ends is massively reduced compared to a grafted sidechain with only one fixated end, the ionic conductivity was expected to drop as well. Ultimately, the ionic conductivity of *PC-net*-PEO1000 was almost exactly one order of magnitude lower compared to *PC-gr*-PEO1000. Interestingly, a network crosslinked completely by BMEE performed very similar to unfunctionalized PAOMEC, despite being completely solid. The ionic conductivity results are plotted in figure 34 on page 68.



Figure 29: Pictures of crosslinked samples are given. The vial on the left contains a swellable gel out of a PAOMEC that was crosslinked using BMEE with 80% thiol per double bond. Samples with a lower crosslinker concentration did not form a stable solid. The picture on the right demonstrates the flexibility of a completely crosslinked polycarbonate network with PEO1000-dithiol as crosslinker.

4.5.2 Microphase Separation

Another potential avenue towards the solidification of the presented polymers relied on the microphase separation of block copolymers. Two immiscible polymers that are covalently connected cannot macroscopically demix. Instead, they form a microphase separation with domains of either polymer on the nanometer scale. In this way, some of the properties of either block are retained instead of being averaged between two miscible polymers. This method was already successfully used in literature to solidify PEO-grafted polymer electrolytes using polystyrene (PS) as additional block.^[126–129] Polystyrene is an ideal candidate to produce microphase-separated polymer electrolyte films due to its high mechanical stability and high T_g of around 100 °C,^[182] its affordable price and it being a nonpolar polymer. On the other side, the polar PC-*gr*-PEO domain should contribute the ionic conductivity. It was of high importance to balance the two polymer blocks properly to produce macroscopically solid block copolymer films. Thus, a controlled polymerization technique was necessary to synthesize a polystyrene of predictable length and with defined endgroups that could then be used to form the block copolymer. For the same reasons as discussed in chapter 4.1.1, ATRP was avoided due to metal-containing catalysts, despite potentially having the most facile access towards an end-functionalized PS with a hydroxy group. Instead, the synthesis depicted in figure 30 was proposed.

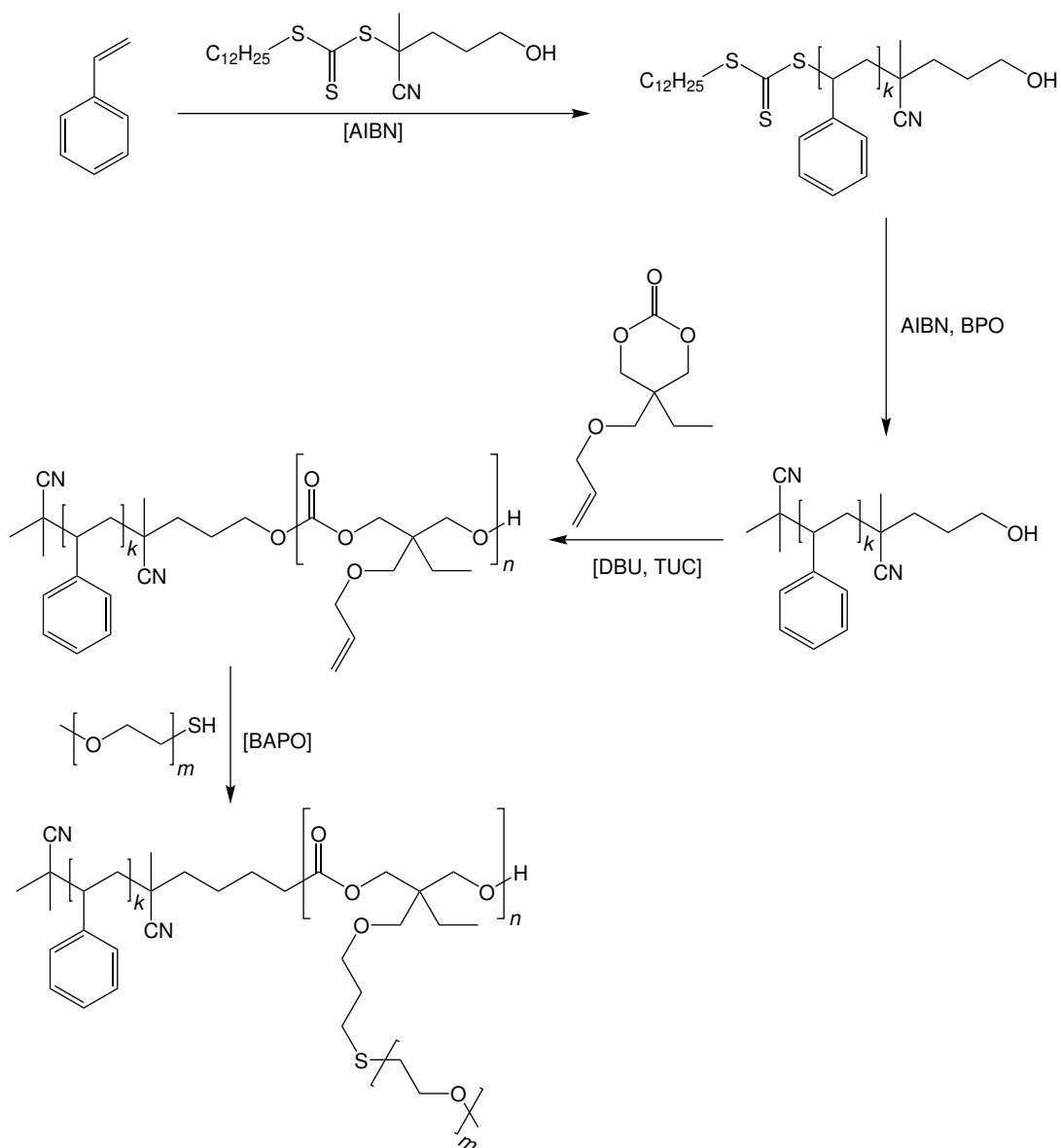


Figure 30: The proposed synthesis route to produce a PS-*b*-(PC-*gr*-PEO) is depicted. Styrene is polymerized using a CTA with a terminal hydroxy group on the initiating moiety. Afterwards, the CTA endgroup is removed by displacement with radicals to avoid side reactions in following steps. The hydroxy group is then used to initiate the polymerization of AOMEAC to form the second block, which is then eventually functionalized with grafted PEO sidechains by radical thiol-ene addition.

A RAFT polymerization with a CTA containing a hydroxy group was planned to be employed to produce the desired PS. Unfortunately, it was necessary to remove the CTA endgroup before the AROP. Firstly, the DBU, which is used during the AROP

as a base, could cleave the CTA group, leaving a thiol. This secondary thiol might have skewed the AROP results by initiating additional chain growth, albeit slower than the primary alcohol. Even then, the PS-thiol would be problematic during the radical thiol-ene addition as well. Even partial reaction between the double bond of PAOMEC and the thiol at the other chain end of PS could inhibit proper microphase separation. Thus, a method was used to remove the CTA endgroup without producing a thiol by displacement with a radical. Benzoyl peroxide (BPO) produces very reactive radicals that could cleave of the CTA endgroup.^[183] A high concentration of BPO and AIBN radicals could then saturate the formed radical at the PS chain end.

The above mentioned examples of PS block copolymers in combination with a PEO-grafted block determined that lamellar microphase separation yielded stable films with high ionic conductivity. With the assumption that the density of polymers are relatively similar, this requires a 1:1 weight ratio between the PS and the PC-*gr*-PEO. It was decided to employ mPEO550 as sidechain for this approach due to the invariance it showed towards the LiTFSI concentration. The motivation was that this invariance meant that other parameters could be varied more freely as well. Initially, it was also the aim to target a PAOMEC block with 35 repeating units to have maximum comparability towards the described grafted system.

Therefore, a PS with 269 repeating units had to be synthesized. A batch with an initial monomer-to-CTA ($[M]/[CTA]$) ratio of 350, resulted only in a degree of polymerization of about 112 after 24 h. Multiple re-initiations were necessary to reach the target. This, however, led to a very broad distribution according to SEC and the endgroup fidelity was expected to be relatively low due to this, despite the continued living nature of the polymerization. Even with an initial $[M]/[CTA]$ ratio of 1000, only a degree of polymerization of 170 was reached in a single initiation. The kinetic studies are plotted in figure 31. Ultimately, it seemed like this particular CTA was not the ideal match with styrene. An even higher $[M]/[CTA]$ would potentially lead to a loss of control due to the very low concentration of CTA and was thus not attempted.

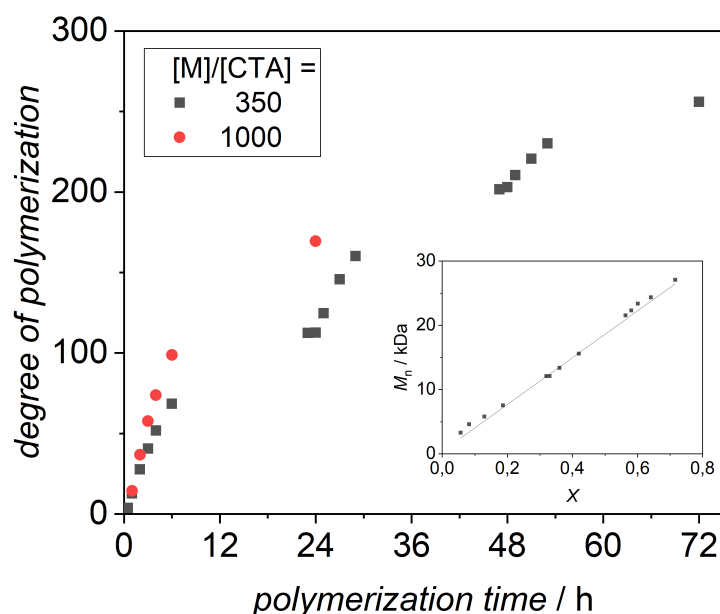


Figure 31: The kinetic study of two RAFT polymerizations of styrene with the hydroxy-terminated CTA is given. Multiple re-initiations (every 24 h) were necessary to come close to the desired degree of polymerization. The inset demonstrates the living nature of the polymerization with a linear growth proportional to the conversion, which is additionally close to the theoretical values represented by the drawn through line. A second polymerization with a higher initial $[M]/[CTA]$ improved the results after a single initiation, but was still significantly below the targeted degree of polymerization of 269.

In the end, multiple hydroxy-terminated PS were synthesized with a degree of polymerization in the range of 80–180. The removal of the CTA endgroup by radical displacement was demonstrated to be successful by the disappearance of the absorbance from the thiocarbonyl at 312 nm according to UV/Vis spectroscopy. As elucidated in chapter 4.1.2, the monomer concentration is a very determining parameter for the equilibrium conversion in the AROP. The much higher molecular mass of the PS compared to the usual initiator of benzyl alcohol together with its considerably lower solubility necessitated a lower AOMEC concentration of 0.5 M for the block copolymer formation. No prior kinetic data for this concentration were available, but an equilibrium conversion of around 25 % was estimated. Nonetheless, the results of the AROP were much worse

than anticipated and seemingly unpredictable, as listed in table 6. Especially, the AROP attempts with a very high initial [AOMECE]/[PS] ratio resulted in nearly no conversion.

Table 6: Overview over attempted AROP chain extensions after radical displacement of CTA endgroup.

$P_n(\text{PS})$	desired $P_n(\text{PC})$	[AOMECE]/[PS]	received $P_n(\text{PC})$	"conversion" ^a	wt%(PS) with PEO
83	10.8	33.2	2.9	8.7 %	78.9 %
83	10.8	51.0	6.1	12.0 %	63.9 %
149	19.4	155.0	1.3	0.8 %	93.7 %
177	23.1	79.0	8.0	10.1 %	74.3 %
177	23.1	185.0	3.3	1.8 %	87.5 %
172 ^b	22.4	50.0	13.3	26.6 %	62.8 %

^a as apparent from received $P_n(\text{PC})$ opposed to starting conditions, ^b no removal of CTA endgroup

A test reaction with a PS that did not have its CTA endgroup removed resulted in a conversion much better than the rest and much closer to the expectation. Either the aminolyzed thiol did initiate a second AROP chain growth, or the radical cleavage of the CTA endgroup somehow interfered with the hydroxy group. The exact reaction that resulted in this phenomenon was not investigated. Still, the second entry with the ratio closest to 50 wt%(PS) was continued with the thiol-ene addition to attach PEO sidechains. Its ionic conductivity results are contained in figure 34 on page 68. A picture of this electrolyte film is included in figure 32.

Another pathway to remove the CTA endgroup was proposed and tested that did not rely on a radical mechanism (figure 33). Instead, the CTA endgroup was cleaved by aminolysis and the resulting thiol linked to an acrylate by thiol-Michael click chemistry. The disappearance of the thiocarbonyl could again be observed by UV/Vis spectroscopy. The acrylate was chosen to yield an easily identifiable signal in NMR spectroscopy. Unfortunately, no such signal was detected, and no quantitative analysis was possible.

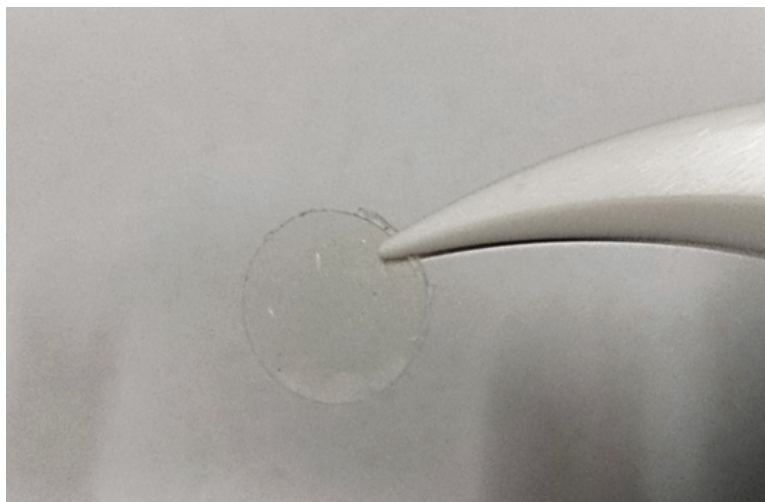


Figure 32: A picture of a PS-*b*-(PC-*gr*-PEO) free-standing film is given. Due to its high PS content of 64 wt%(PS), the film shows relatively low flexibility and a high brittleness.

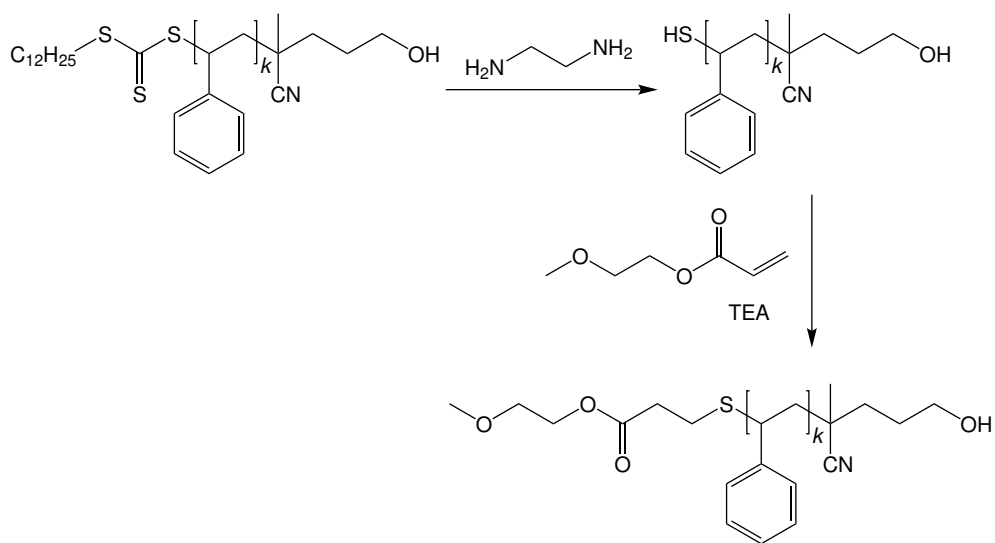


Figure 33: An alternative synthesis route for the removal of the CTA endgroup is illustrated. The aminolysis of the trithiocarbonate results in a thiol. Subsequently, this thiol is converted *via* a thiol-Michael click reaction.

The AROP chain extensions with this polymer is listed in table 7. The apparent

conversion is once again much closer to the expected 25 %, but still not consistently predictable. Once again, the thiol-ene addition of PEO sidechains was performed with the second entry due to the lower wt%(PS). The corresponding ionic conductivity values are depicted in figure 34 on page 68 as well.

Table 7: Overview over attempted AROP chain extensions after aminolysis and thiol-Michael addition.

$P_n(\text{PS})$	desired $P_n(\text{PC})$	[AOMECE]/[PS]	received $P_n(\text{PC})$	"conversion" ^a	wt%(PS) with PEO
138	18.0	40.0	11.0	27.5 %	62.1 %
138	18.0	55.0	11.5	20.9 %	61.0 %

^a as apparent from received $P_n(\text{PC})$ opposed to starting conditions

4.5.3 Characterization of Solidified Samples

The ionic conductivity results for all solid polymer electrolytes are summarized in figure 34. Ultimately, no solidified sample came close to PC-*gr*-PEO550 or PC-*gr*-PEO1000. The solid electrolyte with the highest ionic conductivity was the fully crosslinked PAOMECE network using PEO1000-dithiol as crosslinker. This electrolyte film was very flexible despite its relatively high thickness (400 μm).

The performance of PS-*b*-(PC-*gr*-PEO) as microphase-separated solid polymer electrolyte films were underwhelming. However, it is difficult to judge the overall validity of this approach from these results as the samples had noticeably higher contents of PS than intended. Consequentially, the films were quite brittle and difficult to handle as well. Typically, the range of ratios for which lamellar structures are formed is relatively wide, but further investigation and optimization will be necessary to see if block copolymers with a ratio closer to 50 wt%(PS) will result in more flexible films with higher ionic conductivity, while still remaining mechanically stable solids. Furthermore, this consideration is based on the assumption that PS and PC-*gr*-PEO have a similar density. Due to the high flexibility of both the PAOMECE backbone and the PEO sidechains, as well as the relatively big grafting distance and resulting free volume, it might even be necessary to go to even lower PS contents.

Figure 35 contains DSC measurements for the series of PS-*b*-(PC-*gr*-PEO550). After

the addition of the LiTFSI, two clear T_g could be determined, one corresponding to PS and one for the PC-*gr*-PEO block. This heavily indicated the successful microphase separation. Noteworthy, the T_g of the polar ion-conducting block fell into the same range established for the pure PC-*gr*-PEO after the addition of LiTFSI (compare table 4 on page 46). At the same time, at least partial mixing of the polar and unpolar blocks was observed without LiTFSI. It seems like the addition of the ions was necessary to increase the polarity of the block to effectively form the microphase separation.

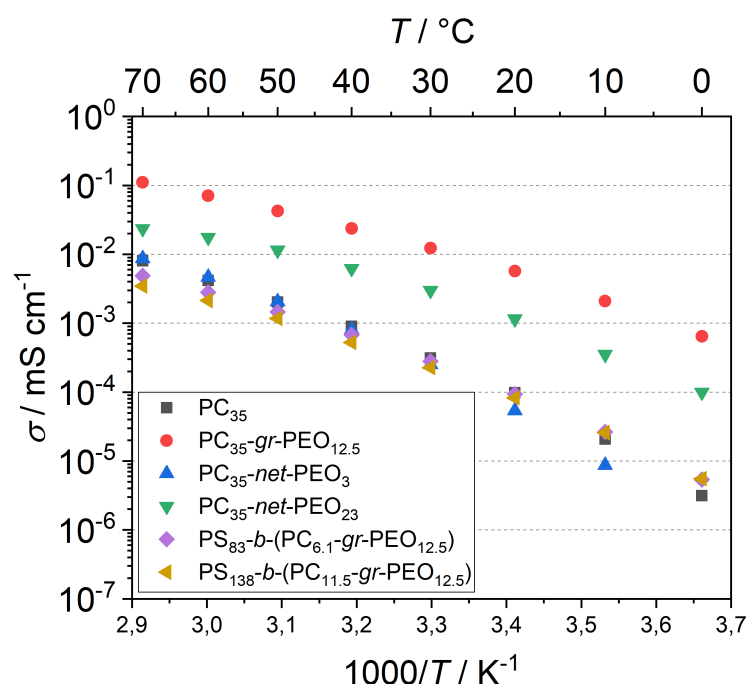


Figure 34: The ionic conductivities derived from EIS for the solidified polymer electrolytes is given. All samples had a $[Li^+]/[O]$ ratio of 1:20. The PEO1000-crosslinked sample (green) performed about one order of magnitude worse than PC-*gr*-PEO550 (red) (and almost exactly one order of magnitude worse than PC-*gr*-PEO1000 (not shown)). The sample crosslinked with BMEE (blue) achieved similar ionic conductivities as pure PAOMEC (black) at high temperatures. The PS-*b*-(PC-*gr*-PEO) after displacement of the CTA endgroup by radicals (purple) achieved nearly the same ionic conductivity as PS-*b*-(PC-*gr*-PEO) after aminolysis and thiol-Michael addition (gold). Both microphase-separated block copolymers had similar PS contents of 64 wt%(PS) and 61 wt%(PS), respectively.

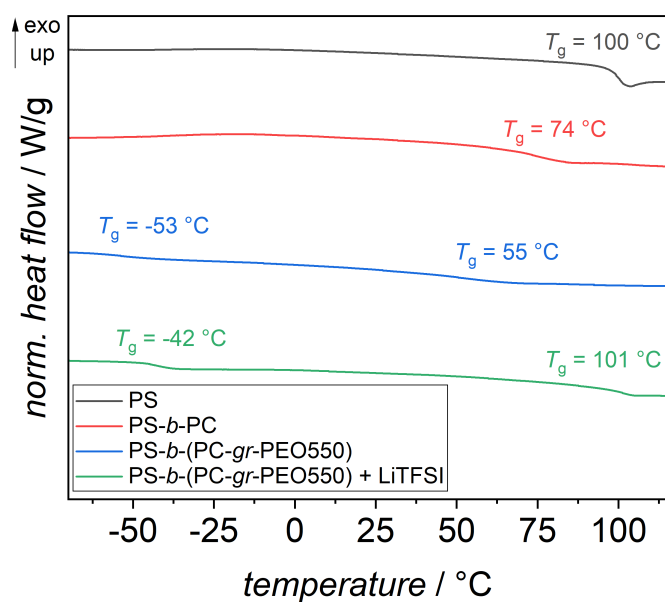


Figure 35: DSC plots for the polymer series resulting from PEO550 are given. The lower integral of the PEO melting peak after the grafting process is a direct indication for the reduction of crystallinity. Additionally, the melting peak vanishes after the addition of LiTFSI as conducting salt, showing the complete suppression of the crystallization of PEO in the polymer electrolyte. The glass transition temperature is reduced with the addition of LiTFSI suggesting an increase in chain mobility.

5 Conclusion and Outlook

The aim of the thesis was to synthesize polycarbonates with PEO sidechains in a systematical fashion to then correlate polymer parameters with the electrochemical performance. This structure-property correlation was intended to gain a deeper understanding and expand the portfolio of detailed studies for PEO-grafted electrolyte systems.

Initially, an adaptable synthesis pathway towards functionalized polycarbonates was established. To that end, a six-membered cyclic carbonate monomer bearing an allyl ether moiety was synthesized and subsequently polymerized in an anionic ring-opening polymerization. Kinetic studies revealed good control and predictability of the resulting polycarbonate up to a maximum of 50 repeating units. To reach higher degrees of polymerization, the monomer concentration would have to be increased, which was not possible due to the viscosity of the solution after a few hours of reaction time. The allyl ether of the polycarbonate was targeted as ene component in a radical thiol-ene addition for a post-polymerization modification. As thiol component, thiol endgroup-functionalized PEO was synthesized in an unusual, but highly efficient pathway by attaching an ethylxanthate to the PEO. The thiol was then liberated by aminolysis under very mild conditions.

The radical thiol-ene addition approach was employed to synthesize aliphatic polycarbonates with PEO sidechains of four different lengths to gauge a potential use as dry polymer electrolyte. In this context, the influences of the sidechain length and the LiTFSI content on the thermal behavior and the ionic conductivity were investigated. It was confirmed that the grafting approach led to a considerable reduction in crystallinity opposed to pure PEO. Even more, the complete suppression of crystallization was observed after the addition of LiTFSI. The glass transition temperatures of the polymer electrolytes with LiTFSI demonstrated only a very low dependency on the sidechain length, suggesting that effects such as sidechain interactions, quasi-ionic crosslinking and plasticizing approximately nullified each other.

Especially PC-*gr*-PEO550 exhibited some unique properties in a slightly lower T_g , a greatly reduced influence of the $[Li^+]/[O]$ ratio on the ionic conductivity, and a significantly higher t_+ , indicating some positive interactions between the polycarbonate backbone and the PEO sidechains. Despite this observation, PC-*gr*-PEO1000 achieved the highest ionic conductivity at all temperatures with $9.90 \times 10^{-3} \text{ mS cm}^{-1}$ at ambient temperature (20 °C) and $2.34 \times 10^{-1} \text{ mS cm}^{-1}$ at 70 °C. The aliphatic polycarbonate backbone was intended to provide high amorphicity and flexibility to the system, as well as potentially offer improvements to the notoriously low lithium transference numbers of PEO-based electrolytes. Indeed, quite high transference numbers were identified with up to 0.194, reaching the upper end in the range associated with PEO-based polymer electrolytes. Unfortunately, the polycarbonate could not provide an increase in transference number beyond other sophisticated PEO architectures.

As is usual, but unfortunate, the amorphized PEO-grafted polycarbonate was very lacking in mechanical stability, resembling a honey-like, highly viscous mass. Two different solidification approaches were examined to improve the mechanical properties of the polymer electrolyte. Controlled crosslinking *via* radical thiol-ene addition with a dithiol required a high degree of crosslinking of at least 80 % to produce a solid network. These films, however, were very flexible and still demonstrated ionic conductivities about one order of magnitude worse than the grafted system.

The second approach relied on the incorporation of a polystyrene as a block with a high T_g . A RAFT polymerization with a hydroxy-terminated CTA that could then initiate the AROP was intended, but control over both polymerizations was very poor. The targeted 50 wt%(PS) was not achieved. Polymer electrolytes with a greater amount of polystyrene were very brittle solid films with a noticeable loss of ionic conductivity. A new route is proposed: The RAFT polymerization of polystyrene is repeated with a more suitable, conventional CTA, which is then aminolyzed to a thiol. At the same time, AROP is initiated by hydroxyethylacrylate. The block copolymer can then be formed by thiol-Michael click chemistry between the thiol and the acrylate.

Nonetheless, a deeper insight into the structure-property relationship of PEO-grafted polymer electrolytes was provided, strengthening the understanding of PEO sidechain

architectures. The demonstrated system of PC-*gr*-PEO showcased some interesting properties that warrant further investigation or attempts of replication of the consistently bigger grafting distance with other backbone chemistries.

6 Experimental Protocols

6.1 Materials

Azobis(isobutyronitrile) (AIBN, Sigma-Aldrich, 98%), benzoyl peroxide (BPO, Sigma-Aldrich, 75%, remainder water), benzyl alcohol (Sigma-Aldrich, 99.8%, anhydrous over inert gas), bis(mercaptoethoxy)ethane (BMEE, TCI, 97%), 3,5-bis(trifluoromethyl)-phenyl isocyanate (abcr, 97%), bis(2,4,6-trimethylbenzoyl)phenylphosphine oxide (BAPO, abcr, 96%), bromine (Alfa Aesar, 99.8%), 2-butyl-2-ethylpropane-1,3-diol (TCI, 98%), calcium hydride (Acros Organics, 93%), celite 545 (VWR), 4-cyano-4[(dodecylsulfanylthiocarbonyl)sulfanyl]pentanol (abcr, 95%), cyclohexylamine (Alfa Aesar, 98%), 1,8-diazabicyclo(5.4.0)undec-7-ene (DBU, Alfa Aesar, 99%), ethyl chloroformate (Acros Organics, 97%), ethylenediamine (Acros Organics, 99%), hydrochloric acid (Roth, 37%), magnesium sulfate hydrate (Roth, 99%, dried), 2-methoxyethyl acrylate (Alfa Aesar, 98%, stabilised), poly(ethylene oxide) (PEO, Acros Organics, M_n : 1000 Da), poly(ethylene oxide) monomethyl ether (mPEO, TCI, M_n : 400 Da/550 Da/1000 Da/2000 Da), potassium ethylxanthate (KXEt, Alfa Aesar, 97%), 1,3-propanediol (TCI, 98%), sodium chloride (Roth, 99.8%), sodium hydrogencarbonate (Roth, 99%), sodium thiosulfate pentahydrate (TCI, 99%), triethylamine (TEA, Acros Organics, 99%), trimethylolpropane monoallyl ether (Aldrich, 98%), tris(2-carboxyethyl)phosphine hydrochloride (TCEP·HCl, abcr, 99%), tosyl chloride (TCI, 99%) were used as received.

Styrene (Merck, 99%, stabilised) was passed through basic aluminum oxide (Acros Organics, Brockmann I, 50–200 μm , 60 \AA) immediately prior to use.

Bis(trifluoromethanesulfonyl)imide lithium salt (LiTFSI, Sigma-Aldrich, 99.95%) was dried at 80 °C under vacuum for 2 days and subsequently stored inside a *MBraun Unilab* glovebox under dry argon atmosphere (<0.1 ppm H₂O, <0.1 ppm O₂). Lithium foil (Honjo Metal, 300 μm thickness) was likewise stored inside the same glovebox.

Mylar foil (Valentia Industries, 100 μm thickness) was cut to shape, dried under vacuum at 40 $^{\circ}\text{C}$ overnight, and then stored in the glovebox as well.

Solvents were ordered from VWR (AnalaR NORMAPUR) and used as received. Designated dry solvents were supplied by Acros Organics and stored over molecular sieves under inert gas atmosphere. Deuterated solvents were purchased from Eurisotop (99.8 % D). Water was deionized by a *Thermo Scientific Barnstead GenPure Pro UV*.

6.2 Instrumentation and Procedures

Nuclear Magnetic Resonance (NMR)

Proton nuclear magnetic resonance (^1H -NMR) and carbon nuclear magnetic resonance (^{13}C -NMR) spectra were recorded on a *Bruker Avance III* equipped with a *Bruker Ascend 400*. The samples were dissolved in CDCl_3 or CD_2Cl_2 and measured at 298 K. The chemical shifts δ are expressed in parts per million (ppm) relative to tetramethylsilane and calibrated on characteristic solvent signals as internal standards (CHCl_3 in CDCl_3 : $\delta_{\text{H}} = 7.26$ ppm, $\delta_{\text{C}} = 77.2$ ppm and CH_2Cl_2 in CD_2Cl_2 : $\delta_{\text{H}} = 5.32$ ppm), $\delta_{\text{C}} = 54.0$ ppm. Coupling constants J are absolute values and are expressed in Hertz (Hz). The multiplicities are abbreviated as following: s (singlet), d (doublet), t (triplet), q (quartet), qnt (quintet), m (multiplet), br (broadened signal).

Size Exclusion Chromatography (SEC)

Size exclusion chromatography (SEC) was conducted on a *Tosoh Bioscience EcoSEC HLC-8320GPC* equipped with a *PSS SDV* guard column (5 μm particle size, 8 \times 50 mm column size) and three *PSS SDV* analytical columns (5 μm particle size, 8 \times 300 mm column size, pore sizes: 100 000 \AA , 1000 \AA , 100 \AA), as well as both a differential refractive index detector and a UV detector (254 nm). THF was used as eluent with a flow rate of 1 mL min^{-1} at 35 $^{\circ}\text{C}$. Typically, 50 μL of a filtered sample solution with a concentration of 2.0 mg mL^{-1} was injected onto the columns. The system was

calibrated using narrow, linear polystyrene (PS) or poly(methyl methacrylate) (PMMA) standards from PSS ranging from 800 Da to 2.2 MDa.

Multiangle Light Scattering (MALS)

Multiangle Light Scattering (MALS) coupled to SEC was performed on a *Agilent Technologies 1260 Infinity II* equipped with a *PSS SDV* guard column (5 μm particle size, 8 \times 50 mm column size) and two *PSS SDV Lux* analytical columns (5 μm particle size, 8 \times 300 mm column size, pore sizes: 100 000 \AA , 1000 \AA). A *PSS SLD9000* was used as the light scattering detector with nine angles ranging from 12° to 164° together with a differential refractive index detector as concentration detector. THF was used as eluent with a flow rate of 1 mL min⁻¹ at 25 °C. For measurements, 50 μL of a filtered sample solution with an exactly determined concentration close to 2.0 mg mL⁻¹ was injected onto the columns.

Differential Scanning Calorimetry (DSC)

Differential scanning calorimetry (DSC) was done on a *TA Instruments DSC 2500* with 1–5 mg of the polymer in a sealed *TA Tzero* sample holder. The samples were subjected to a temperature range from -90 to 150 °C with a heating rate of 10 K min⁻¹ and a cooling rate of 5 K min⁻¹. The relevant thermal behavior was recorded on the second heating scan: the melting temperature T_m as the minimum of the endothermic melting peak and the glass transition temperature T_g as the inflection point.

UV/Vis Spectroscopy

UV/Vis absorbance spectra were recorded using an *Ocean Optics OceanHDX* equipped with an *Ocean Optics DH-mini* light source and an *Ocean Optics qpod 2e* sample compartment. The polymers were dissolved in dry chloroform with a concentration of 1 mg mL⁻¹. Solutions were measured in quartz cuvettes at ambient temperature and corrected against the UV/Vis absorbance of the solvent.

Polymer Electrolyte Preparation and Coin Cell Assembly

The respective polymer was completely dissolved in acetone. At the same time, a separate solution of a corresponding amount of LiTFSI in acetone was prepared to achieve $[\text{Li}^+]/[\text{O}]$ ratios of 1:10, 1:15, or 1:20. Subsequently, the solutions were combined and stirred for another 10 min. After the acetone was removed under reduced pressure again, the polymer electrolytes were dried at 80 °C under reduced pressure for 24 h.

For electrochemical impedance spectroscopy (EIS) measurements, coin cells (CR2032) were assembled using two stainless steel electrodes with a Mylar foil ring spacer (100 μm thickness, 8 mm inner diameter) in between. The dry polymer electrolytes were filled into the cavity of the ring spacer under dry argon atmosphere prior to sealing the cells. For measurements of transference numbers t_+ , an identical cell assembly was used with the addition of lithium foil as electrodes between the Mylar foil and stainless steel electrodes.

Electrochemical Impedance Spectroscopy (EIS)

Electrochemical impedance spectroscopy (EIS) was performed on a *BioLogic VMP-300* potentiostat over a frequency range from 5 MHz to 500 mHz with an amplitude of 10 mV. The measurements were carried out in 10 °C steps from 0 to 70 °C (and reverse) and each temperature step was maintained for 1 h prior to measurement to allow thermal equilibration. Additionally, each sample was measured twice at any given temperature. The ionic conductivity σ was calculated using the following equation:

$$\sigma = \frac{1}{R_b} \frac{d}{A}$$

The bulk resistance R_b can be accessed from the Nyquist plot of the EIS measurement (see figure 36), whereas the electrolyte thickness d (100 μm) and cross-sectional electrode contact area A (50.2655 mm^2) are confined by the Mylar foil ring spacer. For each polymer electrolyte, three coin cells were prepared, measured, and the results averaged.

The transference number t_+ was determined by the Bruce-Vincent method^[179,180] at 60 °C. The symmetric Li||Li cells were initially conditioned for 10 h to guarantee a stable interface between the electrolyte and the lithium metal. Constant current polarization was done by applying a voltage of $\Delta V = 10$ mV for 4 h, while EIS was measured directly before and after the polarization. The calculation of t_+ was done with the following equation:

$$t_+ = \frac{I_{ss} (\Delta V - I_0 R_0)}{I_0 (\Delta V - I_{ss} R_{ss})}$$

The initial current I_0 and the steady-state current I_{ss} can be derived from the polarization plot (see figure 25 on page 54). R_0 and R_{ss} are the interfacial electrode resistances before and after polarization, respectively.

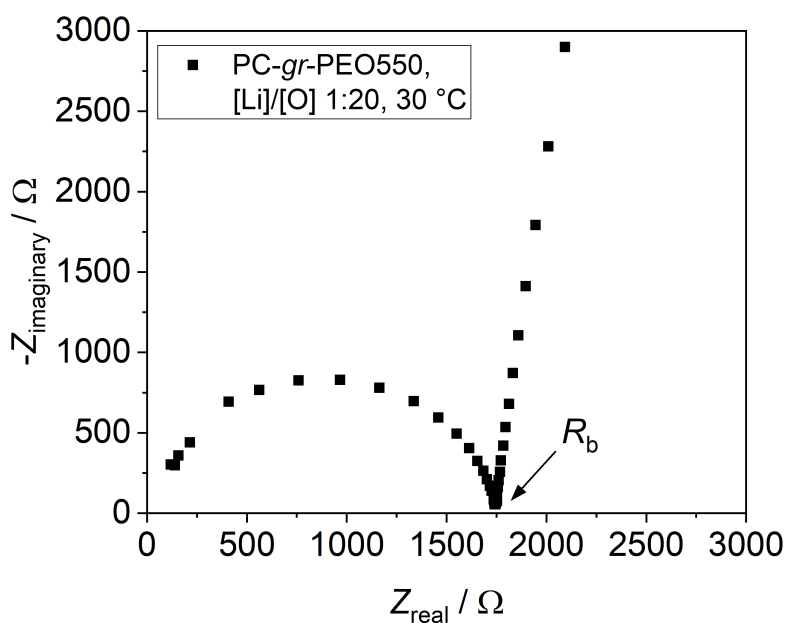
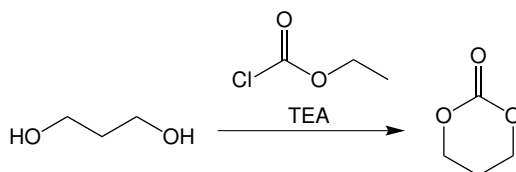


Figure 36: An exemplary EIS spectrum (Nyquist plot) of PC-*gr*-PEO550 at 30 °C with a $[Li^+]/[O]$ ratio of 1:20 is shown. The bulk resistance R_b is determined as the real part of the complex impedance Z at the end of the semicircle.

6.3 Synthesis of Cyclic Carbonates

The general cyclization approach was adapted from literature.^[184,185]

6.3.1 Trimethylene Carbonate (TMC)



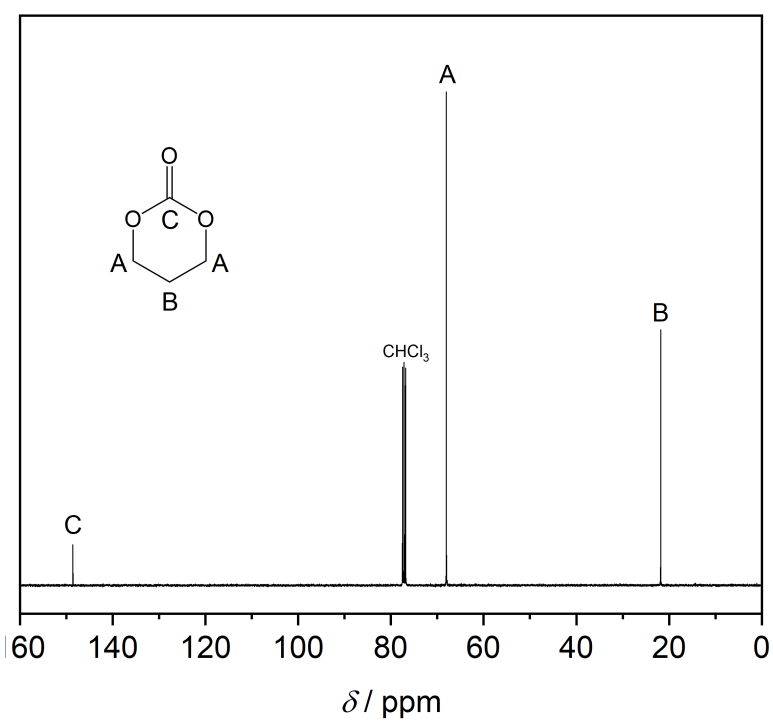
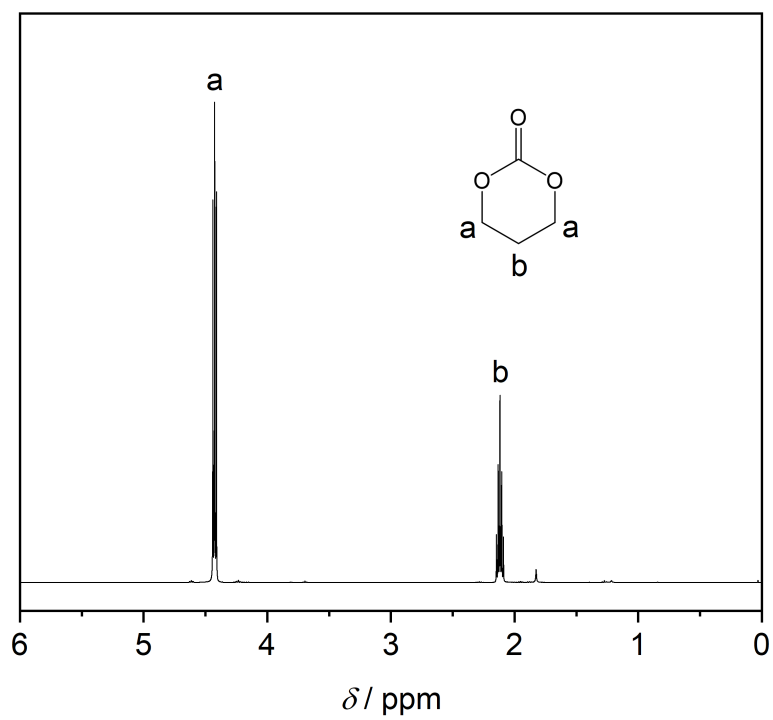
1,3-Propanediol (15.00 g, 197.1 mmol, 1.0 eq) was dissolved in 450 mL of dry THF. The solution was cooled to 0 °C and a solution of ethyl chloroformate (37.7 mL, 42.78 g, 394.2 mmol, 2.0 eq) in 110 mL of dry THF was slowly added. After stirring for 30 min, a solution of TEA (57.4 mL, 41.89 g, 414.0 mmol, 2.1 eq) in 40 mL of dry THF was added dropwise to the reaction mixture. After the addition was completed, the reaction was stirred for further 2 h at 0 °C and was then allowed to warm to ambient temperature and stirred overnight.

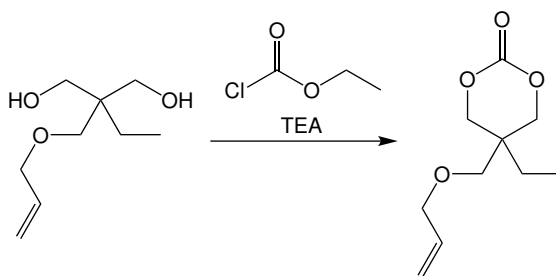
The reaction was filtrated and the solvent removed under reduced pressure. The residue was recrystallized four times from a 1:3 mixture of diethyl ether and THF to receive TMC as colorless crystalline needles (5.68 g, 55.6 mmol, 28 %).

The purity of this compound was not satisfactory for AROP.

¹H-NMR (400 MHz, CDCl₃): δ (ppm) = 4.43 (t, J = 5.7 Hz, 4 H, H_a), 2.12 (qnt, J = 5.7 Hz, 2 H, H_b).

¹³C-NMR (101 MHz, CDCl₃): δ (ppm) = 148.6 (C_C), 68.0 (C_A), 21.8 (C_B).



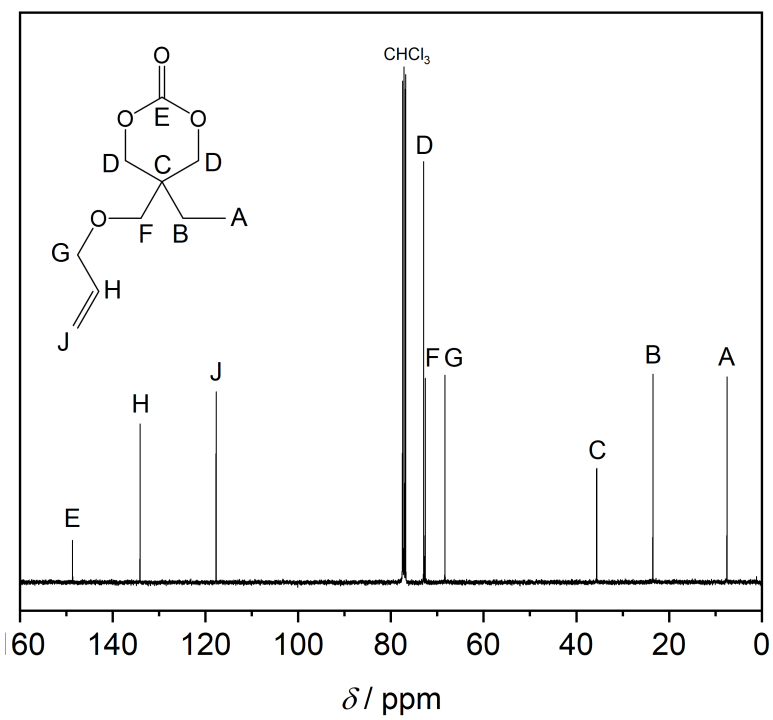
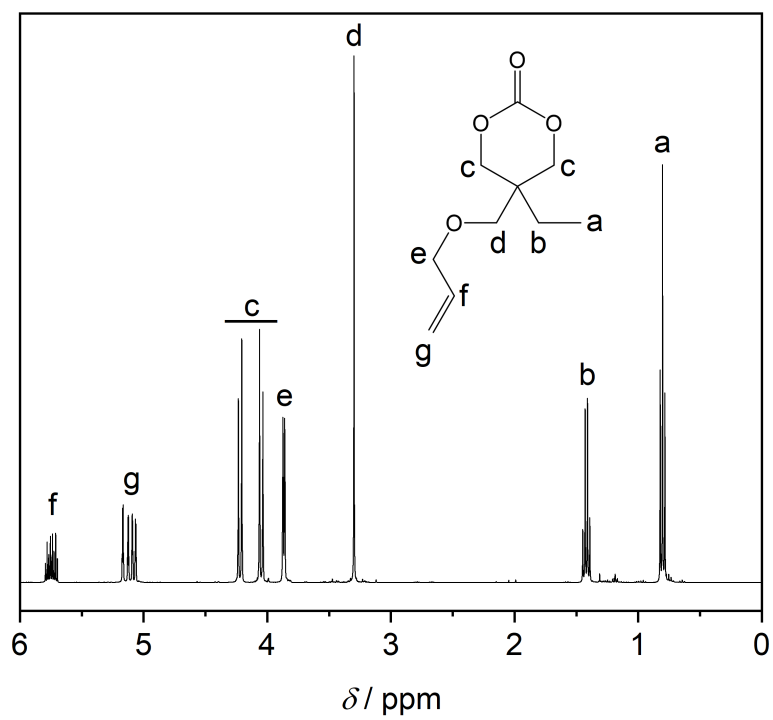
6.3.2 2-Allyloxymethyl-2-Ethyltrimethylene Carbonate (AOMECE)

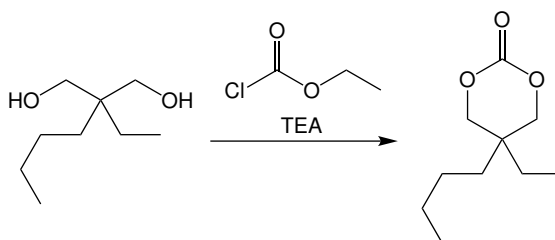
Trimethylolpropane monoallyl ether (80.00 g, 459.1 mmol, 1.0 eq) was dissolved in 1000 mL of dry THF. The solution was cooled to 0 °C and ethyl chloroformate (87.8 mL, 99.65 g, 918.3 mmol, 2.0 eq) was slowly added. After stirring for 30 min, a solution of TEA (127.3 mL, 92.92 g, 918.3 mmol, 2.0 eq) in 600 mL of dry THF was added dropwise to the reaction mixture. After the addition was completed, the reaction was stirred for further 1 h at 0 °C and was then allowed to warm to ambient temperature and stirred overnight.

The reaction was filtrated and the solvent removed under reduced pressure. The residue was redissolved in 400 mL of ethyl acetate. This solution was washed twice with 400 mL of 1 M HCl and twice with 400 mL of H₂O. After the organic phase was dried over MgSO₄, the solvent was removed under reduced pressure. The resulting yellowish oil was purified by vacuum distillation (boiling point: 135 °C at 0.5 mbar) to receive AOMECE as a clear, colorless oil (69.70 g, 348.1 mmol, 76 %).

¹H-NMR (400 MHz, CDCl₃): δ (ppm) = 5.75 (ddt, J = 17.2 Hz, 10.4 Hz, 5.5 Hz, 1 H, H_f), 5.15 (dq, J = 17.3 Hz, 1.7 Hz, 1 H, H_{g,trans}), 5.08 (dq, J = 10.4 Hz, 1.4 Hz, 1 H, H_{g,cis}), 4.13 (dd, J = 68.5 Hz, 10.9 Hz, 4 H, H_c), 3.87 (dt, J = 5.5 Hz, 1.5 Hz, 2 H, H_e), 3.30 (s, 2 H, H_d), 1.42 (q, J = 7.6 Hz, 2 H, H_b), 0.80 (t, J = 7.6 Hz, 3 H, H_a).

¹³C-NMR (101 MHz, CDCl₃): δ (ppm) = 148.7 (C_E), 134.1 (C_H), 117.7 (C_J), 72.9 (C_D), 72.6 (C_F), 68.4 (C_G), 35.6 (C_C), 23.5 (C_B), 7.5 (C_A).



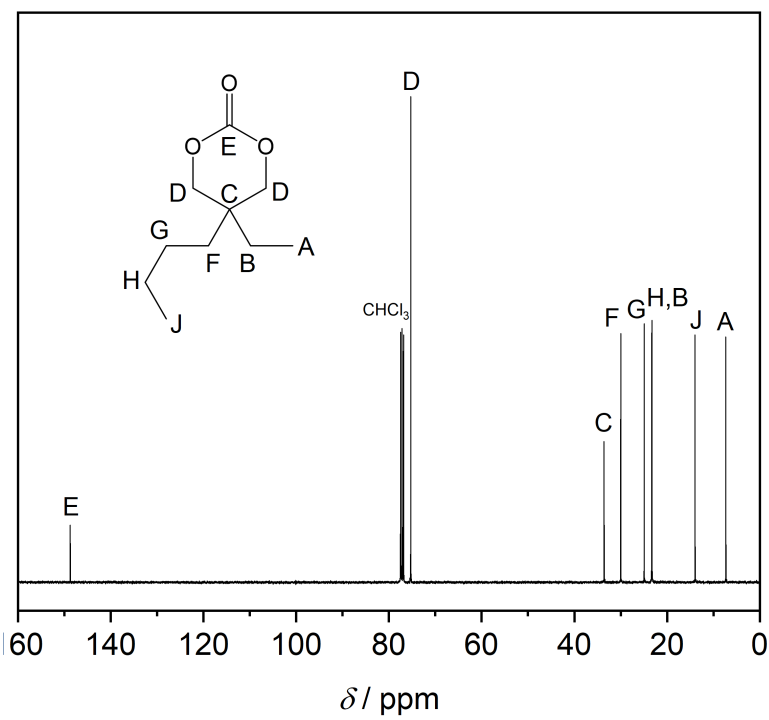
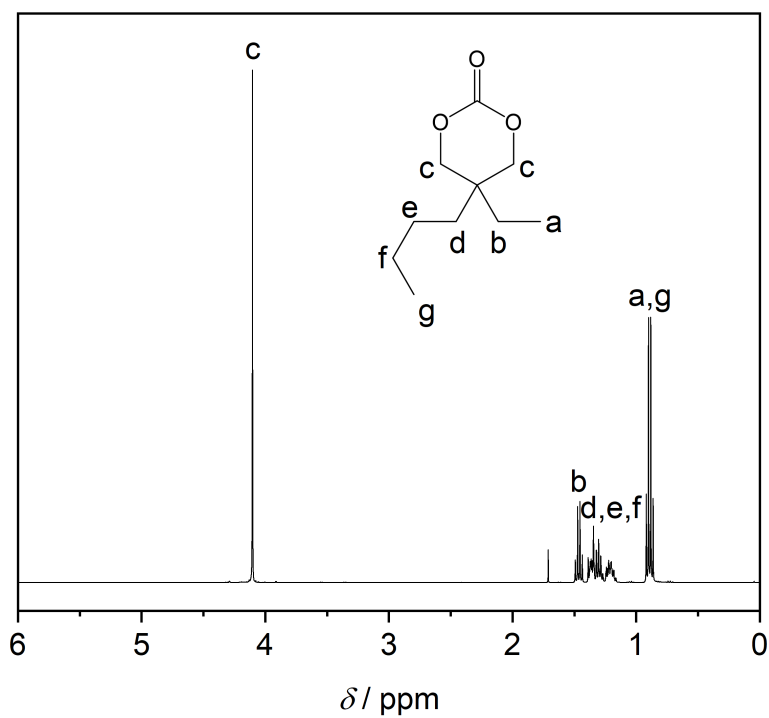
6.3.3 2-Butyl-2-Ethyltrimethylene Carbonate (BEC)

2-Butyl-2-ethyl-1,3-propanediol (25.00 g, 156.0 mmol, 1.0 eq) was dissolved in 320 mL of dry THF. The solution was cooled to 0 °C and ethyl chloroformate (29.9 mL, 33.86 g, 312.0 mmol, 2.0 eq) was slowly added. After stirring for 30 min, a solution of TEA (43.3 mL, 31.57 g, 312.0 mmol, 2.0 eq) in 190 mL of dry THF was added dropwise to the reaction mixture. After the addition was completed, the reaction was stirred for further 1 h at 0 °C and was then allowed to warm to ambient temperature and stirred overnight.

The reaction was filtrated and the solvent removed under reduced pressure. The residue was redissolved in 125 mL of ethyl acetate. This solution was washed twice with 125 mL of 1 M HCl and twice with 125 mL of H₂O. After the organic phase was dried over MgSO₄, the solvent was removed under reduced pressure. The resulting yellowish oil was purified by vacuum distillation (boiling point: 130 °C at 1.0 mbar) to receive BEC as a clear, colorless oil (23.06 g, 123.8 mmol, 79%).

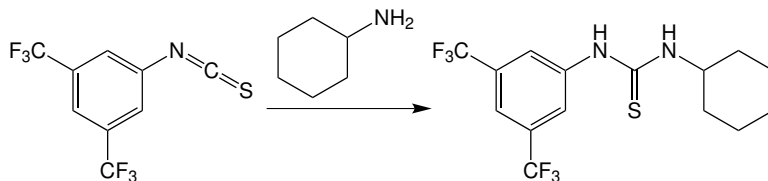
¹H-NMR (400 MHz, CDCl₃): δ (ppm) = 4.10 (s, 4 H, H_C), 1.46 (q, J = 7.6 Hz, 2 H, H_B), 1.39–1.16 (m, 6 H, H_{d,e,f}), 0.89 (q, J = 7.4 Hz, 6 H, H_{a,g}).

¹³C-NMR (101 MHz, CDCl₃): δ (ppm) = 148.7 (C_E), 75.3 (C_D), 33.6 (C_C), 30.0 (C_F), 24.9 (C_G), 23.3 (C_H), 23.2 (C_B), 14.0 (C_J), 7.3 (C_A).



6.4 Anionic Ring-Opening Polymerization

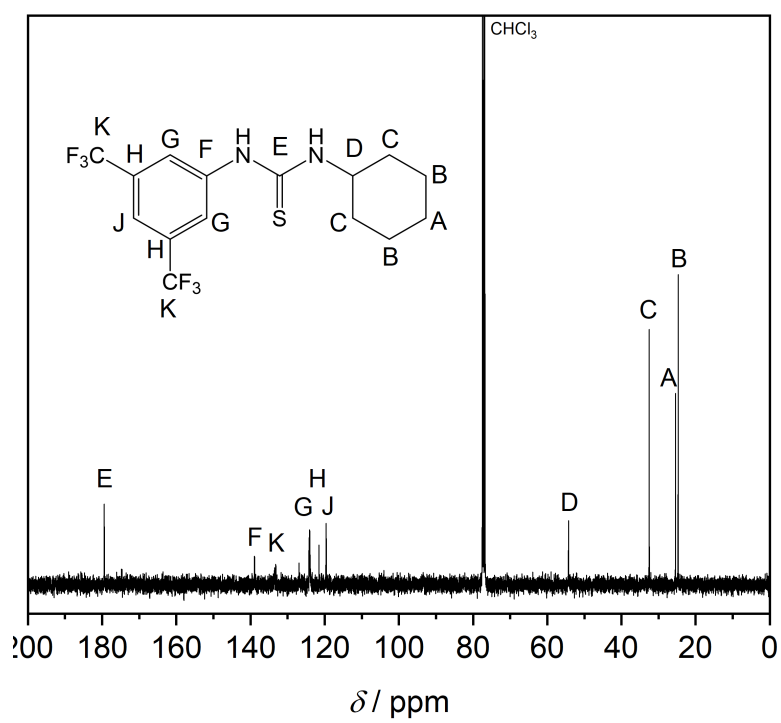
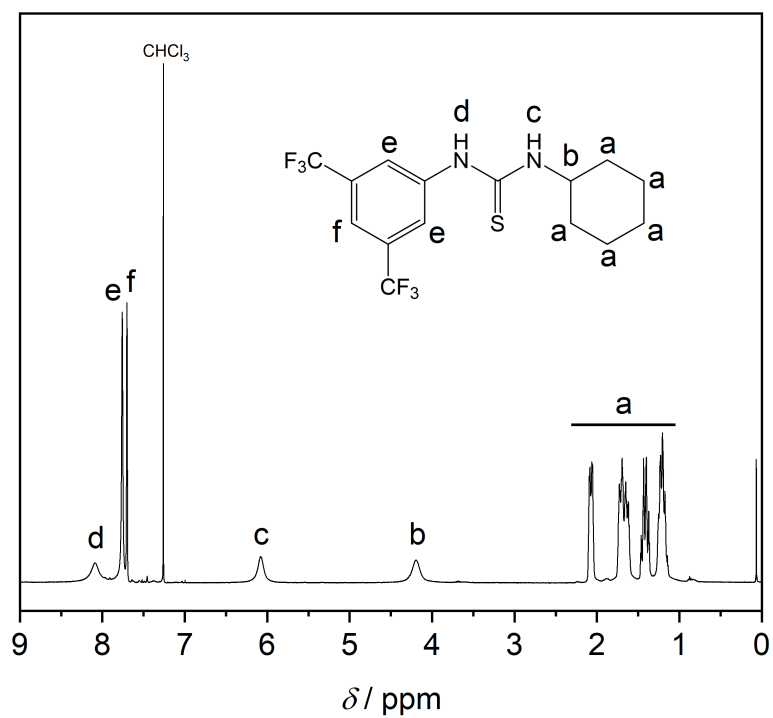
6.4.1 Synthesis of Thiourea Cocatalyst (TUC)



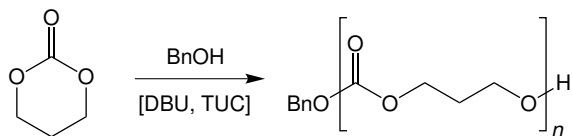
The synthesis of *N*-(3,5-bis(trifluoromethyl)phenyl)-*N'*-cyclohexylthiourea was done according to literature.^[166] A solution of 3,5-bis(trifluoromethyl)phenyl isocyanate (10.0 g, 36.88 mmol, 1.0 eq) in 40 mL of dry THF was prepared under inert gas and cooled to 0 °C. After cyclohexylamine (4.23 mL, 3.66 g, 36.88 mmol, 1.0 eq) was added, the reaction mixture was allowed to warm to ambient temperature and stirred overnight. The solvent was then removed under reduced pressure and the residue was recrystallized from chloroform and dried *in vacuo* to yield TUC as a colorless powder (11.891 g, 32.11 mmol, 87 %).

¹H-NMR (400 MHz, CDCl₃): δ (ppm) = 8.09 (br, 1 H, H_d), 7.76 (s, 2 H, H_e), 7.70 (s, 1 H, H_f), 6.08 (br, 1 H, H_c), 4.19 (br, 1 H, H_b), 2.09–1.17 (m, 10 H, H_a).

¹³C-NMR (101 MHz, CDCl₃): δ (ppm) = 179.8 (C_E), 139.8 (C_F), 132.9 (q, J = 34.9 Hz, C_K), 124.1 (C_G), 121.5 (C_H), 119.5 (C_J), 54.2 (C_D), 32.7 (C_C), 25.7 (C_A), 25.1 (C_B).



6.4.2 Polymerization of TMC



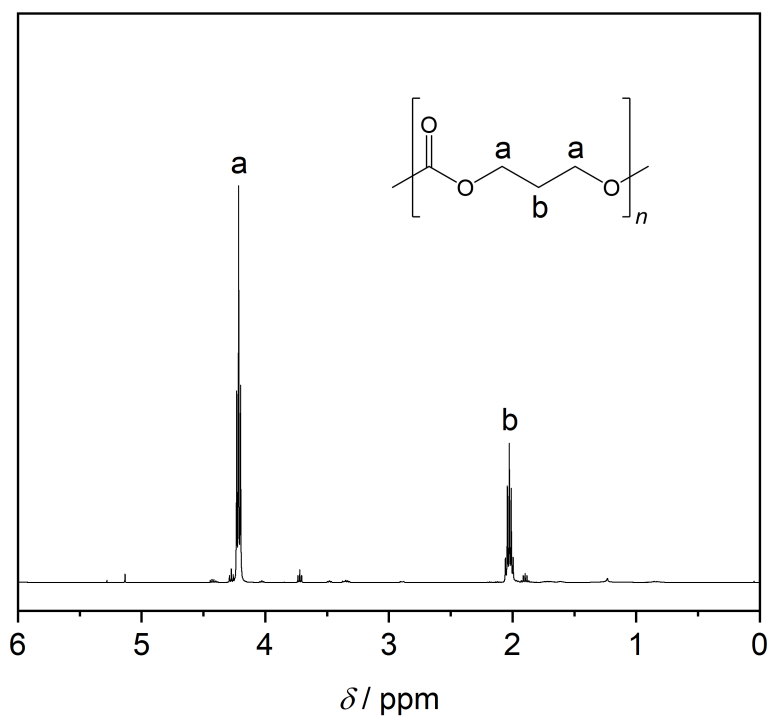
TMC (2.00 g, 19.6 mmol, 100.0 eq) was dissolved in 9.8 mL of dry DCM ($[M] = 2 \text{ M}$) under inert gas in a thoroughly dried flask. This solution was kept stirring over CaH_2 overnight.

Afterwards, the solution was transferred to a different thoroughly dried flask through a syringe filter. The solution was pre-heated to 30°C and then in quick succession firstly DBU (73 μL , 74.5 mg, 0.49 mmol, 2.5 eq) and secondly benzyl alcohol (20.3 μL , 21.2 mg, 0.196 mmol, 1.0 eq) were added.

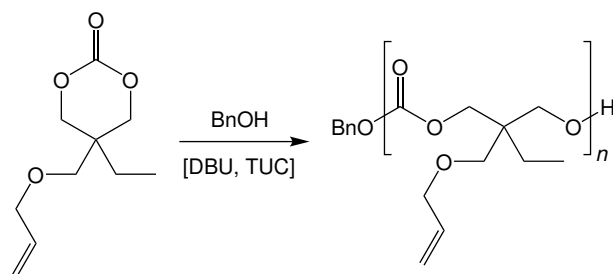
After 24 h polymerization time, the reaction was stopped by adding 375 mg of benzoic acid dissolved in little DCM to the solution. The polymer was recovered by precipitation into 60 mL of methanol in an ethyl acetate/liquid nitrogen cooling bath (-84°C) and subsequently decanting the supernatant. Drying the polymer *in vacuo* resulted in PTMC as a colorless viscous mass (typical monomer conversion 90 %).

The received polymer always featured a bimodal distribution.

$^1\text{H-NMR}$ (400 MHz, CDCl_3): δ (ppm) = 4.22 (t, $J = 6.3 \text{ Hz}$, 4 H, H_a), 2.03 (qnt, $J = 6.2 \text{ Hz}$, 2 H, H_b).



6.4.3 Polymerization of AOMEAC



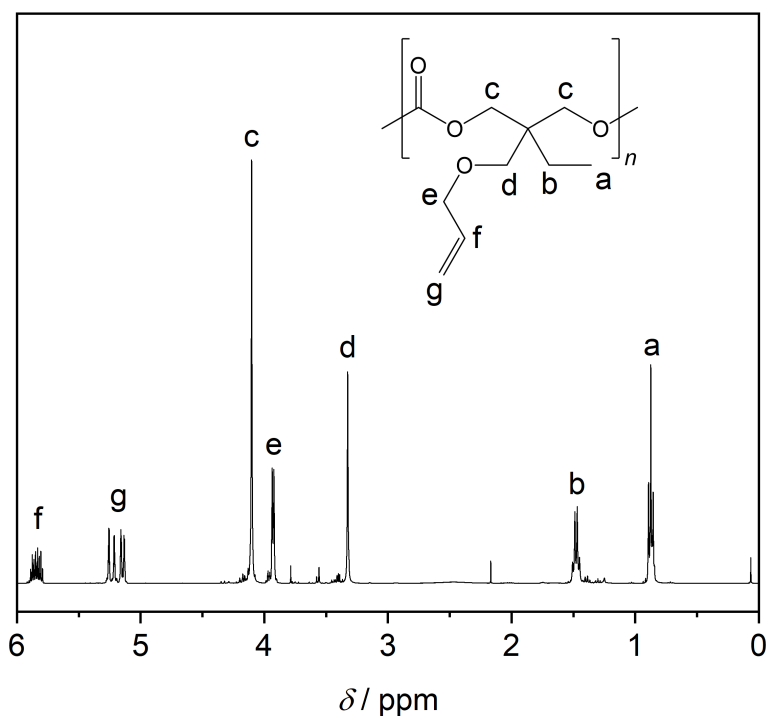
AOMEAC (29.0 g, 144.8 mmol, 50.0 eq) was dissolved in 72.5 mL of dry DCM ($[M] = 2 \text{ M}$) under inert gas in a thoroughly dried flask. To that solution, TUC (2682 mg, 7.24 mmol, 2.5 eq) was added. This solution was kept stirring over CaH_2 overnight.

Afterwards, the solution was transferred to a different thoroughly dried flask through a syringe filter. The solution was pre-heated to 30°C and then in quick succession firstly DBU (1083 μL , 1102.4 mg, 7.24 mmol, 2.5 eq) and secondly benzyl alcohol (300 μL , 313.2 mg, 2.90 mmol, 1.0 eq) were added.

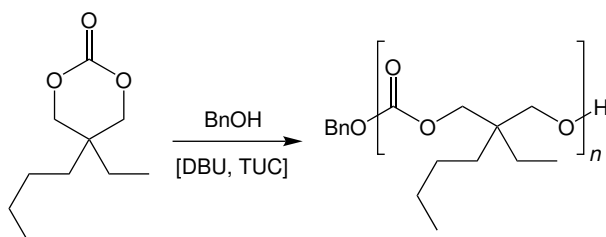
After 24 h polymerization time, the reaction was stopped by adding 5510 mg of benzoic

acid dissolved in little DCM to the solution. The polymer was recovered by precipitation into 435 mL of methanol in an ethyl acetate/liquid nitrogen cooling bath ($-84\text{ }^{\circ}\text{C}$) and subsequently decanting the supernatant. Drying the polymer *in vacuo* resulted in PAOMEC as a colorless viscous mass (typical monomer conversion 73%).

$^1\text{H-NMR}$ (400 MHz, CDCl_3): δ (ppm) = 5.84 (ddt, $J = 17.3\text{ Hz}, 10.7\text{ Hz}, 5.5\text{ Hz}, 1\text{ H}, \text{H}_f$), 5.23 (dq, $J = 17.3\text{ Hz}, 1.7\text{ Hz}, 1\text{ H}, \text{H}_{g,\text{trans}}$), 5.15 (dq, $J = 10.5\text{ Hz}, 1.5\text{ Hz}, 1\text{ H}, \text{H}_{g,\text{cis}}$), 4.10 (s, 4 H, H_c), 3.93 (dt, $J = 5.5\text{ Hz}, 1.5\text{ Hz}, 2\text{ H}, \text{H}_e$), 3.33 (s, 2 H, H_d), 1.48 (q, $J = 7.6\text{ Hz}, 2\text{ H}, \text{H}_b$), 0.87 (t, $J = 7.6\text{ Hz}, 3\text{ H}, \text{H}_a$).



6.4.4 Polymerization of BEC

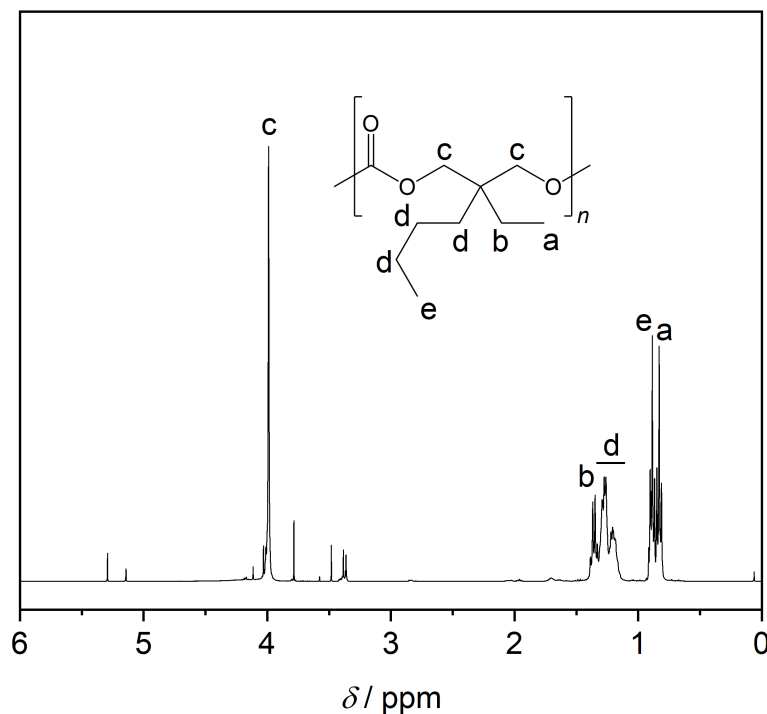


BEC (9.0 g, 48.3 mmol, 50.0 eq) was dissolved in 24 mL of dry DCM ($[M] = 2 \text{ M}$) under inert gas in a thoroughly dried flask. To that solution, TUC (895 mg, 2.42 mmol, 2.5 eq) was added. This solution was kept stirring over CaH_2 overnight.

Afterwards, the solution was transferred to a different thoroughly dried flask through a syringe filter. The solution was pre-heated to 30°C and then in quick succession firstly DBU (361 μL , 367.8 mg, 2.42 mmol, 2.5 eq) and secondly benzyl alcohol (100 μL , 104.5 mg, 0.97 mmol, 1.0 eq) were added.

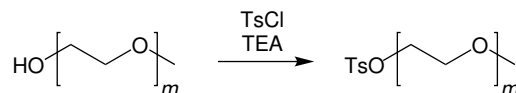
After 24 h polymerization time, the reaction was stopped by adding 1840 mg of benzoic acid dissolved in little DCM to the solution. The polymer was recovered by precipitation into 145 mL of methanol in an ethyl acetate/liquid nitrogen cooling bath (-84°C) and subsequently decanting the supernatant. Drying the polymer *in vacuo* resulted in PBEC as a colorless viscous mass (typical monomer conversion 65%).

$^1\text{H-NMR}$ (400 MHz, CDCl_3): δ (ppm) = 3.99 (s, 4 H, H_c), 1.36 (q, $J = 7.5 \text{ Hz}$, 2 H, H_b), 1.31–1.16 (m, 6 H, H_d), 0.89 (t, $J = 7.2 \text{ Hz}$, 3 H, H_e), 0.83 (t, $J = 7.5 \text{ Hz}$, 3 H, H_a).



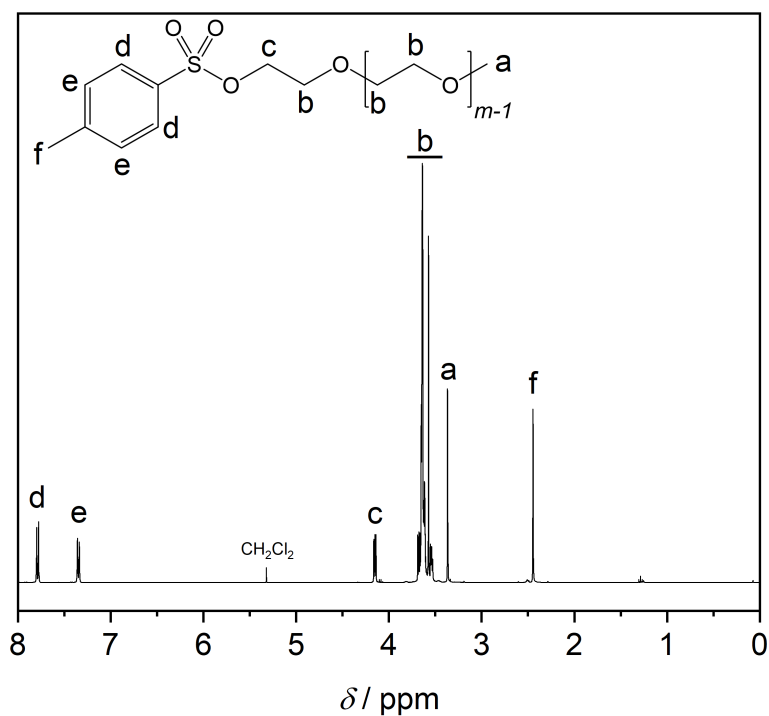
6.5 Thiolation of PEO

6.5.1 Tosylation

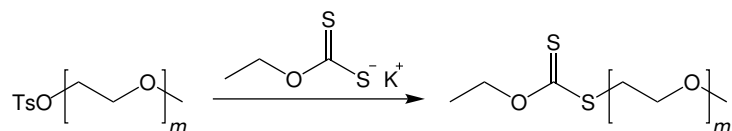


A solution of mPEO-OH (100 g, 1.0 EG eq) in 500 mL of dry DCM was prepared under inert gas at 0 °C, to which triethylamine (1.5 eq) was added. After stirring for 20 min, tosyl chloride (1.2 eq) was added in portions over further 20 min to the reaction. The solution was kept stirring for 1 h at 0 °C and then at ambient temperature overnight. Afterwards, the reaction was washed three times with 300 mL of 1 M HCl, once with 300 mL of saturated NaHCO₃ solution and twice with 300 mL of H₂O. The combined aqueous phases were then extracted twice with 400 mL of DCM. The combined organic phases were then dried over MgSO₄ and the solvent was removed under reduced pressure. The resulting oil was mixed with 400 mL of H₂O and washed four times with 400 mL of hexane. Afterwards, the aqueous phase was extracted twice with 400 mL of DCM and dried over MgSO₄. The removal of the solvent under reduced pressure resulted in mPEO-OTs as either a slightly yellow oil or an offwhite wax-like solid depending on polymerization degree (typical yields: 80–90 %).

¹H-NMR (400 MHz, CD₂Cl₂): δ (ppm) = 7.79 (d, *J* = 8.4 Hz, 2 H, H_d), 7.35 (d, *J* = 8.1 Hz, 2 H, H_e), 4.15 (t, *J* = 4.8 Hz, 2 H, H_c), 3.80–3.43 (m, (4*m*-2) H, H_b), 3.37 (s, 3 H, H_a), 2.45 (s, 3 H, H_f).



6.5.2 Xanthation

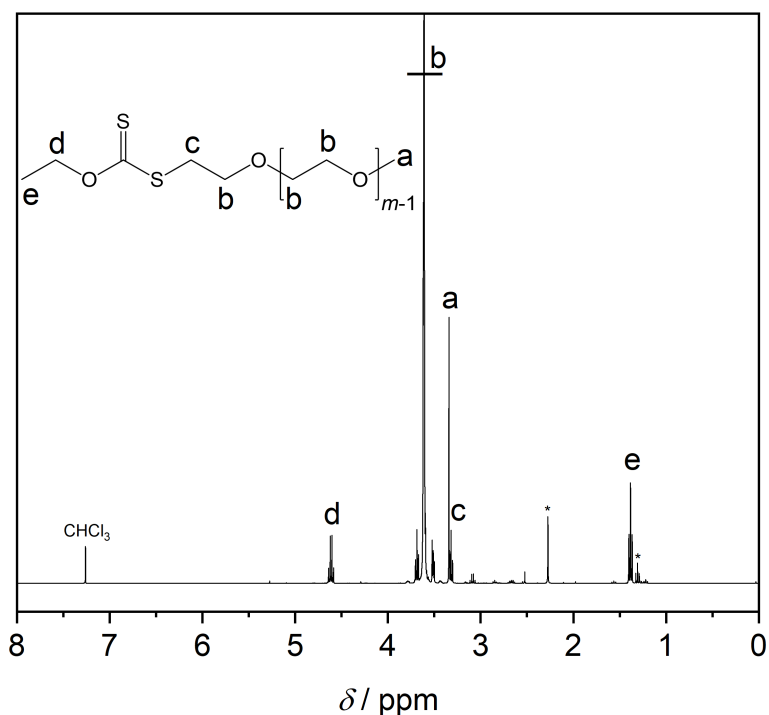


mPEO-OTs (75 g, 1.0 EG eq) was dissolved in 1200 mL of dry acetonitrile under inert gas and cooled to 0 °C. This solution was stirred vigorously and potassium ethylxanthate (1.5 eq) was added in portions over 40 min. After stirring for further 2 h at 0 °C the reaction was allowed to warm to ambient temperature overnight under continued vigorous stirring.

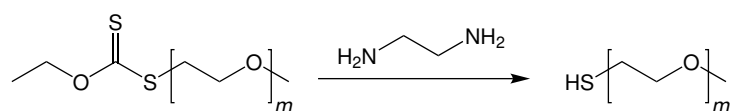
This mixture was then mixed with Celite (2–3 times the weight of xanthate added) and filtered. After thoroughly washing the precipitate with further acetonitrile, the solvent was removed under reduced pressure. The residue was redissolved in 250 mL of DCM and washed four times with 200 mL of H₂O. The organic phase was dried over MgSO₄ and the solvent removed under reduced pressure to yield mPEO-XEt as either a bright yellow oil or a yellow wax-like solid depending on polymerization degree (typical yields:

70–80 %).

$^1\text{H-NMR}$ (400 MHz, CDCl_3): δ (ppm) = 4.57 (q, $J = 7.1$ Hz, 2 H, H_d), 3.66–3.46 (m, $(4m-2)$ H, H_b), 3.30 (s, 3 H, H_a), 3.28 (t, $J = 6.6$ Hz, 2 H, H_c), 1.35 (t, $J = 7.1$ Hz, 3 H, H_e).



6.5.3 Aminolysis

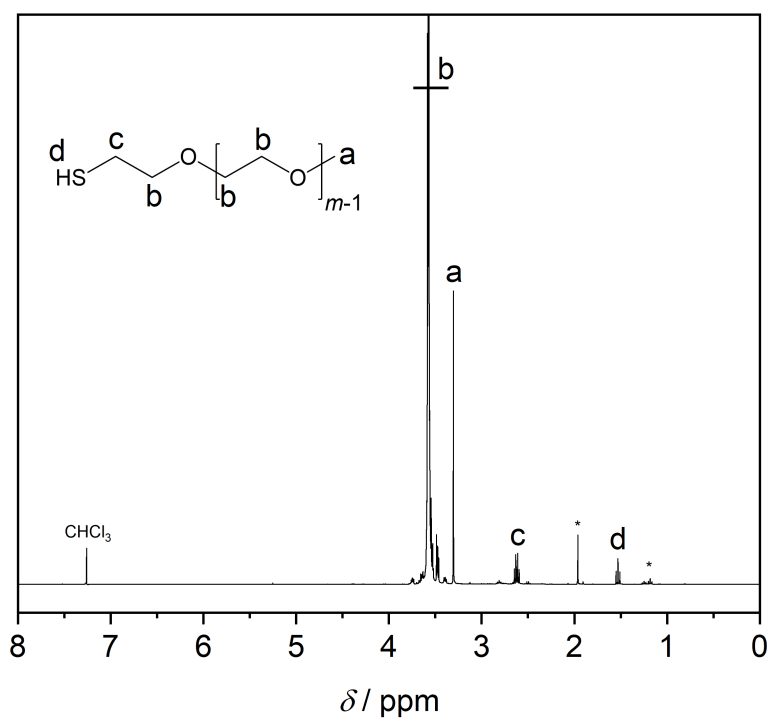


The mPEO-XEt (30 g, 1.0 EG eq) was dissolved in a mixture of 400 mL of H_2O and 100 mL of THF under inert gas. To this solution, ethylenediamine (10.0 eq) was added and stirred at ambient temperature overnight.

Afterwards, 250 mL of 1 M HCl was added to the solution and the reaction was extracted three times with 250 mL of DCM. After washing the combined organic phases twice with 250 mL of saturated NaCl solution, the solution was dried over MgSO_4 . The removal of

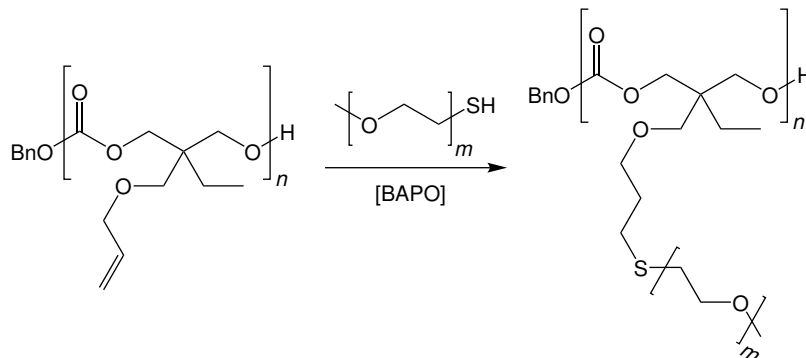
the solvent under reduced pressure resulted in mPEO-SH as either a colorless oil or an offwhite wax-like solid depending on polymerization degree (typical yields: 85–95%). In the case that a batch had been stored for longer than a month, the thiol was reduced prior to use by the following protocol: The potential thiol/disulfide mixture of PEO (8 g, 1.0 EG eq) was dissolved in 150 mL of H₂O under inert gas. TCEP·HCl (1.0 eq) was added and the solution stirred at ambient temperature overnight. Afterwards, the reaction solution was extracted three times with 100 mL of DCM. The organic phase was dried over MgSO₄ and the solvent removed under reduced pressure.

¹H-NMR (400 MHz, CDCl₃): δ (ppm) = 3.44–3.37 (m, (4*m*-2) H, H_b), 3.14 (s, 3 H, H_a), 2.46 (dt, *J* = 8.2 Hz, 6.4 Hz, 2 H, H_c), 1.41 (t, *J* = 8.2 Hz, 1 H, H_d).



6.6 Thiol-ene Addition

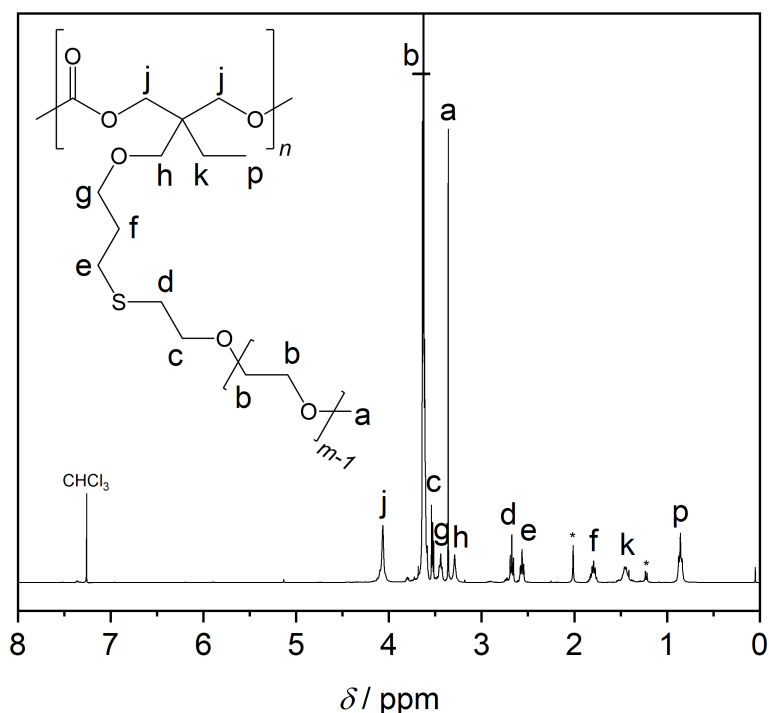
6.6.1 General Procedure for Post-Polymerization Modification



Typically, PAOMEC (350 mg, 1.0 RU eq) was dissolved in dry dioxane (5 mL per 1 g combined mass of reactants). Afterwards, the desired amount of mPEO-SH (2.0 EG eq for mPEO400, mPEO550, and mPEO1000; 4.0 EG eq for mPEO2000) and BAPO (0.1 eq) were added. The solution was sparged with dry nitrogen and then irradiated with an Osram Dulux Blue UVA lamp (32 W, 355–390 nm, max. 370 nm) for 4 h.

The solution was then diluted with THF equal to 1.5 times the amount of solvent. Spectra/Por 7 RC membranes (MWCO: 8 kDa for mPEO400; 15 kDa for mPEO550; 25 kDa for mPEO1000; 50 kDa for mPEO2000) was thoroughly rinsed with water and then submerged in water for at least 30 min. Afterwards, the tubing was loaded with the sample, closed off with dialysis clips and dialyzed against 2 L of THF. The dialysate was exchange daily and the dialysis time was typically 7 d for mPEO400, mPEO550, and mPEO1000; and 30 d for mPEO2000. After removal of the solvent, the polymer was extensively dried *in vacuo* (typically quantitative double bond conversion).

¹H-NMR (400 MHz, CDCl₃): δ (ppm) = 4.07 (s, 4 H, H_i), 3.73–3.57 (m, (4*m*-4) H, H_b), 3.54–3.52 (m, 2 H, H_c), 3.44 (t, *J* = 6.2 Hz, 2 H, H_g), 3.36 (s, 3 H, H_a), 3.29 (s, 2 H, H_h), 2.68 (t, *J* = 7.1 Hz, 2 H, H_d), 2.56 (t, *J* = 7.2 Hz, 2 H, H_e), 1.80 (tt, *J* = 7.2 Hz, 6.2 Hz, 2 H, H_f), 1.44 (q, *J* = 7.6 Hz, 2 H, H_k), 0.86 (t, *J* = 7.6 Hz, 3 H, H_p).



6.6.2 Crosslinking

PAOMEC (300.0 mg, 1.0 RU eq) was dissolved in 2.5 mL of dry THF. BMEE (134.5 mg, 738 μmol , 0.5 eq), LiTFSI (106.5 mg, [Li]/[O] ratio 1:20), and BAPO (61.8 mg, 148 μmol , 0.1 eq) were added to the solution. The mixture was stirred to homogeneity and then filled into a PTFE petridish (diameter 4 cm).

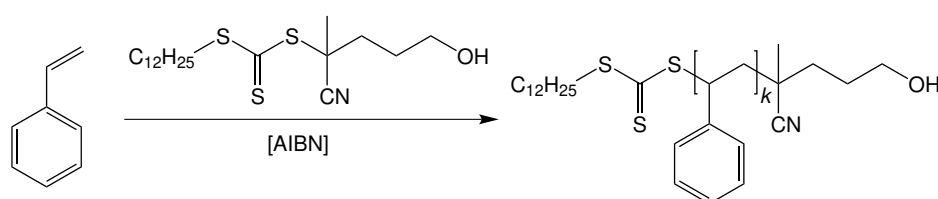
Alternatively, PAOMEC (300.0 mg, 1.0 RU eq) was dissolved in 5 mL of THF. PEO1000-dithiol, synthesized from bishydroxy-PEO1000 following the aforementioned protocol (0.5 EG eq), LiTFSI (318.4 mg, [Li]/[O] ratio 1:20), and BAPO (61.8 mg, 148 μmol , 0.1 eq) were added to the solution. The mixture was stirred to homogeneity and then filled into a PTFE petridish (diameter 6 cm).

In both cases, the reaction was irradiated with an Osram Dulux Blue UVA lamp (32 W, 355–390 nm, max. 370 nm) for 4 h. The remaining solvent was slowly evaporated and the resulting polymer film thoroughly dried *in vacuo* at 80 °C. No analysis in terms of conversion was conducted. Discs with a diameter of 16 mm were cut out from the films, their thickness determined (850 μm for the first network, 400 μm for the second

network), and then placed in a coin cell assembly in place of the Mylar foil spacer. The coin cells were conditioned at 80 °C for 24 h prior to following the general procedure for EIS measurements.

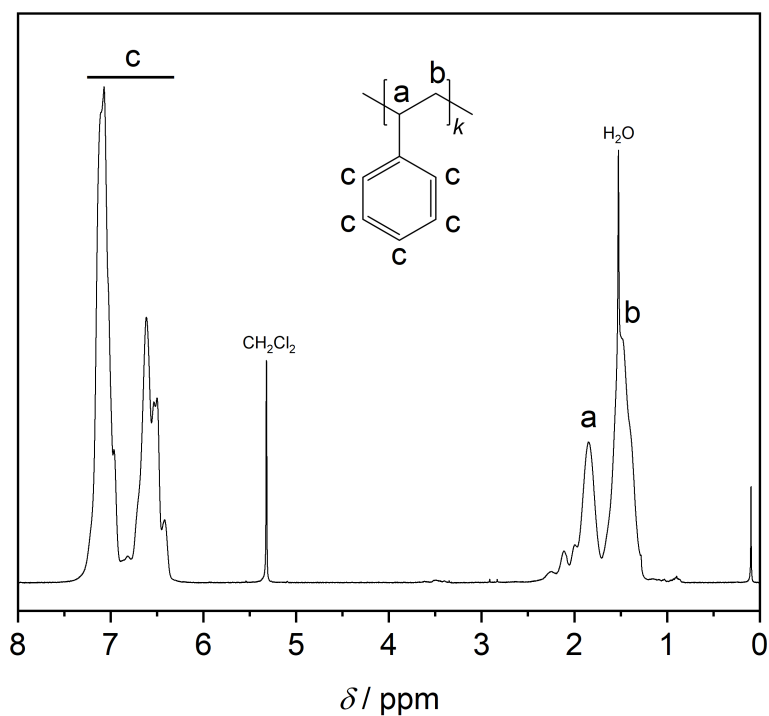
6.7 PS Block Copolymerization Approach

6.7.1 RAFT Polymerization of Styrene

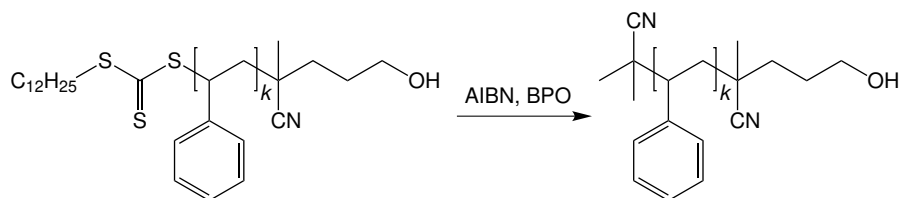


Styrene (32.00 g, 307.243 mmol, 1000.0 eq) was dissolved in 64 mL of dry toluene under inert gas. After 4-cyano-4-[(dodecylsulfanylthiocarbonyl)sulfanyl]pentanol (119.7 mg, 307 μ mol, 1.0 eq) and AIBN (10.1 mg, 61 μ mol, 0.2 eq) were added, the solution was degassed by three freeze-pump-thaw cycles. The reaction was then placed in a preheated oil bath at 70 °C. After 24 h of reaction time, the polymerization was stopped by brief cooling in liquid nitrogen. The polymer was then precipitated into 1200 mL of icecold methanol twice. The resulting yellowish powder was dried *in vacuo* (typical monomer conversion 17%).

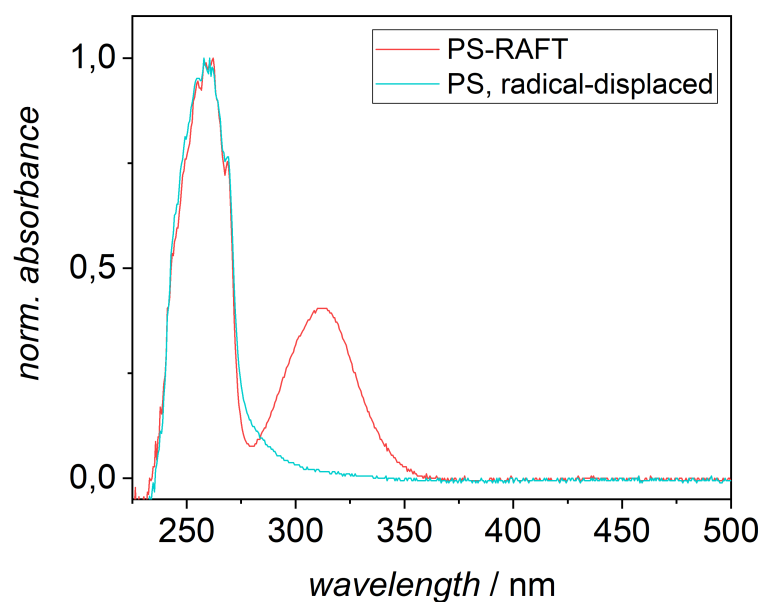
$^1\text{H-NMR}$ (400 MHz, CD_2Cl_2): δ (ppm) = 7.15–6.40 (m, 5 H, H_c), 2.12–1.80 (m, 1 H, H_a), 1.59–1.29 (m, 2 H, H_b).



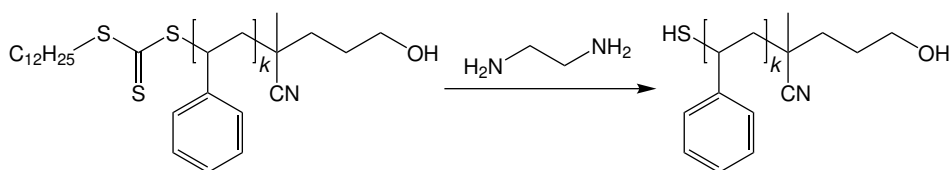
6.7.2 CTA Endgroup Removal *via* Radical Displacement



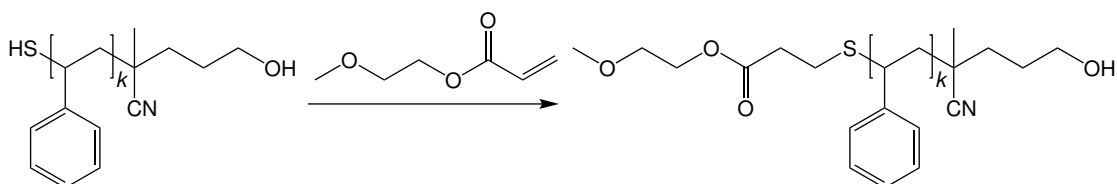
The hydroxy-PS-RAFT (2.00 g, 1.0 EG eq) was dissolved in 40 mL of dry toluene. Afterwards, AIBN (20.0 eq) and BPO (5.0 eq) were added and the solution sparged with dry nitrogen. The reaction mixture was heated to 90 °C. The same amount of AIBN and BPO were added after 4 h once again. After further 4 h, the polymer was precipitated into 800 mL of icecold methanol twice and dried *in vacuo* to yield a colorless powder.



6.7.3 CTA Endgroup Removal via Aminolysis

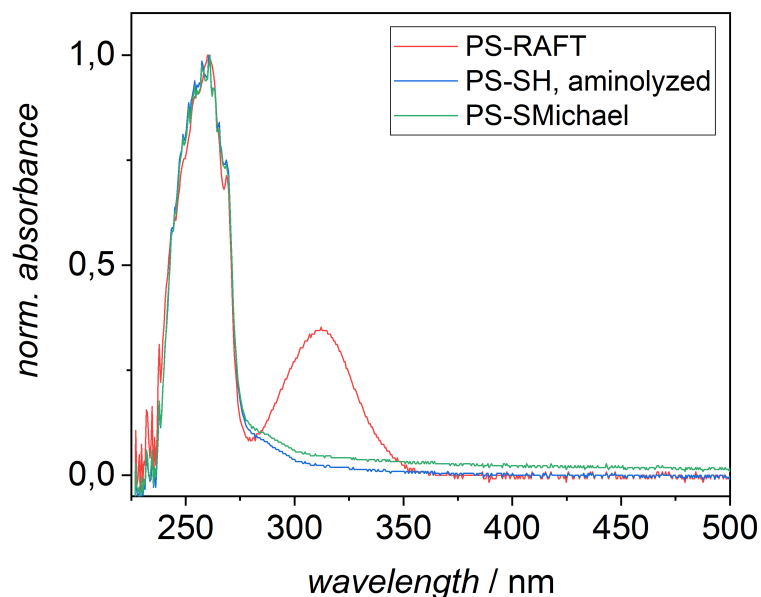


The hydroxy-PS-RAFT (2.50 g, 1.0 EG eq) was dissolved in 50 mL of ethyl acetate. Afterwards, ethylenediamine (60.0 eq) was added and the solution stirred at ambient temperature overnight. The polymer was precipitated into 1000 mL of icecold methanol twice and dried *in vacuo* to yield a colorless powder.

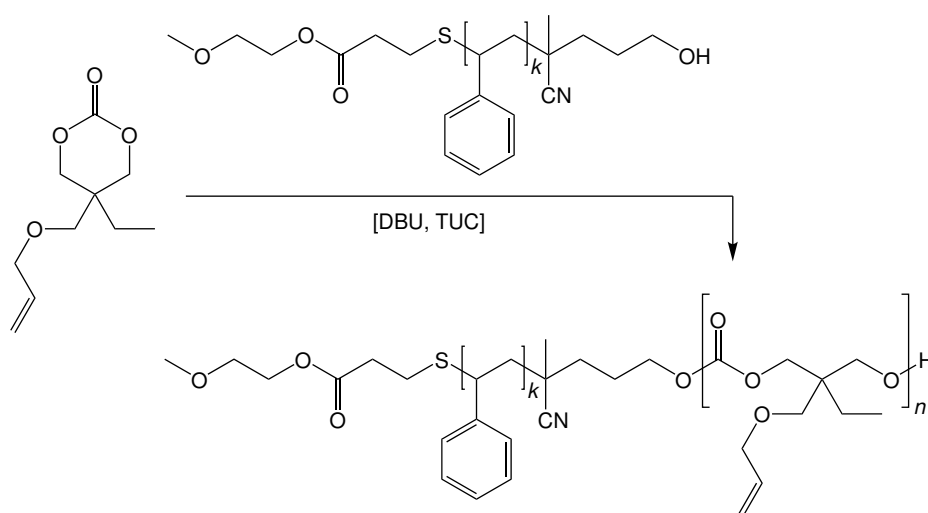


The previously aminolyzed hydroxy-PS-SH (2.00 g, 1.0 EG eq) was dissolved in 50 mL of dry THF. Then, triethylamine (1.2 eq) and 2-methoxyethyl acrylate (2.2 eq) were

added and the solution was stirred at ambient temperature overnight. The polymer was precipitated into 1000 mL of icecold methanol twice and dried in vacuo to yield a colorless powder.



6.7.4 AROP Chain Extension



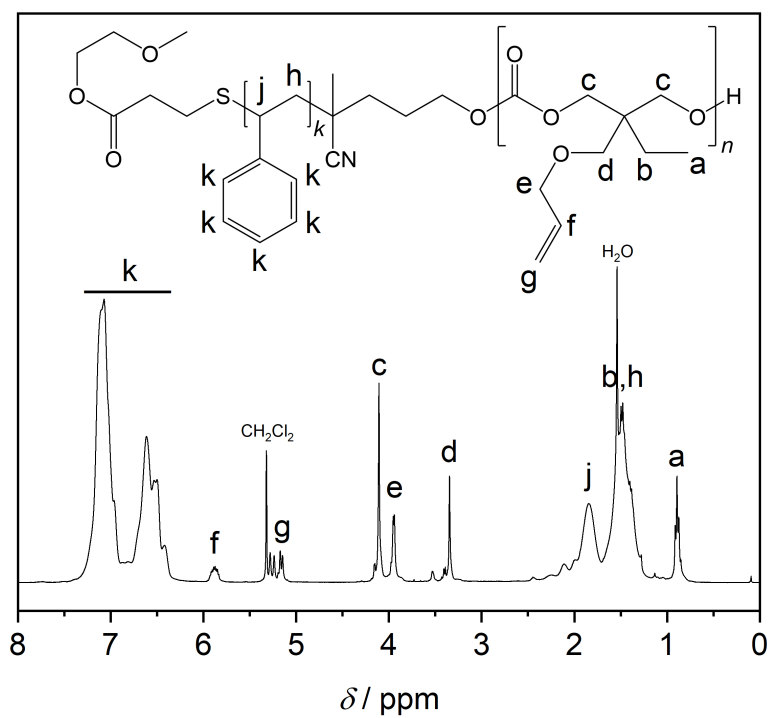
AOMEC (x eq) was dissolved in dry DCM under inert gas in a thoroughly dried flask. To that solution, TUC (2.5 eq) was added. This solution was kept stirring over CaH_2

overnight. Additionally, a solution of hydroxy-PS (1.00 g, 1.0 EG eq, cleaved by aminolysis) in dry DCM under inert gas in a thoroughly dried flask was prepared and likewise kept stirring over CaH_2 overnight.

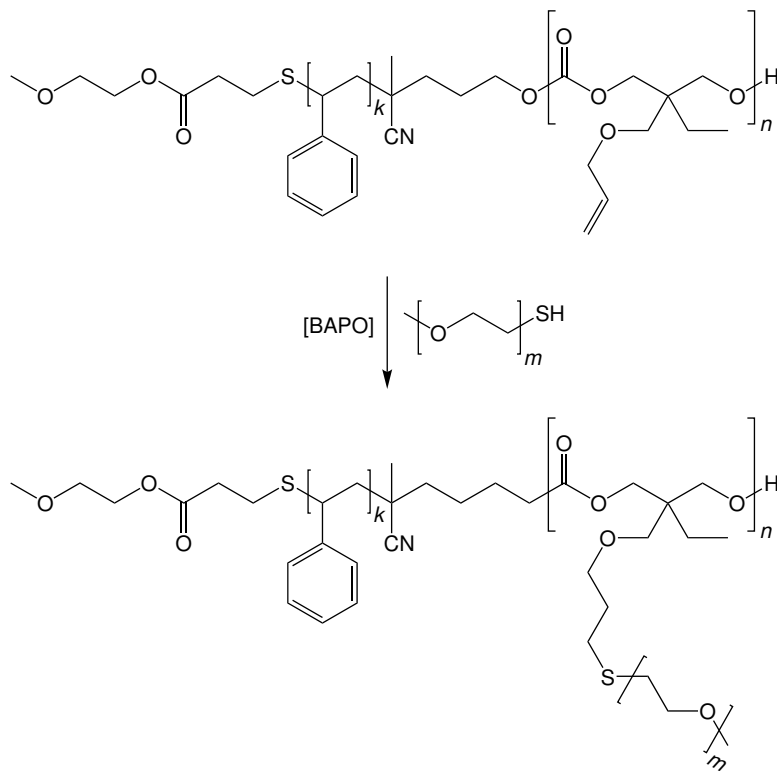
Afterwards, the monomer solution was transferred to a different thoroughly dried flask through a syringe filter. The solution was pre-heated to 30°C and then in quick succession firstly DBU (2.5 eq) and secondly the likewise filtered hydroxy-PS solution was added ($[\text{M}]$ with combined solutions = 0.5 M).

After 24 h polymerization time, the reaction was stopped by adding benzoic acid dissolved in little DCM to the solution. The polymer was recovered by precipitation into methanol at ambient temperature and the precipitation was repeated twice. Drying the polymer *in vacuo* resulted in a colorless powder (typical monomer conversion 20–30 %).

$^1\text{H-NMR}$ (400 MHz, CD_2Cl_2): δ (ppm) = 7.23–6.41 (m, (5k) H, H_k), 5.89 (ddt, J = 16.1 Hz, 10.6 Hz, 5.4 Hz, (1n) H, H_f), 5.27 (d, J = 17.2 Hz, (1n) H, $\text{H}_{g,\text{trans}}$), 5.17 (d, J = 10.2 Hz, (1n) H, $\text{H}_{g,\text{cis}}$), 4.12 (s, (4n) H, H_c), 3.96 (d, J = 5.5 Hz, (2n) H, H_e), 3.36 (s, (2n) H, H_d), 2.12–1.80 (m, (1k) H, H_i), 1.55–1.29 (m, (2n+2k) H, H_{b+h}), 0.90 (t, J = 7.7 Hz, (3n) H, H_a).



6.7.5 Thiol-ene Addition and Electrolyte Film Preparation

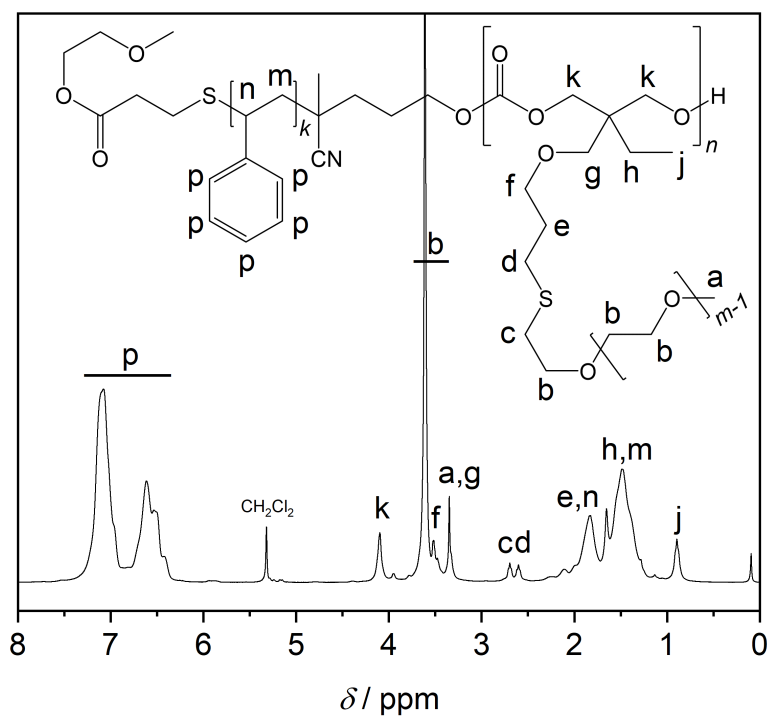


PS-*b*-PC (300 mg, 1.0 PC–RU eq) was dissolved in 5 mL of dry dioxane. Afterwards, mPEO550-SH (2.0 EG eq) and BAPO (0.1 eq) were added. The solution was sparged with dry nitrogen and then irradiated with an Osram Dulux Blue UVA lamp (32 W, 355–390 nm, max. 370 nm) for 4 h.

After removal of the solvent, the slimy residue was cooled to $-20\text{ }^{\circ}\text{C}$ for a few minutes and then mixed with methanol and mechanically stirred to produce a precipitate of the polymer. The solid was filtrated and dissolved in little DCM. This procedure was repeated two to four times, until the residue after removal of the solvent seemed solid instead of slimy. After a last cycle, the polymer was extensively dried *in vacuo*.

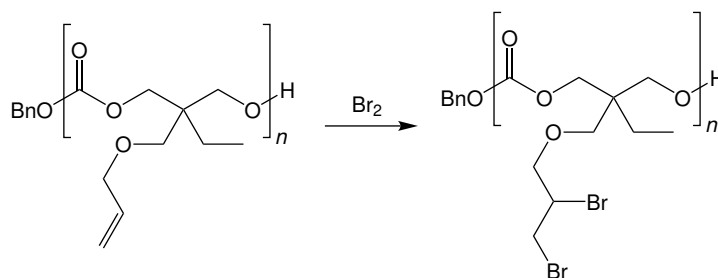
133 mg of the resulting polymer was completely dissolved in acetone and then combined with a separate solution of LiTFSI in acetone ([Li]/[O] ratio 1:20). The mixture was stirred to homogeneity and then filled into a PTFE petridish (diameter 4 cm). The solvent was slowly evaporated and the resulting polymer film thoroughly dried *in vacuo* at $80\text{ }^{\circ}\text{C}$. Discs with a diameter of 10 mm were cut out from the films, their thickness determined ($135\text{ }\mu\text{m}$), and then placed in a coin cell assembly in place of the Mylar foil spacer. The coin cells were conditioned at $80\text{ }^{\circ}\text{C}$ for 24 h prior to following the general procedure for EIS measurements.

$^1\text{H-NMR}$ (400 MHz, CD_2Cl_2): δ (ppm) = 7.23–6.41 ((5*k*) H, H_p), 4.11 ((4*n*) H, H_k), 3.79–3.46 ((4*nm*) H, H_{b+f}), 3.35 ((5*n*) H, H_{a+g}), 2.70 ((2*n*) H, H_c), 2.60 ((2*n*) H, H_d), 2.20–1.72 ((2*n+k*) H, H_{e+n}), 1.72–1.19 ((2*n+2k*) H, H_{h+m}), 0.89 ((3*n*) H, H_j).



6.8 Multifunctionalization

6.8.1 Bromination of PAOMEC

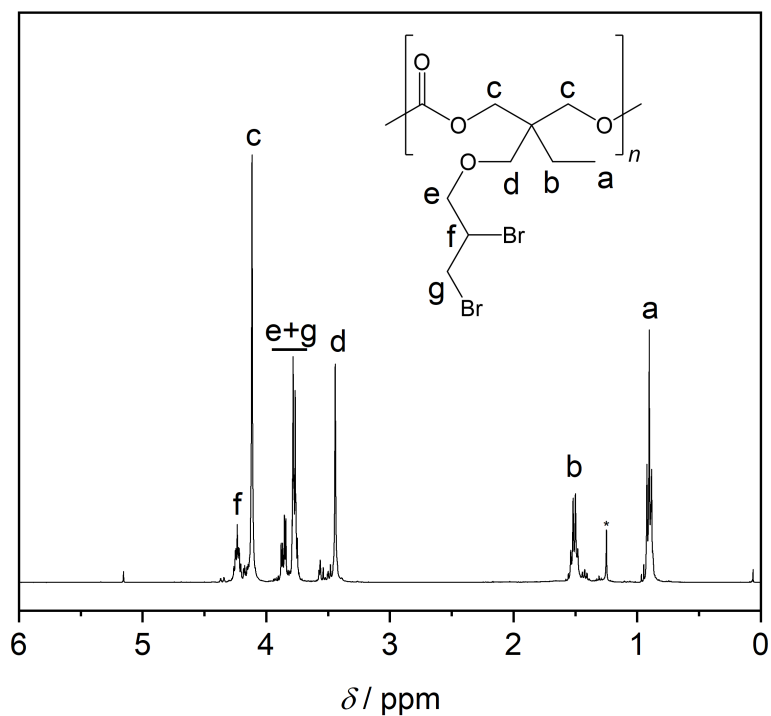


PAOMEC (3.00 g, 1.0 RU eq) was dissolved in 30 mL of dry chloroform under inert gas and cooled to 0 °C. Afterwards, liquid bromine (0.76 mL, 2.36 g, 14.76 mmol, 1.0 eq) was added dropwise to the solution, until no further decolorization was observed. The reaction was then kept stirring at ambient temperature for further 2 h.

Afterwards, the reaction solution was washed twice with 30 mL of a 10% Na₂S₂O₃ solution and three times with 30 mL of water. The organic phase was dried over MgSO₄

and the solvent removed under reduced pressure. Drying the polymer *in vacuo* resulted in a colorless viscous mass (5.22 g, 97%).

¹H-NMR (400 MHz, CDCl₃): δ (ppm) = 4.23 (tt, $J = 6.8$ Hz, 4.6 Hz, 1 H, H_f), 4.12 (s, 4 H, H_c), 3.91–3.73 (m, 4 H, H_{e+g}), 3.44 (s, 2 H, H_d), 1.51 (q, $J = 7.7$ Hz, 2 H, H_b), 0.90 (t, $J = 7.6$ Hz, 3 H, H_a).



List of Abbreviations

Some abbreviations are only used once for general information or only for a single paragraph. Such are not listed here.

Established physical quantities and units, as well as chemical atom symbols are excluded as well.

AIBN	azobis(isobutyronitrile)
AOMEC	2-allyloxymethyl-2-ethyltrimethylene carbonate
AROP	anionic ring-opening polymerization
ATRP	atom transfer radical polymerization
<i>b</i>	<i>block</i>
BAPO	bis(2,4,6-trimethylbenzoyl)phenylphosphine oxide, Irgacure 819
BEC	2-butyl-2-ethyltrimethylene carbonate
BMEE	bis(mercaptoethoxy)ethane
Bn	benzyl
BPO	benzoyl peroxide
br	broadened signal
CD₂Cl₂	deutero-dichloromethane
CDCl₃	deutero-chloroform
CTA	chain transfer agent
d	doublet
DBU	1,8-diazabicyclo(5.4.0)undec-7-ene
DCM	dichloromethane
Da	Dalton

DSC	differential scanning calorimetry
δ	chemical shift
EG	end group
EIS	electrochemical impedance spectroscopy
eq	equivalent(s)
Et	ethyl
FRP	free radical polymerization
<i>gr</i>	<i>graft</i>
J	coupling constant
LIB	lithium-ion battery
m	multiplet
M_n	number-average molecular mass
M_p	peak molecular mass
MALS	multiangle light scattering
mPEO	poly(ethylene oxide) monomethyl ether
MWCO	molecular weight cutoff
<i>net</i>	<i>network</i>
NMR	nuclear magnetic resonance
P_n	degree of polymerization
PAOMEC	poly(2-allyloxymethyl-2-ethyltrimethylene carbonate)
PBEC	poly(2-butyl-2-ethyltrimethylene carbonate)
PC	polycarbonate
PEC	poly(ethylene carbonate)
PEO	poly(ethylene oxide)

PMMA	poly(methyl methacrylate)
ppm	parts per million
PS	polystyrene
PTMC	poly(trimethylene carbonate)
q	quartet
qnt	quintet
RAFT	reversible addition-fragmentation chain transfer
ROP	ring-opening polymerization
RU	repeating unit
s	singlet
SCE	saturated calomel electrode
SEC	size exclusion chromatography
SEI	solid electrolyte interphase
SPE	solid polymer electrolyte
σ	ionic conductivity
t	triplet
t_+	cation transference number
T_g	glass transition temperature
T_m	melting temperature
TCEP·HCl	tris(2-carboxyethyl)phosphine hydrochloride
TEA	triethylamine
TFSI	bis(trifluoromethanesulfonyl)imide
THF	tetrahydrofuran
TMC	trimethylene carbonate

Ts	tosyl (<i>p</i> -toluenesulfonyl)
TUC	thiourea cocatalyst, <i>N</i> -(3,5-bis(trifluoromethyl)phenyl)- <i>N'</i> -cyclohexylthiourea
UV	ultraviolet (light)
UV/Vis	ultraviolet and visible light
XEt	<i>O</i> -ethylxanthate

List of Figures

1	Examples of Step-Growth Polymerizations	3
2	Mechanism of FRP	5
3	Mechanism of ATRP	6
4	Mechanism of RAFT	7
5	Two Different Mechanisms of AROP	9
6	Mechanism of Radical Thiol-ene Addition	12
7	Lithium-Ion Battery Schematic	15
8	Lithium Dendrite Growth	16
9	PEO Coordination	19
10	Some PEO-grafted Structures from Literature	20
11	PEC and PTMC	21
12	Kinetic Study for PTMC	27
13	Abandoned Initial Synthesis Pathway	29
14	Outline of Synthetis Route	31
15	Influence of TUC on Conversion of AROP	33
16	Kinetic Studies for AROP	34
17	Various Routes for Thiolation	36
18	Conversion of Thiol-ene Addition	39
19	SEC Traces for PC- <i>gr</i> -PEO1000	40
20	Comparison of MALS Results with SEC Column Calibration	42
21	DSC Plots for the Polymer Series of PEO550	45
22	Pictures of PC- <i>gr</i> -PEO2000 Before and After Amorphization by LiTFSI	47
23	Overview of Ionic Conductivity Plots	50
24	Comparison of Ionic Conductivities Depending on Length of Sidechain	52
25	Polarization Plot for the Bruce-Vincent Test of PC- <i>gr</i> -PEO550	54
26	Ionic Conductivity Corrected by Transference Number	56
27	Reaction Scheme for the Bromination and Subsequent Substitution Approach	57

List of Figures

28	SEC and NMR from Unsuccessful Bromine Substitution Attempts	58
29	Pictures of Crosslinked Samples	60
30	Proposed Synthesis Route for PS- <i>b</i> -(PC- <i>gr</i> -PEO)	62
31	Kinetics of PS Polymerization	64
32	Picture of a Microphase-Separated Solid Film	66
33	Removal of CTA Endgroup by Aminolysis with Subsequent Thiol-Michael Click	66
34	Ionic Conductivity of Solidified Electrolytes	68
35	DSC Plots for the Polymer Series of PEO550	69
36	Exemplary Nyquist Plot	77

List of Tables

1	Overview over a selection of typical cyclic monomers and their usual ring-opening polymerization mechanism (adapted from literature ^[45]).	10
2	¹ H-NMR and SEC results of the examined polymers.	41
3	Thermal properties of the examined polymers as determined by DSC measurements, as well as a comparison with pure PEO.	43
4	Thermal properties of the polymer electrolytes after the addition of LiTFSI	46
5	Lithium ion transference numbers t_+ of selected polymers at 60 °C.	55
6	Overview over attempted AROP chain extensions after radical displacement of CTA endgroup.	65
7	Overview over attempted AROP chain extensions after aminolysis and thiol-Michael addition.	67

Bibliography

- [1] N. Nitta, F. Wu, J. T. Lee, G. Yushin, *Mater. Today* **2015**, *18*, 252–264.
- [2] M. Tran, D. Banister, J. D. Bishop, M. D. McCulloch, *Nat. Clim. Chang.* **2012**, *2*, 328–333.
- [3] Z. Yang, H. Huang, F. Lin, *Adv. Energy Mater.* **2022**, *12*, 2200383.
- [4] T. Kim, W. Song, D. Y. Son, L. K. Ono, Y. Qi, *J. Mater. Chem. A* **2019**, *7*, 2942–2964.
- [5] G. E. Blomgren, *J. Electrochem. Soc.* **2017**, *164*, A5019–A5025.
- [6] M. Armand, P. Axmann, D. Bresser, M. Copley, K. Edström, C. Ekberg, D. Guyomard, B. Lestriez, P. Novák, M. Petranikova, W. Porcher, S. Trabesinger, M. Wohlfahrt-Mehrens, H. Zhang, *J. Power Sources* **2020**, *479*, 228708.
- [7] J. B. Goodenough, Y. Kim, *Chem. Mater.* **2010**, *22*, 587–603.
- [8] Q. Wang, P. Ping, X. Zhao, G. Chu, J. Sun, C. Chen, *J. Power Sources* **2012**, *208*, 210–224.
- [9] N. Williard, W. He, C. Hendricks, M. Pecht, *Energies* **2013**, *6*, 4682–4695.
- [10] J. Janek, W. G. Zeier, *Nat. Energy* **2016**, *1*, 1–4.
- [11] Y. Zheng, Y. Yao, J. Ou, M. Li, D. Luo, H. Dou, Z. Li, K. Amine, A. Yu, Z. Chen, *Chem. Soc. Rev.* **2020**, *49*, 8790–8839.
- [12] C. Monroe, J. Newman, *J. Electrochem. Soc.* **2005**, *152*, A396.
- [13] A. L. Robinson, J. Janek, *MRS Bull.* **2014**, *39*, 1046–1047.
- [14] J. Nanda, C. Wang, P. Liu, *MRS Bull.* **2018**, *43*, 752–758.
- [15] R. Chen, Q. Li, X. Yu, L. Chen, H. Li, *Chem. Rev.* **2020**, *120*, 6820–6877.
- [16] W. Xu, J. Wang, F. Ding, X. Chen, E. Nasybulin, Y. Zhang, J. G. Zhang, *Energy Environ. Sci.* **2014**, *7*, 513–537.
- [17] Z. Hu, G. Li, A. Wang, J. Luo, X. Liu, *Batter. Supercaps* **2020**, *3*, 331–335.

- [18] Q. Zhao, S. Stalin, C. Z. Zhao, L. A. Archer, *Nat. Rev. Mater.* **2020**, *5*, 229–252.
- [19] Z. Xue, D. He, X. Xie, *J. Mater. Chem. A* **2015**, *3*, 19218–19253.
- [20] J. Mindemark, M. J. Lacey, T. Bowden, D. Brandell, *Prog. Polym. Sci.* **2018**, *81*, 114–143.
- [21] I. Osada, H. De Vries, B. Scrosati, S. Passerini, *Angew. Chemie - Int. Ed.* **2016**, *55*, 500–513.
- [22] C. Sun, J. Liu, Y. Gong, D. P. Wilkinson, J. Zhang, *Nano Energy* **2017**, *33*, 363–386.
- [23] A. Varzi, K. Thanner, R. Scipioni, D. Di Lecce, J. Hassoun, S. Dörfler, H. Altheus, S. Kaskel, C. Prehal, S. A. Freunberger, *J. Power Sources* **2020**, *480*, 228803.
- [24] R. G. Jones, E. S. Wilks, W. V. Metanomski, J. Kahovec, M. Hess, R. Stepto, T. Kitayama, *Compendium of Polymer Terminology and Nomenclature - IUPAC Recommendations 2008*, RSC Publishing, **2009**.
- [25] J. K. Stille, *J. Chem. Educ.* **1981**, *58*, 862–866.
- [26] K. Pang, R. Kotek, A. Tonelli, *Prog. Polym. Sci.* **2006**, *31*, 1009–1037.
- [27] M. Winnacker, *Biomater. Sci.* **2017**, *5*, 1230–1235.
- [28] F. E. Golling, R. Pires, A. Hecking, J. Weikard, F. Richter, K. Danielmeier, D. Dijkstra, *Polym. Int.* **2019**, *68*, 848–855.
- [29] G. Odian, *Principles of Polymerization*, 4th Ed., Wiley, Hoboken, **2004**.
- [30] K. Hong, H. Zhang, J. W. Mays, A. E. Visser, C. S. Brazel, J. D. Holbrey, W. M. Reichert, R. D. Rogers, *Chem. Commun.* **2002**, *13*, 1368–1369.
- [31] D. Colombani, **1997**, *22*, 1649–1720.
- [32] P. Nesvadba, *Radical Polymerization in Industry*, **2012**.
- [33] M. Szwarc, *Nature* **1956**, *178*, 1168–1169.
- [34] H. Frey, T. Ishizone, *Macromol. Chem. Phys.* **2017**, *218*, 3–5.
- [35] A. D. Jenkins, R. G. Jones, G. Moad, *Pure Appl. Chem.* **2010**, *82*, 483–491.
- [36] M. Destarac, *Polym. Chem.* **2018**, *9*, 4947–4967.

- [37] P. Krys, K. Matyjaszewski, *Eur. Polym. J.* **2017**, *89*, 482–523.
- [38] M. Najafi, H. Roghani-Mamaqani, V. Haddadi-Asl, M. Salami-Kalajahi, *Adv. Polym. Technol.* **2011**, *30*, 257–268.
- [39] J.-S. Wang, K. Matyjaszewski, *J. Am. Chem. Soc.* **1995**, *117*, 5614–5615.
- [40] M. Kato, M. Kamigaito, M. Sawamoto, T. Higashimura, *Macromolecules* **1995**, *28*, 1721–1723.
- [41] D. A. Shipp, *Polym. Rev.* **2011**, *51*, 99–103.
- [42] J. Chiefari, Y. K. Chong, F. Ercole, J. Krstina, J. Jeffery, T. P. Le, R. T. Mayadunne, G. F. Meijs, C. L. Moad, G. Moad, E. Rizzardo, S. H. Thang, *Macromolecules* **1998**, *31*, 5559–5562.
- [43] S. Perrier, *Macromolecules* **2017**, *50*, 7433–7447.
- [44] O. Nuyken, S. D. Pask, *Polymers* **2013**, *5*, 361–403.
- [45] D. J. Brunelle, *Ring-Opening Polymerization. Mechanisms, Catalysis, Structure, Utility*. Hanser Publishers, **1993**.
- [46] P. Dubois, O. Coulembier, J.-M. Raquez, *Handbook of Ring-Opening Polymerization*, WILEY-VCH, **2009**.
- [47] P. Théato, H.-A. Klok, *Functional Polymers by Post-Polymerization Modification: Concepts, Guidelines, and Applications*, Wiley-VCH, **2013**.
- [48] W. Xue, H. Mutlu, P. Theato, *Eur. Polym. J.* **2020**, *130*, 109660.
- [49] M. A. Gauthier, M. I. Gibson, H. A. Klok, *Angew. Chemie - Int. Ed.* **2009**, *48*, 48–58.
- [50] W. A. Cunningham, *J. Chem. Educ.* **1935**, *12*, 120–124.
- [51] A. B. Lowe, *Polym. Chem.* **2010**, *1*, 17–36.
- [52] G. Delaittre, N. K. Guimard, C. Barner-Kowollik, *Acc. Chem. Res.* **2015**, *48*, 1296–1307.
- [53] A. Das, P. Theato, *Macromolecules* **2015**, *48*, 8695–8707.

- [54] H. C. Kolb, M. G. Finn, K. B. Sharpless, *Angew. Chemie - Int. Ed.* **2001**, *40*, 2004–2021.
- [55] C. E. Hoyle, T. Y. Lee, T. Roper, *J. Polym. Sci. Part A Polym. Chem.* **2004**, *42*, 5301–5338.
- [56] The Royal Swedish Academy of Sciences, *Nobel Prize Chem.* **2022**.
- [57] M. Benaglia, A. Alberti, L. Giorgini, F. Magnoni, S. Tozzi, *Polym. Chem.* **2013**, *4*, 124–132.
- [58] G. B. Desmet, M. K. Sabbe, D. R. D’Hooge, P. Espeel, S. Celasun, G. B. Marin, F. E. Du Prez, M. F. Reyniers, *Polym. Chem.* **2017**, *8*, 1341–1352.
- [59] C. Remzi Becer, R. Hoogenboom, U. S. Schubert, *Angew. Chemie - Int. Ed.* **2009**, *48*, 4900–4908.
- [60] A. B. Lowe, *Polym. Chem.* **2014**, *5*, 4820–4870.
- [61] V. S. Khire, A. W. Harant, A. W. Watkins, K. S. Anseth, C. N. Bowman, *Macromolecules* **2006**, *39*, 5081–5086.
- [62] M. W. Jones, G. Mantovani, S. M. Ryan, X. Wang, D. J. Brayden, D. M. Haddleton, *Chem. Commun.* **2009**, 5272–5274.
- [63] J. W. Chan, C. E. Hoyle, A. B. Lowe, *J. Am. Chem. Soc.* **2009**, *131*, 5751–5753.
- [64] R. Hoogenboom, *Angew. Chemie - Int. Ed.* **2010**, *49*, 3415–3417.
- [65] A. Masias, J. Marcicki, W. A. Paxton, *ACS Energy Lett.* **2021**, *6*, 621–630.
- [66] E. Fan, L. Li, Z. Wang, J. Lin, Y. Huang, Y. Yao, R. Chen, F. Wu, *Chem. Rev.* **2020**, *120*, 7020–7063.
- [67] The Royal Swedish Academy of Sciences, *Nobel Prize Chem.* **2019**.
- [68] M. Armand, J.-M. Tarascon, *Nature* **2008**, *451*, 652–657.
- [69] S. Liang, W. Yan, X. Wu, Y. Zhang, Y. Zhu, H. Wang, Y. Wu, *Solid State Ionics* **2018**, *318*, 2–18.
- [70] J. Asenbauer, T. Eisenmann, M. Kuenzel, A. Kazzazi, Z. Chen, D. Bresser, *Sustain. Energy Fuels* **2020**, *4*, 5387–5416.

- [71] X. B. Cheng, R. Zhang, C. Z. Zhao, Q. Zhang, *Chem. Rev.* **2017**, *117*, 10403–10473.
- [72] A. Hammami, N. Raymond, M. Armand, *Nature* **2003**, *424*, 635–636.
- [73] R. Khurana, PhD thesis, Cornell University, **2014**, p. 13.
- [74] J. W. Fergus, *J. Power Sources* **2010**, *195*, 4554–4569.
- [75] K. Edström, D. Brandell, T. Gustafsson, L. Nyholm, *Electrochem. Soc. Interface* **2011**, *20*, 41–46.
- [76] M. A. Ratner, D. F. Shriver, *Chem. Rev.* **1988**, *88*, 109–124.
- [77] C. A. Angell, *Solid State Ionics* **1983**, *9-10*, 3–16.
- [78] Y. Wang, F. Fan, A. L. Agapov, T. Saito, J. Yang, X. Yu, K. Hong, J. Mays, A. P. Sokolov, *Polymer (Guildf)*. **2014**, *55*, 4067–4076.
- [79] J. Lopez, D. G. Mackanic, Y. Cui, Z. Bao, *Nat. Rev. Mater.* **2019**, *4*, 312–330.
- [80] S. Honary, H. Orafai, *Drug Dev. Ind. Pharm.* **2002**, *28*, 711–715.
- [81] D. T. Hallinan, N. P. Balsara, *Annu. Rev. Mater. Res.* **2013**, *43*, 503–525.
- [82] G. G. Eshetu, D. Mecerreyes, M. Forsyth, H. Zhang, M. Armand, *Mol. Syst. Des. Eng.* **2019**, *4*, 294–309.
- [83] D. E. Fenton, J. M. Parker, P. V. Wright, *Polymer (Guildf)*. **1973**, *14*, 589–594.
- [84] P. V. Wright, *Br. Polym. J.* **1975**, *7*, 319–327.
- [85] M. Armand, J. M. Chabagno, M. J. Duclot, *Second Int. Meet. Solid Electrolytes* **1978**, 20–22.
- [86] M. Armand, J. M. Chabagno, M. J. Duclot, *Fast Ion Transp. Solids* **1979**, 131.
- [87] C. Berthier, W. Gorecki, M. Minier, M. Armand, J. M. Chabagno, P. Rigaud, *Solid State Ionics* **1983**, *11*, 91–95.
- [88] B. Scrosati, J. Garche, *J. Power Sources* **2010**, *195*, 2419–2430.
- [89] V. Di Noto, S. Lavina, G. A. Giffin, E. Negro, B. Scrosati, *Electrochim. Acta* **2011**, *57*, 4–13.
- [90] A. Magistris, C. Fisica, *Polym. Int.* **1992**, *28*, 277–280.

- [91] W. H. Meyer, *Adv. Mater.* **1998**, *10*, 439–448.
- [92] R. C. Agrawal, G. P. Pandey, *J. Phys. D. Appl. Phys.* **2008**, *41*, 223001.
- [93] E. Quartarone, P. Mustarelli, *Chem. Soc. Rev.* **2011**, *40*, 2525–2540.
- [94] N. Molinari, J. P. Malloa, B. Kozinsky, *Chem. Mater.* **2018**, *30*, 6298–6306.
- [95] L. Stolz, G. Homann, M. Winter, J. Kasnatscheew, *Mater. Adv.* **2021**, *2*, 3251–3256.
- [96] D. Devaux, R. Bouchet, D. Glé, R. Denoyel, *Solid State Ionics* **2012**, *227*, 119–127.
- [97] D. Diddens, A. Heuer, O. Borodin, *Macromolecules* **2010**, *43*, 2028–2036.
- [98] Y. Takahashi, H. Tadokoro, *Macromolecules* **1973**, *6*, 672–675.
- [99] L. Zhu, J. Li, Y. Jia, P. Zhu, M. Jing, S. Yao, X. Shen, S. Li, F. Tu, *Int. J. Energy Res.* **2020**, *44*, 10168–10178.
- [100] V. Bocharova, A. P. Sokolov, *Macromolecules* **2020**, *53*, 4141–4157.
- [101] S. Sylla, J. Y. Sanchez, M. Armand, *Electrochim. Acta* **1992**, *37*, 1699–1701.
- [102] L. R. A. K. Bandara, M. A. K. L. Dissanayake, B. Mellander, *Electrochim. Acta* **1998**, *43*, 10–14.
- [103] I. Nicotera, G. A. Ranieri, M. Terenzi, A. V. Chadwick, M. I. Webster, *Solid State Ionics* **2002**, *146*, 143–150.
- [104] S. N. Banitaba, D. Semnani, E. Heydari-Soureshjani, B. Rezaei, A. A. Ensafi, *Solid State Ionics* **2020**, *347*, 115252.
- [105] S. Choudhury, R. Mangal, A. Agrawal, L. A. Archer, *Nat. Commun.* **2015**, *6*, 10101.
- [106] S. Qian, H. Chen, Z. Wu, D. Li, X. Liu, Y. Tang, S. Zhang, *Batter. Supercaps* **2021**, *4*, 39–59.
- [107] L. Xu, J. Li, W. Deng, L. Li, G. Zou, H. Hou, L. Huang, X. Ji, *Mater. Chem. Front.* **2021**, *5*, 1315–1323.

- [108] Z. Wen, T. Itoh, Y. Ichikawa, M. Kubo, O. Yamamoto, *Solid State Ionics* **2000**, *134*, 281–289.
- [109] S. K. Patla, R. Ray, K. Asokan, S. Karmakar, *J. Appl. Phys.* **2018**, *123*, 125102.
- [110] J. R. MacCallum, M. J. Smith, C. A. Vincent, *Solid State Ionics* **1984**, *11*, 307–312.
- [111] R. Khurana, J. L. Schaefer, L. A. Archer, G. W. Coates, *J. Am. Chem. Soc.* **2014**, *136*, 7395–7402.
- [112] Y. Zhang, W. Lu, L. Cong, J. Liu, L. Sun, A. Mauger, C. M. Julien, H. Xie, J. Liu, *J. Power Sources* **2019**, *420*, 63–72.
- [113] X. Ji, S. Li, M. Cao, R. Liang, L. L. Xiao, K. Yue, S. Liu, X. Zhou, Z. H. Guo, *Batter. Supercaps* **2022**, *5*, e202100319.
- [114] X. Ji, Y. Zhang, M. Cao, Q. Gu, H. Wang, J. Yu, Z. H. Guo, X. Zhou, *J. Adv. Ceram.* **2022**, *11*, 835–861.
- [115] D. J. Bannister, G. R. Davies, I. M. Ward, J. E. McIntyre, *Polymer (Guildf)*. **1984**, *25*, 1600–1602.
- [116] D. Rosenbach, N. Mödl, M. Hahn, J. Petry, M. A. Danzer, M. Thelakkat, *ACS Appl. Energy Mater.* **2019**, *2*, 3373–3388.
- [117] T. Itoh, K. Fujita, T. Uno, M. Kubo, *Ionics (Kiel)*. **2017**, *23*, 257–264.
- [118] A. J. Butzelaar, K. L. Liu, P. Röring, G. Brunklaus, M. Winter, P. Théato, *ACS Appl. Polym. Mater.* **2021**, *3*, 1573–1582.
- [119] S. Li, K. Jiang, J. Wang, C. Zuo, Y. H. Jo, D. He, X. Xie, Z. Xue, *Macromolecules* **2019**, *52*, 7234–7243.
- [120] A. Arya, A. L. Sharma, *Polymer electrolytes for lithium ion batteries: a critical study*, Vol. 23, *Ionics*, **2017**, pp. 497–540.
- [121] E. D. Gomez, A. Panday, E. H. Feng, V. Chen, G. M. Stone, A. M. Minor, C. Kisielowski, K. H. Downing, O. Borodin, G. D. Smith, N. P. Balsara, *Nano Lett.* **2009**, *9*, 1212–1216.

- [122] D. Sharon, P. Bennington, M. A. Webb, C. Deng, J. J. De Pablo, S. N. Patel, P. F. Nealey, *J. Am. Chem. Soc.* **2021**, *143*, 3180–3190.
- [123] R. Bouchet, T. N. Phan, E. Beaudoin, D. Devaux, P. Davidson, D. Bertin, R. Denoyel, *Macromolecules* **2014**, *47*, 2659–2665.
- [124] V. Sethuraman, S. Mogurampelly, V. Ganesan, *Soft Matter* **2017**, *13*, 7793–7803.
- [125] A.-V. G. Ruzette, P. P. Soo, D. R. Sadoway, A. M. Mayes, *Journal of The Electrochemical Society* **2001**, *148*, A537.
- [126] C. Wang, T. Sakai, O. Watanabe, K. Hirahara, T. Nakanishi, *Journal of The Electrochemical Society* **2003**, *150*, A1166.
- [127] J. Rolland, J. Brassinne, J. P. Bourgeois, E. Poggi, A. Vlad, J. F. Gohy, *J. Mater. Chem. A* **2014**, *2*, 11839–11846.
- [128] A. J. Butzelaar, P. Röring, T. P. Mach, M. Hoffmann, F. Jeschull, M. Wilhelm, M. Winter, G. Brunklus, P. Théato, *ACS Appl. Mater. Interfaces* **2021**, *13*, 39257–39270.
- [129] A. J. Butzelaar, P. Röring, M. Hoffmann, J. Atik, E. Paillard, M. Wilhelm, M. Winter, G. Brunklus, P. Theato, *Macromolecules* **2021**, *54*, 11101–11112.
- [130] K. S. Ngai, S. Ramesh, K. Ramesh, J. C. Juan, *Ionics (Kiel)*. **2016**, *22*, 1259–1279.
- [131] Q. Zhang, K. Liu, F. Ding, X. Liu, *Nano Res.* **2017**, *10*, 4139–4174.
- [132] M. T. Ong, O. Vernal, E. W. Draeger, A. C. Van Duin, V. Lordi, J. E. Pask, *J. Phys. Chem. B* **2015**, *119*, 1535–1545.
- [133] E. F. Spiegel, K. J. Adamic, B. D. Williams, A. F. Sammells, *Polymer (Guildf)*. **2000**, *41*, 3365–3369.
- [134] Y. Tominaga, V. Nanthana, D. Tohyama, *Polym. J.* **2012**, *44*, 1155–1158.
- [135] Y. Tominaga, K. Yamazaki, *Chem. Commun.* **2014**, *50*, 4448–4450.
- [136] B. Sun, J. Mindemark, K. Edström, D. Brandell, *Solid State Ionics* **2014**, *262*, 738–742.

- [137] B. Sun, J. Mindemark, K. Edström, D. Brandell, *Electrochem. commun.* **2015**, *52*, 71–74.
- [138] G. Rokicki, *Progress in Polymer Science (Oxford)* **2000**, *25*, 259–342.
- [139] H. Tomita, F. Sanda, T. Endo, *Journal of Polymer Science Part A: Polymer Chemistry* **2001**, *39*, 162–168.
- [140] Y. Tominaga, *Polym. J.* **2017**, *49*, 291–299.
- [141] J. Mindemark, B. Sun, E. Törmä, D. Brandell, *J. Power Sources* **2015**, *298*, 166–170.
- [142] K. Kimura, M. Yajima, Y. Tominaga, *Electrochem. commun.* **2016**, *66*, 46–48.
- [143] T. Okumura, S. Nishimura, *Solid State Ionics* **2014**, *267*, 68–73.
- [144] K. Kimura, H. Matsumoto, J. Hassoun, S. Panero, B. Scrosati, Y. Tominaga, *Electrochim. Acta* **2015**, *175*, 134–140.
- [145] B. Sun, J. Mindemark, E. V. Morozov, L. T. Costa, M. Bergman, P. Johansson, Y. Fang, I. Furó, D. Brandell, *Phys. Chem. Chem. Phys.* **2016**, *18*, 9504–9513.
- [146] P. C. Barbosa, L. C. Rodrigues, M. M. Silva, M. J. Smith, *Solid State Ionics* **2011**, *193*, 39–42.
- [147] K. Kimura, J. Motomatsu, Y. Tominaga, *Journal of Physical Chemistry C* **2016**, *120*, 12385–12391.
- [148] M. Forsyth, J. Sun, D. R. Macfarlane, A. J. Hill, *Journal of Polymer Science Part B: Polymer Physics* **2000**, *38*, 341–350.
- [149] J. Mindemark, L. Imholt, D. Brandell, *Electrochim. Acta* **2015**, *175*, 247–253.
- [150] J. Mindemark, L. Imholt, J. Montero, D. Brandell, *J. Polym. Sci. Part A Polym. Chem.* **2016**, *54*, 2128–2135.
- [151] M. D. Konieczynska, X. Lin, H. Zhang, M. W. Grinstaff, *ACS Macro Lett.* **2015**, *4*, 533–537.
- [152] Y. Tominaga, T. Shimomura, M. Nakamura, *Polymer (Guildf)*. **2010**, *51*, 4295–4298.

- [153] M. Ebadi, T. Eriksson, P. Mandal, L. T. Costa, C. M. Araujo, J. Mindemark, D. Brandell, *Macromolecules* **2020**, *53*, 764–774.
- [154] J. Mindemark, B. Sun, D. Brandell, *Polym. Chem.* **2015**, *6*, 4766–4774.
- [155] B. Sun, H. D. Asfaw, D. Rehnlund, J. Mindemark, L. Nyholm, K. Edström, D. Brandell, *ACS Appl. Mater. Interfaces* **2018**, *10*, 2407–2413.
- [156] W. He, Z. Cui, X. Liu, Y. Cui, J. Chai, X. Zhou, Z. Liu, G. Cui, *Electrochim. Acta* **2017**, *225*, 151–159.
- [157] Y. Chen, G. Chen, C. Niu, W. Shang, R. Yu, C. Fang, P. Ouyang, J. Du, *Polymer (Guildf)*. **2021**, *223*, 123695.
- [158] L. Meabe, T. V. Huynh, N. Lago, H. Sardon, C. Li, L. A. O'Dell, M. Armand, M. Forsyth, D. Mecerreyes, *Electrochim. Acta* **2018**, *264*, 367–375.
- [159] L. Meabe, T. V. Huynh, D. Mantione, L. Porcarelli, C. Li, L. A. O'Dell, H. Sardon, M. Armand, M. Forsyth, D. Mecerreyes, *Electrochim. Acta* **2019**, *302*, 414–421.
- [160] L. Meabe, N. Goujon, C. Li, M. Armand, M. Forsyth, D. Mecerreyes, *Batter. Supercaps* **2020**, *3*, 68–75.
- [161] F. Chen, B. G. Amsden, *J. Polym. Sci. Part A Polym. Chem.* **2016**, *54*, 544–552.
- [162] H. Ajiro, Y. Takahashi, M. Akashi, *Macromolecules* **2012**, *45*, 2668–2674.
- [163] X. Zhang, Z. Zhang, X. Su, H. Dong, Z. Zhong, R. Zhuo, *Macromol. Chem. Phys.* **2015**, *216*, 1712–1717.
- [164] Y. Haramiishi, N. Chanthaset, K. Kan, M. Akashi, H. Ajiro, *Polym. Degrad. Stab.* **2016**, *130*, 78–82.
- [165] T. Morioka, K. Ota, Y. Tominaga, *Polymer (Guildf)*. **2016**, *84*, 21–26.
- [166] R. C. Pratt, B. G. G. Lohmeijer, D. A. Long, P. N. P. Lundberg, A. P. Dove, H. Li, C. G. Wade, R. M. Waymouth, J. L. Hedrick, *Macromolecules* **2006**, *39*, 7863–7871.
- [167] F. Suriano, O. Coulembier, J. L. Hedrick, P. Dubois, *Polym. Chem.* **2011**, *2*, 528–533.

- [168] A. W. Snow, E. E. Foos, *Synthesis (Stuttg)*. **2003**, 509–512.
- [169] C. Tsiamantas, S. J. Dawson, I. Huc, *Comptes Rendus Chim.* **2016**, *19*, 132–142.
- [170] D. Lee, R. L. Donkers, J. M. DeSimone, R. W. Murray, *J. Am. Chem. Soc.* **2003**, *125*, 1182–1183.
- [171] Y. Liu, M. K. Shipton, J. Ryan, E. D. Kaufman, S. Franzen, D. L. Feldheim, *Anal. Chem.* **2007**, *79*, 2221–2229.
- [172] D. M. Mizrahi, M. Omer-Mizrahi, J. Goldshtein, N. Askinadze, S. Margel, *J. Polym. Sci. Part A Polym. Chem.* **2010**, *48*, 5468–5478.
- [173] M. W. Ali, Z. Muhammad, Q. Jia, L. Li, M. Saleem, M. Siddiq, Y. Chen, Y. Chen, *Polym. Chem.* **2020**, *11*, 4164–4171.
- [174] M. L. Miller, E. E. Roller, R. Y. Zhao, B. A. Leece, O. Ab, E. Baloglu, V. S. Goldmacher, R. V. Chari, *J. Med. Chem.* **2004**, *47*, 4802–4805.
- [175] R. Nicolaÿ, Y. Kwak, K. Matyjaszewski, *Chem. Commun.* **2008**, 5336–5338.
- [176] G. G. D’Ayala, M. Malinconico, P. Laurienzo, A. Tardy, Y. Guillaneuf, M. Lansalot, F. D’Agosto, B. Charleux, *J. Polym. Sci. Part A Polym. Chem.* **2014**, *52*, 104–111.
- [177] J. A. Faucher, J. V. Koleske, E. R. Santee, J. J. Stratta, C. W. Wilson, *J. Appl. Phys.* **1966**, *37*, 3962–3964.
- [178] S. Lascaud, M. Perrier, A. Vallée, S. Besner, J. Prud’homme, M. Armand, *Macromolecules* **1994**, *27*, 7469–7477.
- [179] J. Evans, C. A. Vincent, P. G. Bruce, *Polymer (Guildf)*. **1987**, *28*, 2324–2328.
- [180] P. G. Bruce, C. A. Vincent, *J. Electroanal. Chem.* **1987**, *225*, 1–17.
- [181] K. Pożyczka, M. Marzantowicz, J. R. Dygas, F. Krok, *Electrochim. Acta* **2017**, *227*, 127–135.
- [182] J. Rieger, *J. Therm. Anal.* **1996**, *46*, 965–972.
- [183] H. Zipse, *Top. Curr. Chem.* **2006**, *263*, 163–189.

- [184] Y. He, H. Keul, M. Möller, *React. Funct. Polym.* **2011**, *71*, 175–186.
- [185] A. W. Thomas, P. K. Kuroishi, M. M. Pérez-Madrigo, A. K. Whittaker, A. P. Dove, *Polym. Chem.* **2017**, *8*, 5082–5090.
- [186] M. Subarew, A. J. Butzelaar, P. Théato, *xxx* **2023**, *xxx*, *xxx*.

Author Information

Marvin Subarew

Education

09/2018 – 12/2022 **Doctorate**

Karlsruhe Institute of Technology (Karlsruhe)

Poly(ethylene oxide)-grafted Polycarbonates as Solvent-free Polymer Electrolytes for Lithium-Metal Batteries, supervised by Prof. Dr. Patrick Théato, within the BMBF Cluster "FestBatt"

04/2016 – 09/2018 **Chemistry M. Sc.**

Karlsruhe Institute of Technology (Karlsruhe)

Focus on polymer chemistry, focus thesis: The Usage of Thiol-ene Photopolymerization and Retro-Hetero-Diels-Alder Debonding on Demand in a Stereolithography Process, supervised by Prof. Dr. Christopher Barner-Kowollik

Master thesis: Hyaluronic Acid Hydrogels Bearing Nanopatterned Gold Nanoparticles for Biomedical Applications, supervised by Dr. Cornelia Lee-Thedieck

10/2012 – 04/2016 **Chemistry B. Sc.**

Karlsruhe Institute of Technology (Karlsruhe)

Bachelor thesis: Renewable Polyamides Derived from Terpenes, supervised by Prof. Dr. Michael Meier

09/2004 – 07/2012 **Abitur**

Copernicus Gymnasium (Philippsburg)

Work

09/2018 – 04/2022 **Doctoral Researcher**

Karlsruhe Institute of Technology (Karlsruhe)

06/2012 – 07/2012 **Lab Assistant**

TECHPharm GmbH Technische Dienste & Pharma (Bruchsal)

Publications

Parts of chapters 4.1.4, 4.2, and 4.3 are currently under internal review for publication:

M. Subarew, A. J. Butzelaar, P. Théato, xxx **2023**, xxx, xxx

Die vorliegende Arbeit wurde im Zeitraum von September 2018 bis Oktober 2022 am Institut für Technische Chemie und Polymerchemie (ITCP) am Karlsruher Institut für Technologie (KIT) unter der wissenschaftlichen Betreuung von Prof. Dr. Patrick Théato angefertigt.

Hiermit versichere ich, dass ich die vorliegende Arbeit selbstständig verfasst und keine anderen als die angegebenen Quellen und Hilfsmittel verwendet habe. Insbesondere habe ich wörtlich oder inhaltlich übernommene Inhalte aus anderen Werken als solche kenntlich gemacht. Die Satzung des Karlsruher Instituts für Technologie (KIT) zur Sicherung guter wissenschaftlicher Praxis in der jeweils gültigen Fassung wurde beachtet. Des Weiteren erkläre ich, dass ich mich derzeit in keinem laufenden Promotionsverfahren befinde, und auch keine vorausgegangenen Promotionsversuche unternommen habe. Die elektronische Version der Arbeit stimmt mit der schriftlichen Version überein und die Primärdaten sind gemäß Abs. A (6) der Regeln zur Sicherung guter wissenschaftlicher Praxis des KIT beim Institut abgegeben und archiviert.

02. November 2022 **Karlsruhe**